SCUOLA DI DOTTORATO
UNIVERSITÀ DEGLI STUDI *MEDITERRANEA* DI REGGIO CALABRIA
DIPARTIMENTO DI INGEGNERIA CIVILE, DELL'ENERGIA, DELL'AMBIENTE E DEI MATERIALI (DICEAM)

DOTTORATO DI RICERCA IN
INGEGNERIA MARITTIMA, DEI MATERIALI E DELLE STRUTTURE
S.S.D. ICAR/08
XXVII CICLO

SEISMIC ANALYSIS OF OFFSHORE WIND TURBINES ON BOTTOM FIXED SUPPORT STRUCTURES: COUPLED AND UNCOUPLED ANALYSIS

PHD STUDENT:
Natale Alati

SUPERVISORS:
Ing. Giuseppe Failla

Prof. Felice Arena

HEAD OF THE DOCTORAL SCHOOL
Prof. Felice Arena

REGGIO CALABRIA, JANUARY 2016

NATALE ALATI

SEISMIC ANALYSIS OF OFFSHORE WIND TURBINES ON BOTTOM FIXED SUPPORT STRUCTURES: COUPLED AND UNCOUPLED ANALYSIS

Il Collegio dei docenti del Dottorato di Ricerca in
Ingegneria Marittima, dei Materiali e delle Strutture
è composto da:

Felice Arena (coordinatore)
Giuseppe Barbaro
Guido Benassai
Paolo Boccotti
Vittoria Bonazinga
Michele Buonsanti
Salvatore Caddemi
Enzo D'Amore
Giuseppe Failla
Vincenzo Fiamma
Pasquale Filianoti
Enrico Foti
Paolo Fuschi
Sofia Giuffrè
Carlos Guedes Soares
Giovanni Leonardi
Antonina Pirrotta
Aurora Angela Pisano
Alessandra Romolo
Adolfo Santini
Francesco Scopelliti
Pol D. Spanos
Alba Sofi

Abstract

Offshore wind energy is one of the most import renewable energy resources worldwide. In the last year, the growth of energy demand and the great potential of wind resources in the sea have encouraged the realization of offshore wind turbines (OWTs).

The present thesis investigates the seismic response of a horizontal axis wind turbine on two bottom-fixed support structures for transitional water depths (30-60 m), a tripod and a jacket, both resting on pile foundations. Fully-coupled, non-linear time-domain simulations on full system models are carried out with the software BLADED© under combined wind-wave-earthquake loadings, for different load cases, considering fixed and flexible foundation models. A comparison with some typical design load cases given by international guidelines is implemented.

Although fully-coupled non-linear time domain simulations provide the “exact” numerical solutions, they involve some significant disadvantages: (i) a dedicated software package is needed, capable of accounting for inherent interactions between aerodynamic, hydrodynamic and seismic responses; (ii) computational costs are significant, almost prohibitive when several analyses have to be implemented for different environmental states and system parameters, as in the early stages of design.

For these reasons, in this thesis, the results of uncoupled analysis, obtained as linear superposition of separate wind, wave and earthquake responses with an additional damping referred to as *aerodynamic damping*, will be compared with fully-coupled non-linear time domain simulations. Important conclusions will be drawn on the reliability of uncoupled analyses for seismic assessment of OWTs.

Contents

Figures

Introduction

The demand for energy will continue to increase in the coming years and offshore wind energy shows great potential to become a key player in renewable energy future. The wind flow offshore is more stable and the average wind velocity is higher than onshore, in particular in the North Sea where the first installation of offshore wind turbines began in 1990s. In 2002 and 2003, the first large, utility-scale offshore farms were commissioned. The Horns Rev and Nysted wind farms, both in Denmark, were the first farms built with capacities exceeding 100 MW. As of the end of 2008, there was over 1000 MW of installed wind capacity, most of it in Europe.

Offshore wind energy has several promising attributes. These include:

- ✓ greater area available for siting large projects;
- ✓ proximity to cities and other load centers;
- ✓ general higher wind speeds compared with onshore locations;
- ✓ lower intrinsic turbulence intensities;
- ✓ lower wind shear.

There are some differences than onshore wind turbines, as;

- ✓ higher project costs due to a necessity for specialized installation and service vessels and equipment and more expensive support structures;
- ✓ more difficult working conditions;
- ✓ more difficult and expensive installaion procedures;
- ✓ decreased availability due to limited accessibility for maintenance;
- ✓ necessity for special corrosion prevention measures.

According to the IEC 2009, the offshore wind turbine is defined as “a wind turbine with a support structure which is subject to the hydrodynamic loading”. This type of turbine consists of the following components (see Figure 0.1):

- ✓ Rotor-nacelle assembly (RNA): is the part of a wind turbine that capture the kinetic energy of the wind and converts its to electrical power. It includes:
  - rotor: part of a wind turbine consisting of the blades and hub;
  - nacelle assembly: part of wind turbine consisting of all components above the tower that are not part of the rotor. This includes the drive train, bed plate, yaw system, and the nacelle enclosure.

✓ Support structure: this consists of the tower, substructure and foundation:

- tower: part of the support structure which connects the substructure to the rotor-nacelle assembly;
- substructure: part of the support structure which extends upwards from the seabed and connects the foundation to the tower;
- foundation: part of the support structure which transfers the loads acting on the structure into the seabed.

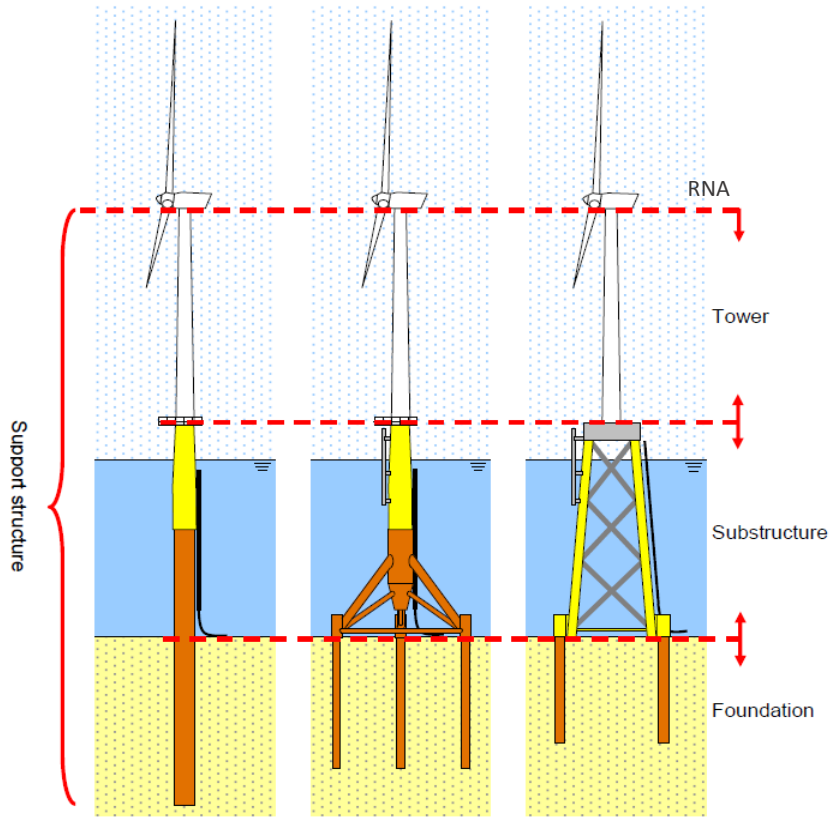

Figure 0.1: Components of offshore wind turbines

This dissertation is focused on the seismic response of offshore wind turbines on two different fixed support structures for transitional water depths.

Chapter 1 contains the general aspects that influence the design of offshore wind turbines, illustrates the basis for the estimation of aerodynamic and hydrodynamic loads and the structural model adopted for the simulation of the full system.

Chapter 2 provides an introduction about the seismic demand of horizontal axis wind turbines and analyses the aspects of international standard and certification guidelines for the load combinations with seismic excitations.

Chapter 3 shows the results of fully-coupled non-linear time domain simulations of offshore wind turbines on two bottom fixed support structures (tripod and jacket) for different foundation models: fixed and flexible.

Chapter 4 presents the result of uncoupled analysis for the support structures tripod and jacket with fixed foundation model.

1. Offshore wind turbines

The design of offshore wind turbines is one of the most fascinating challenges in renewable energy. Meeting the objective of increasing power production with reduced installation and maintenance costs requires a multi-disciplinary approach, bringing together the expertise in different fields of engineering. The purpose of this chapter is to offer a broad perspective on some crucial aspects of offshore wind turbines design, discussing the basis of aerodynamic and hydrodynamic loads and presenting the approaches adapted to performing integrated design load calculations for offshore wind turbines.

1.1. Introduction

In the last decades offshore wind energy has attracted a growing interest from scientists and engineers worldwide. After the first offshore wind farm, built in 1991 in relatively shallow waters (2-5 m) off the coast of Denmark at Vindeby, many others have been constructed, especially in the North and Baltic Seas, and new ones are being developed in Europe, United States, China and other countries [1]. Offshore wind energy still represents a small quote part of the total wind energy in the world, about 7 GW out of 393 GW at the half of 2015, but has an enormous potential (see Figure 1.1). The European Wind Energy Association (EWEA), for instance, estimates that offshore wind energy production in Europe will increase from the 6.5 GW at the end of 2013 to 150 GW in 2030, meeting approximately 14% of Europe's electricity demand [2-3]. Offshore sites offer indeed some considerable advantages over onshore sites, as:

- ✓ in the sea, the wind blows more stronger and constant respect land wind; as consequence the turbines are more efficient since they can produce more electricity and they can maintain higher levels of electricity generation for longer periods;

- ✓ with the offshore wind farms the noise and the visual imapct are significantly reduced, allowing for the designers of the wind turbines to produce larger wind turbines with longer blades that can effectively produce more electricity;
- ✓ vast expanses of uninterrupted open sea are available and the installations will not occupy land, interfering with other land uses.

However, due to several issues as more difficult and specialised installation procedures, more expensive support structures, more difficult environmental and working conditions, offshore wind energy may still be more expensive not only than onshore wind energy, but also than conventional power resources. Therefore, closing this gap has become a key step a future sustainable exploitation of offshore wind energy potential.

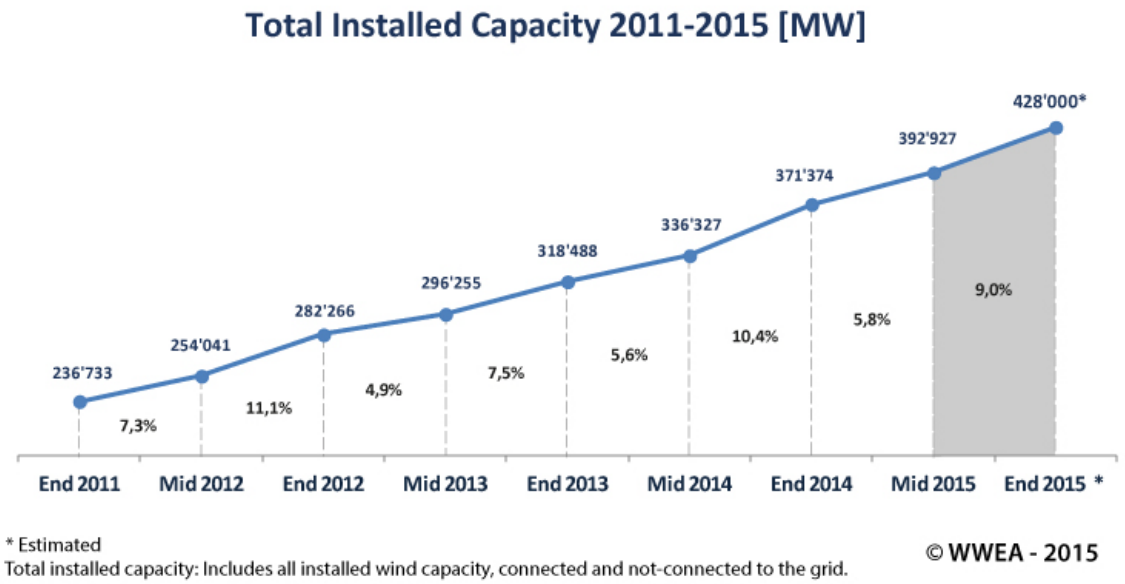

Figure 1.1: Global cumulative installed wind capacity until 2014 (Source WWEA).

Wind energy converters have a very long history, that in Europe traces back to the Middle Ages (for more information on the historical development, see Manwell [4]). Nowadays an offshore wind turbine is a complex ensemble of different components and subsystems: rotor, nacelle with powertrain, control and safety systems [5], and a support structure generally composed of a tower mounted on either a bottom-fixed substructure or a floating device moored to the seabed. Three-bladed, upwind rotors with horizontal axis are the conventional design solution in the industry, although alternative options (two blades, downwind rotor position or vertical axis) are under study. In the twenty-three years since the Vindeby offshore wind farm was built off the coast of Denmark, turbine size has

increased from 450 kW to 3-5 MW and even larger turbines, with rated power up to 10 MW, are being tested to be released in a near future [1].

Most of the existing offshore wind farms are in shallow waters, generally less than 20 m deep. At these sites wind turbines are mounted on monopiles driven into the seabed or resting on concrete gravity bases [6]. As the water depth increases, however, monopile solutions may require too large diameters to counteract the overturning moment and, for this reason, are not generally considered as economically feasible in waters deeper than 30 m. In transitional water depths, i.e. between 30 m and 60 m, wind turbines mounted on space multi-footing substructures such as tripods and jackets are presently considered as a best option [7]. Tripods and jackets have been used at the Alpha Ventus wind farm (Germany) in approximately 30 m of water, and jackets at the Beatrice wind farm (UK) in nearly 45 m of water, for 5-MW turbines. For waters deeper than 60 m, however, current research is investigating wind turbines on floating devices as the most economically sustainable option [8-11]. Configurations under study are generally classified based on the primary physical principles adopted to achieve static stability: the spar-buoy (or ballast stabilised floater), whose stability is provided by a ballast lowering the centre of gravity below the centre of buoyancy; the tension leg platform (TLP) (or mooring stabilised floater), where stability is achieved through mooring lines kept under tension by excess buoyancy in the platform; the barge (or buoyancy stabilised floater), where stability is achieved through the waterplane area. The spar-buoy and barge are generally moored by catenary lines, but the spar-buoy may be moored also by taut lines. Hybrid concepts using features from the three classes, such as semisubmersible floaters, are also a possibility [9]. The technical feasibility of multi-megawatt floating wind turbines has been already demonstrated by three prototypes, Hywind in the North Sea (2.3-MW turbine on a spar-buoy), WindFloat in the Atlantic (2-MW turbine on a semisubmersible floater) and Fukushima-FORWARD Phase 1 in Japan (2-MW turbine on a semisubmersible floater) [3, 12-13]. This natural progression is illustrated in Figure 1.2.

Several other prototypes are under development and, at this stage, the current effort in industry and research is primarily focused on designing economic floating systems which can compete with bottom-fixed offshore turbines in terms of cost of energy. This has become a crucial goal in the perspective of moving wind turbines further offshore, with the purpose of minimising visual impact and harnessing the large resources available; it has been estimated, for instance, that only the wind resource potential at 5 to 50 nautical miles

off the U.S. coast could provide the total electrical generating capacity currently installed in the U.S. (more than 900 GW) [14]. Several other prototypes are under development and, at this stage, the current effort in industry and research is primarily focused on designing economic floating systems which can compete with bottom-fixed offshore turbines in terms of cost of energy.

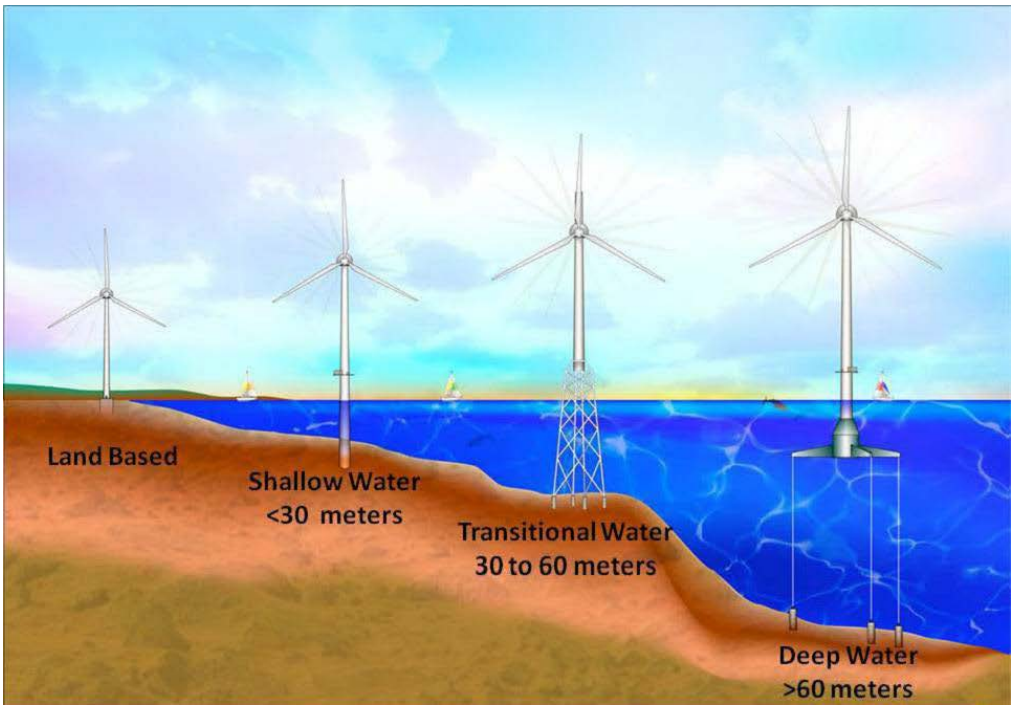

Figure 1.2: Natural progression of substructure design for different water depth.

In the last years, a number of international Standards and Guidelines have been released for design and assessment of offshore wind turbines [15-17]. In the meanwhile, numerical modelling has progressed toward more sophisticated descriptions of structural components, mechanical and electrical subsystems of modern offshore wind turbines, along with an appropriate treatment of the incident wind and wave fields. Existing numerical models rely on modal representation, multi-body, finite element (FE) concepts, sometimes combined in mixed approaches, and involve system motion equations to be solved by fully-coupled non-linear time domain integration, to account for inherent interactions between aerodynamic and hydrodynamic responses. In fact, while aerodynamic loads on the rotor are to be derived from aeroelastic models, considering the complex interaction between air flow and rotor blades, the influence of control systems and support structure dynamics, the latter affects the calculation of the hydrodynamic loads. Hence, although in some cases and

especially in the early stages of design, simplified analyses are implemented with responses to wind and wave loads computed separately and next superposed [18-19], only fully-integrated time-domain simulations are currently recommended as the basis of final, detailed wind turbine design calculations, due to the role played by system non-linearities inherent to rotor aerodynamics, hydrodynamics, and control systems [20-22].

For either existing solutions in shallow-transitional waters or future projects in deeper waters, the objective of an efficient and cost-effective design poses engineering challenges and numerical modelling complexities, which can be solved only by an integrated approach combining the expertise in diverse fields such as, among others, aerodynamics, hydrodynamics, structural and foundation engineering; also, vibration control and health monitoring play an important role, in view of ensuring a reliable and continuous power production for sustainable investments [23-24].

1.2. Aerodynamics

Aerodynamic is the base of any theoretical and experimental study on wind turbines. Since the early days of the wind industry, the Blade Element Momentum (BEM) theory has been awarded particular favour as a robust and computationally inexpensive tool to model the rotor aerodynamics and calculate aerodynamic loads. This method was developed from helicopter aerodynamics and due to its convenience and reliability has remained the most widely-used method for calculating the aerodynamic forces on wind turbines. BEM theory couples the momentum flow theory and the blade element theory.

The momentum flow theory was introduced by Betz in 1926; the turbine is represented by a uniform “actuator disk” which creates a discontinuity of pressure in the stream tube of air flowing through it. The assumption of this model are:

- ✓ homogeneous, incompressible, steady state fluid;
- ✓ no frictional drag;
- ✓ an infinite number of blades;
- ✓ uniform thrust over the disc or rotor area;
- ✓ a non-rotating wake;
- ✓ the static pressure far upstream and far downstream of the rotor is equal to the undisturbed ambient static pressure.

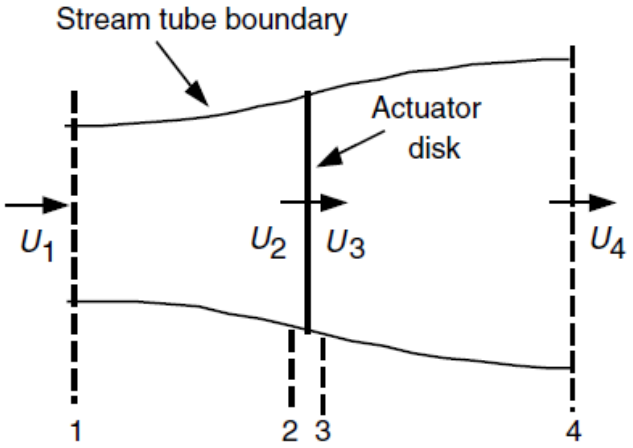

Figure 1.3: Actual disk model of wind turbine.

The analysis assumes a control volume, in which the control volume boundaries are the surface of a stream tube and two cross-sections of the stream tube (see Figure 1.3). Applying the conservation of linear momentum to the control volume enclosing the whole system, one can find the net force on the contents of the control volume. That force is equal and opposite to the thrust, T, which is the force of the wind on the wind turbine. From the conservation of linear momentum for a one-dimensional, incompressible, time-invariant flow, the thrust is equal and opposite to the rate of change of momentum of the air stream:

$$T = U_1\left(\rho AU\right)_1 - U_4\left(\rho AU\right)_4 \tag{1.1}$$

where ρ is the air density, A is the cross-sectional area, U is the air velocity, and the subscripts indicate values at numbered cross-sections in Figure 1.3.

For steady state flow, the thrust can be expressed as follow:

$$T = \dot{m}\left(U_1 - U_4\right) \tag{1.2}$$

where $\dot{m}$ is the mass flow rate.

The thrust is positive so the velocity behind the rotor, U_4, is less than the free stream velocity U_1. Since no work is done on either side of the rotor, the Bernoulli function can be used upstream and downstream of the disc:

$$p_1 + \frac{1}{2}\rho U_1^2 = p_2 + \frac{1}{2}\rho U_2^2 \tag{1.3}$$

$$p_3 + \frac{1}{2}\rho U_3^2 = p_4 + \frac{1}{2}\rho U_4^2 \tag{1.4}$$

The pressure far upstream and far downstream of the stream tube are equal (p_1=p_4) and the velocity across the disc remains the same (U_2=U_3).
The thrust can also be expressed as the net forces on each side of the actuator disc:

$$T = A_2\left(p_2 - p_3\right) \tag{1.5}$$

If one solves for (p_2 - p_3) using equations (1.3) and (1.4) and substitutes that in equations (1.5), one obtains:

$$T = \frac{1}{2}\rho A_2\left(U_1^2 - U_4^2\right) \tag{1.6}$$

Equating the thrust value from equations (1.2) and (1.6) and recognizing that the mass flow rate is also $\rho A_2 U_2$, one obtains:

$$U_2 = \frac{U_1 + U_4}{2} \tag{1.7}$$

Thus, the wind velocity at the rotor plane, using the simple model, is the average of the upstream and downstream wind speeds.

If one defines the axial induction factor a, as the fractional decrease in the wind velocity between the free stream and the rotor plane, then

$$a = \frac{U_1 - U_2}{U_1} \tag{1.8}$$

$$U_2 = U_1\left(1 - a\right) \tag{1.9}$$

and

$$U_4 = U_1(1-2a) \tag{1.10}$$

The quantity U_1a is often referred to as the induced velocity at the rotor, in which case the velocity of the wind at the rotor is a combination of the free stream velocity and the induced

wind velocity. As the axial induction factor increases from 0, the wind speed behind the rotor slows more and more. If a = 1/2, the wind has slowed to zero velocity behind the rotor and the simple theory is no longer applicable.

The power P, extracted by the wind, is equal to the thrust times the velocity at the disc:

$$P = \frac{1}{2}\rho A_2\left(U_1^2 - U_4^2\right)U_2 = \frac{1}{2}\rho A_2 U_2\left(U_1 + U_4\right)\left(U_1 - U_4\right) \tag{1.11}$$

Substituting for U_2 and U_4 from equations (1.9) and (1.10) gives:

$$P = \frac{1}{2}\rho A U^3 4a\left(1-a\right)^2 \tag{1.12}$$

where the control volume area at the rotor, A_2, is replaced by A, the rotor area, and the free stream velocity U_1 is replaced by U.

The performance of the wind rotor is usually characterized by its power coefficient, C_p:

$$C_P = \frac{P}{\frac{1}{2}\rho U^3 A} = 4a(1-a)^2 \tag{1.13}$$

that represents the fraction of the power in the wind that is extracted by the rotor.

The maximum C_P is determined by taking the derivate of the power coefficient (equation (1.13)) with respect to a and setting it equal to zero, yielding a = 1/3. Thus:

$$C_{P,\max} = 16/27 = 0.5926 \tag{1.14}$$

when a=1/3. For this case, the flow through the disc corresponds to a stream tube with an upstream cross-sectional area of 2/3 the disc area that expands to twice the disc area downstream. This result indicates that, if an ideal rotor were designed and operated such that the wind speed at the rotor were 2/3 of the free stream wind speed, then it would be operating at the point of maximum power production. Furthermore, given the basic laws of physics, this is the maximum power possible.

From equations (1.6), (1.9) and (1.10), the axial thrust on the disc is:

$$T = \frac{1}{2}\rho A U^2 \left[4a\left(1-a\right)\right] \tag{1.15}$$

Similarly to the power, the thrust on a wind turbine can be characterized by a non-dimensional thrust coefficient:

$$C_T = \frac{T}{1/2\,\rho U^2 A} = 4a(1-a) \tag{1.16}$$

C_T has a maximum of 1.0 when a = 0.5 and the downstream velocity is zero. At maximum power output (a =1/3), C_T has a value of 8/9. A graph of the power and thrust coefficients for an ideal Betz turbine and the non-dimensionalized downstream wind speed are illustrated in Figure 1.4.

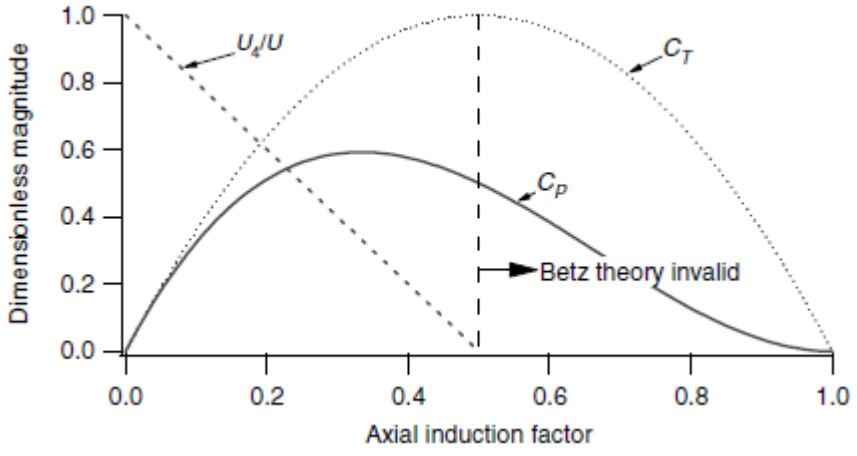

Figure 1.4: Power and thrust coefficient C_P and C_T as a function of axial induction factor for an ideal horizontal axis wind turbine.

The Betz limit, $C_{P,\max} = 16/27$, is the maximum theoretically possible rotor power coefficient. In practice, three effects lead to a decrease in the maximum achievable power coefficient:

- ✓ rotation of the wake behind the rotor;
- ✓ finite number of blades and associated tip losses;
- ✓ non-zero aerodynamic drag.

The first correction take into account the rotation that the rotor imparts to the flow; in the case of a rotating wind turbine rotor, the flow behind the rotor rotates in the opposite direction to the rotor, in reaction to the torque exerted by the flow on the rotor. An annular stream tube model of this flow, illustrating the rotation of the wake, is shown in Figure 1.5.

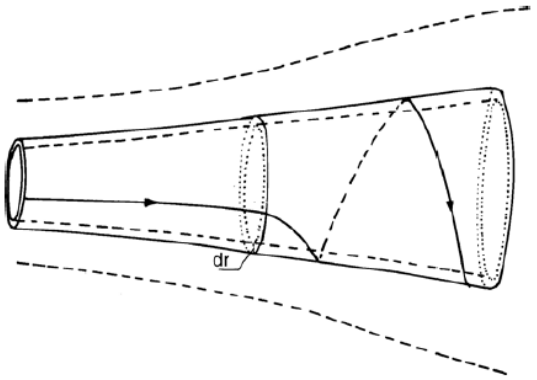

Figure 1.5: Stream tube model of flow behind rotating wind turbine blade.

The generation of rotational kinetic energy in the wake results in less energy extraction by the rotor than would be expected without wake rotation. In general, the extra kinetic energy in the wind turbine wake will be higher if the generated torque is higher. Thus, as will be shown here, slow-running wind turbines (with a low rotational speed and a high torque) experience more wake rotation losses than high-speed wind machines with low torque. Figure 1.6 gives a schematic of the parameters involved in this analysis. Subscripts denote values at the cross-sections identified by numbers. If it is assumed that the angular velocity imparted to the flowstream, ω, is small compared to the angular velocity, Ω, of the wind turbine rotor, then it can also be assumed that the pressure in the far wake is equal to the pressure in the free stream. The analysis that follows is based on the use of an annular stream tube with a radius r and a thickness dr, resulting in a cross-sectional area equal to $2\pi r dr$ (see Figure 1.6). The pressure, wake rotation, and induction factors are all assumed to be functions of radius.

If one uses a control volume that moves with the angular velocity of the blades, the energy equation can be applied in the sections before and after the blades to derive an expression for the pressure difference across the blades (see Glauert, 1935 for the derivation). Note that across the flow disc, the angular velocity of the air relative to the blade increases from Ω to $\Omega+\omega$, while the axial component of the velocity remains constant.

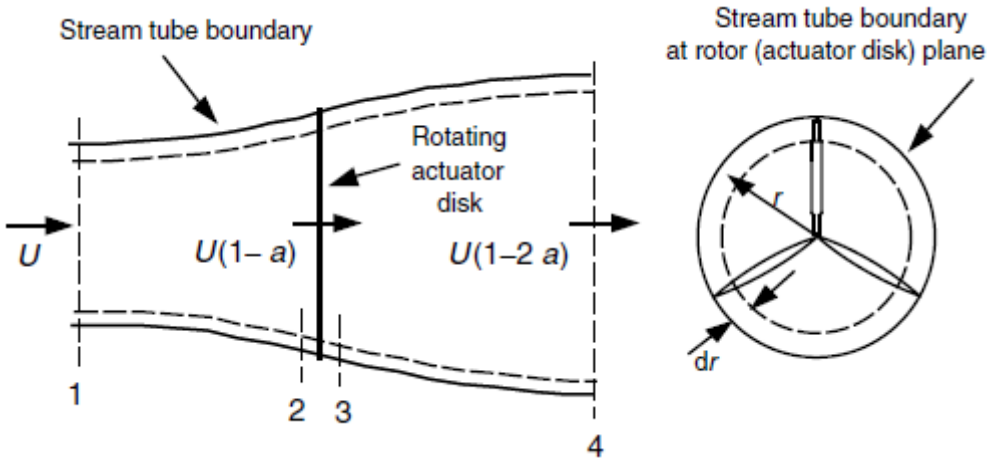

Figure 1.6: Stream tube model of flow behind rotating wind turbine blade.

The resulting thrust force on an annular element, dT, is:

$$dT = \left(p_2 - p_3\right) dA = \left[\rho\left(\Omega + \frac{1}{2}\omega\right)\omega r^2\right] 2\pi r dr \tag{1.17}$$

An angular induction factor, a', is defined as:

$$a' = \omega / 2\Omega \tag{1.18}$$

The expression for the thrust becomes:

$$dT = 4a'\left(1 + a'\right)\frac{1}{2}\rho\Omega^2 r^2 2\pi r dr \tag{1.19}$$

Following the previous linear moment analysis, the thrust force on an annular cross-section is:

$$dT = 4a(1-a)\frac{1}{2}\rho U^2 2\pi r dr \tag{1.20}$$

Equating the two equations for the thrust force, it is possible to define a local speed ratio λ_r:

$$\frac{a(1-a)}{a'(1+a')} = \frac{\Omega^2 r^2}{U^2} = \lambda_r \tag{1.21}$$

The local speed ratio is defined as the ratio of the speed at some intermediate radius to the wind speed.

Next, one can derive an expression for the torque on the rotor by applying the conservation of angular momentum. For this situation, the torque exerted on the rotor, *Q*, must equal the change in angular momentum of the wake. On an incremental annular area element gives:

$$dQ = d\dot{m}(\omega r)(r) = (\rho U_2 2\pi r dr)(\omega r)(r) = 4a'(1-a)\frac{1}{2}\rho U \Omega r^2 2\pi r dr \tag{1.22}$$

The blade element theory is used to calculate the aerodynamic forces on the blade as functions of lift and drag coefficients and angle of attack. As shown in Figure 1.7, the blade is assumed to be divided into N sections with the following assumptions:

- ✓ there is no aerodynamic interaction between the elements (no radial flow);
- ✓ the forces on the blades are determined solely by the lift and drag characteristics of the airfoil shapes of the blades.

The lift and drag forces are perpendicular and parallel to a relative wind velocity that is the vector sum of the wind velocity at the rotor, *U(1-a)*, and the velocity due to the rotation of the blade. This rotational component is the vector sum of the blade section velocity, *Ωr*, and the induced angular velocity at the blades from conservation of angular momentum, $\omega r/2$, or

$$\Omega r + (\omega/2)r = r\Omega(1+a') \tag{1.23}$$

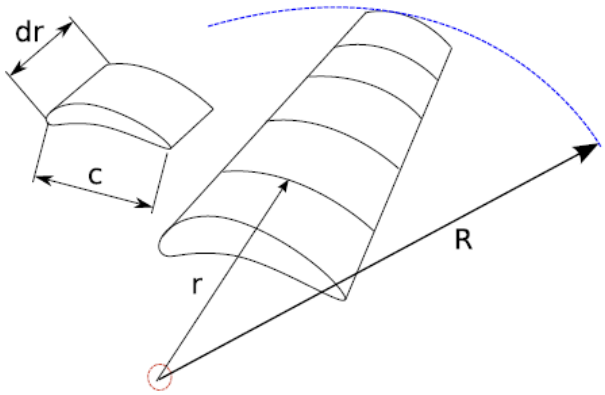

Figure 1.7: Blade element model.

The relationships of the various forces, angles, and velocities at the blade, looking down from the blade tip, are shown in Figure 1.8.

Here, θ_p is the section pitch angle, which is the angle between the chord line and the plane of rotation; $\theta_{p,0}$ is the blade pitch angle at the tip; θ_T is the blade twist angle; a is the angle of attack (the angle between the chord line and the relative wind); φ is the angle of relative wind; dF_L is the incremental lift force; dF_D is the incremental drag force; dF_N is the incremental force normal to the plane of rotation (this contributes to thrust); and dF_T is the incremental force tangential to the circle swept by the rotor. This is the force creating useful torque. Finally, U_{rel} is the relative wind velocity.

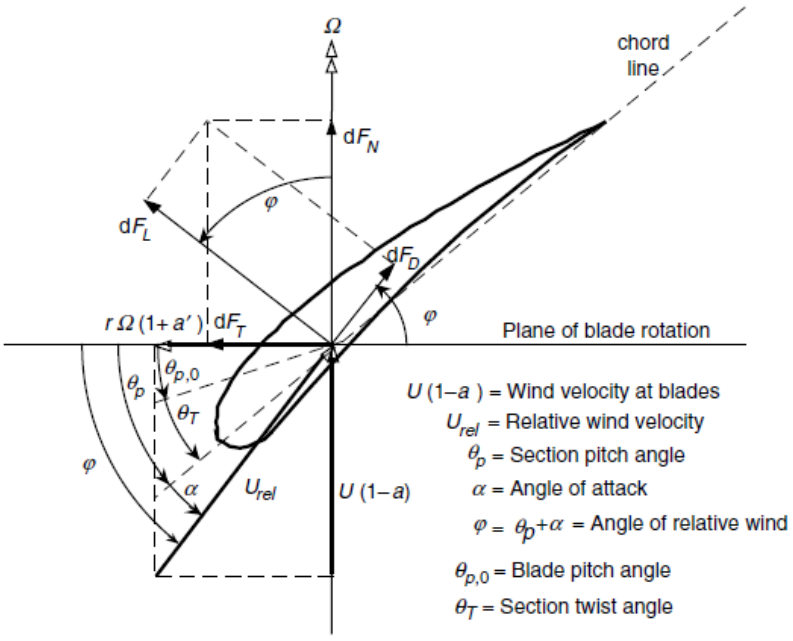

Figure 1.8: Blade geometry for analysis of horizontal axis wind turbine.

From Figure 1.8, it is possible to define the following relationships:

$$\tan\varphi = \frac{U\left(1-a\right)}{r\Omega\left(1+a'\right)} \tag{1.24}$$

$$U_{rel} = U\left(1-a\right)/\sin\varphi \tag{1.25}$$

$$dF_L = C_L \frac{1}{2}\rho U_{rel}^2 c dr \tag{1.26}$$

$$dF_D = C_D \frac{1}{2}\rho U_{rel}^2 c dr \tag{1.27}$$

$$dF_N = dF_L \cos\varphi + dF_D \sin\varphi \tag{1.28}$$

$$dF_T = dF_L \sin\varphi + dF_D \cos\varphi \tag{1.29}$$

Combing the Blade Element and Momentum theory, it is possible to define the axial and angular induction factors as:

$$a = 1/\left[1+4\sin^2\varphi/\left(\sigma' C_L\cos\varphi\right)\right] \tag{1.30}$$

$$a' = 1/\left[\left(4\cos\varphi/\left(\sigma' C_L\right)\right)-1\right] \tag{1.31}$$

where σ' is the local solidity, defined by:

$$\sigma' = Bc/2\pi r \tag{1.32}$$

Now the equations of BEM theory have been introduced and the method provides the aerodynamic loads by the following iterative procedure [25]:

- ✓ Initialize *a* and *a'*;

- ✓ Compute the angle of relative wind φ using equation (1.24)
- ✓ Compute the local angle of attack α with equation $\alpha = \varphi - \theta_p$;
- ✓ Read $C_L(a)$ and $C_D(a)$ from airfoil table;
- ✓ Calculate a and a' from equations (1.30) and (1.31);
- ✓ If a and a' change with respect to the initial value of the step more than a certain tolerance, restart with these values or else finish.
- ✓ Compute the local loads on the segment of the blades and integrate to compute the global aerodynamic loads.

The BEM theory relies, however, on some oversimplifying approximations, such as assuming a steady, axial and 2D air flow, and a disk-like modelling of the rotor [26-27]. Most of these limitations have been addressed by incorporating in the original BEM theory appropriate sub-models [27], for instance dynamic stall and dynamic inflow models to correct the steady-state assumption, models of yaw and tilt flows to correct the axial flow assumption, correction to 2D airfoil data to account for 3D effects (e.g. see [25] and references therein), and models of tip loss to compensate for rotor disk modelling [27]. With these important modifications, the BEM model is still the most used for rotor aerodynamics in commercial aeroelastic codes.

Considering, however, that reducing uncertainties and approximations in the calculation of aerodynamic loads is essential for an efficient design, a better understanding of rotor aerodynamics has been sought by alternative methods. Also, more sophisticated descriptions have become of particular interest in view of modelling the aerodynamics of floating wind turbines, where flow conditions may be more complex than in bottom-fixed wind turbines and can hardly be captured by BEM theory, due to significant low-frequency platform motion (significant pitching motion is encountered at the incident-wave frequency) or severe yaw conditions [28].

Among alternatives to BEM theory, computational fluid dynamics (CFD) methods are certainly the most accurate ones [29]. CFD methods typically solve the Navier-Stokes equations governing the turbulent air flow, assumed to be either compressible or incompressible depending on the ratio between local wind speed and sound speed [25], in conjunction with appropriate turbulence models [29]. Turbulence models are necessary to deal with the wide range of time and length scales involved in a full solution of the Navier-Stokes equation (while in the atmospheric boundary layer the turbulence scales may vary from the order of 1 km to the order of 1 mm, inside the blade boundary layers scales may

be even smaller [29]). Turbulence modelling is involved in the Large Eddy Simulation (LES) method, where effects of unresolved small scales are included based on the behaviour of larger scales, in the Reynolds-averaged Navier-Stokes (RANS) method and a combination of the two, commonly referred to as Detached Eddy Simulation (DES) method [25,29]. Also, the solution of the Navier-Stokes equations is generally coupled with appropriate models of the wind turbine, such as an "exact" direct modelling of the blades through a body-fitted grid, or the actuator disk (AD), the actuator line (AL) and the actuator surface (AS) models [29]. The first approach may be computationally expensive especially for modelling the boundary layer on the blades, including possible transition, separation and stall, and requires the generation of a high-quality moving mesh, commonly done with different overlapping grids communicating with each other [29]. Mainly to overcome these disadvantages, the AD, AL and AS models have been developed, where the aerodynamic loads are represented in the computational grid by body forces, computed using the wind velocity field obtained from the Navier-Stokes equations and based on tabulated airfoil data in the same way as in the BEM theory [25]. In the AD model the body forces are distributed on the entire rotor disc, whereas in the AL/AS models the loads are distributed around lines/planar surfaces along the actual blade positions. Alternative methods to CFD methods solving the Navier-Stokes equations are the so called free vortex wake methods, where the motion of fluid particles carrying vorticity is tracked in time and space [25,30]. The advantage over CFD methods is that only part of the space needs to be accounted for, namely the positions of the vorticity elements [26].

1.3. Hydrodynamics

The estimation of aerodynamic loads is influenced by the support structure adopted. For bottom-fixed support structures, Morison's equation is generally used, assuming that wave diffraction and radiation effects are negligible. This assumption is acceptable for slender bodies, i.e. with a small diameter with respect to wavelength of incident waves, and small motion of the support structure. The Morison's equation calculates the hydrodynamic loads per unit length:

$$f_{Morison}(x,z,t) = C_m \cdot \rho_w \frac{\pi D^2}{4} \dot{u}_w(x,z,t) + C_d \cdot \rho_w \frac{D}{2} \left| u_w(x,z,t) \right| u_w(x,z,t) \tag{1.33}$$

The first term of the equation 1.33 is the inertia contribution, which depends on the water density ρ, the inertia coefficient C_m , the cylinder diameter D and the water acceleration $\dot{u_w}$, while last term in equation 1.33 is the drag force, which depends on the structure diameter D, the drag coefficient C_d and the water velocity u_w. Figure 1.9 shows the representation of a slender vertical members under hydrodynamic loads.

The wave particle kinematics can be obtained by linear wave theory according to Airy. The following equations describe the wave particle velocity and acceleration, with the z-axis pointing upwards from the free water surface ($-d \leq z \leq 0$) and position x horizontally in the wave direction:

$$u(x,z,t) = \hat{\zeta}\, 2\pi f \frac{\cosh k_{wave}(z+d)}{\sinh k_{wave} d} \cos(k_{wave} x - 2\pi ft)$$

$$\dot{u}(x,z,t) = \hat{\zeta}\, (2\pi f)^2 \frac{\cosh k_{wave}(z+d)}{\sinh k_{wave} d} \sin(k_{wave} x - 2\pi ft) \tag{1.34}$$

where $\hat{\zeta}$ is the wave amplitude, k_{wave} is the wave number, f is the wave frequency, d is the water depth and t is the time.

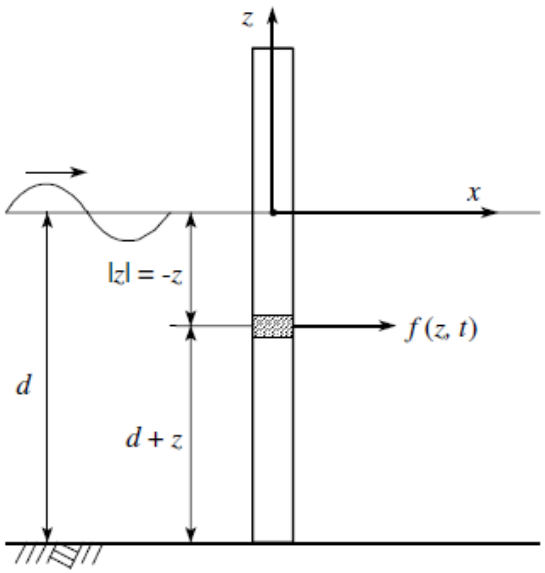

Figure 1.9: Slender vertical members with hydrodynamic loads.

The resulting horizontal force F on the cylinder can be found by integration of Morison's equation for values of z from $-d$ to 0.

For floating supports alternative methods are adopted to compute hydrodynamic loads, as for instance methods based on first-order hydrodynamics theory [28], where radiation and diffraction effects are modelled by introducing, in the motion equations of the floating support, frequency-dependent hydrodynamic added-mass and damping terms (radiation), and wave excitation terms depending on frequencies and direction of the incident waves (diffraction), computed in the frequency domain using potential flow theory for regular or irregular sea states [31]. Second-order hydrodynamic theory has been applied in some cases, as second-order loads may excite slow-drift motion in soft-moored platforms, typically those with catenary moorings, or ringing effects in TLPs [32]. Hydrodynamic loads on floating supports can be computed also by CFD methods solving the Navier-Stokes equations [33-34].

1.4. Structural model

The most accurate simulation of offshore wind turbines (OWT) with complex sub structures is achieved if the complete set of equations of motion of the entire offshore model is solved in one numerical solver. The traditional use of standard, commercial finite element analysis software packages for solving problems of structural dynamics is challenging in the case of wind turbines. This is because of the presence of rigid body motion of one structural component, i.e. the rotor, with respect to another, i.e. the tower or another support structure type. In principle, the standard finite element method only considers structures in which the deflection occurs about an initial reference position, and for this reason the finite element models that have been developed for wind turbine in the past have been tailored to deal with this problem. The multi-body method and the finite element method are the approaches more reliable for the dynamic analysis of wind turbines.

The multi-body method can be formulated using different ways. A motion can be represented by superimposing a rigid body motion and a relative flexible motion in multibody systems. If additionally the relative flexible motion is given in a body fixed frame (non-inertial frame), this is the classical flexible multibody formulation. In the classical formulation, there exist the rigid body variables for each flexible body as unknown variables. The classical formulation can be characterized by the superimposed motion with

the rigid body variables and a relative displacement vector given in a non-inertial body fixed frame. The classical formulation comes from rigid multi-body mechanics by adding flexibility to the bodies. GH Bladed software code [35] uses a multi-body approach combined with a modal representation of the flexible components like the blades and the tower. This approach has the major advantage of giving an accurate and reliable representation of the dynamics of a wind turbine with relatively few degrees of freedom, making it a fast and efficient means of computation. In the last version of multibody code, the structure can now be modelled with any number of separate bodies, each with individual modal properties, which are coupled together using the equations of motion.

Each mode is defined in terms of the following parameters:

- ✓ modal frequency;
- ✓ modal damping coefficient;
- ✓ mode shape represented by a vector of displacements.

The mode shapes and frequencies of the blade and tower (the main flexible components in a standard wind turbine model) are calculated based on the position of the neutral axis, mass distribution along the body and bending stiffness along the body, as well as other parameters specific to the body in question. The modal damping for each mode is a user input to the model.

The use of multibody dynamics enables a completely self-consistent, rigorous formulation of the structural dynamics of a wind turbine. The blade modes are modelled individually with fully coupled flapwise, edgewise and torsional degrees of freedom, and are valid for any pitch angle. Advanced definition options are available for the blade geometry and structure, and additional degrees of freedom in the drive train and

gearbox can be easily modelled.

The Finite Element Method (FEM) is a numerical technique to solve the equations of motion by minimizing an integral error on the domain. The idea of this method is to minimize a functional which it has the spatial model and time as a domain. When this method is applied to a solid structure the Energy becomes the functional that the FEM minimizes. That means the method searches for the displacements on the nodes of the body mesh which equals the work done by the internal displacements on the body and the work done by the applied forces, the displacements must fulfilled the boundary conditions contrails. The FEM is used for detailed analysis and for each body is required a mesh. Create the mesh of a body is not straight forward process although exist automatic meshers.

The automatic meshers usually are designed to create tetrahedral mesh on the bodies and they do not have the capability to create quad meshes. A quad mesh gives higher accuracy on the FEM analysis, the disadvantage is

the user has to do the mesh manually and this process is time consuming. A parametric mesh is created when the user has to simulate different modifications of a mechanism or optimize a mechanism which is an iterative process. A parametric mesh decreases the time to create the mesh because the model is meshing automatically. The first stages of a mechanism design do not require a detailed analysis but many simulations of different mechanism configuration, that is the reason why this method is commonly used only on the final and detailed analysis of the mechanism.

Many methods are developed based on the FEM with the objective to find an efficient way to use the FEM method in early stages of the design. The intuitive approach is to use only the degrees of freedom of some nodes instead of all the degrees of freedom on the mesh. That concept is the same as model the mechanical part with a coarse mesh, the problem is the method has large errors for coarse meshes.

This error decreases when the right nodes on the mesh are selected to represent the mechanism. The selection of the nodes are based on which dynamic behavior the model represents for the specific prescribed boundaries conditions. Three important methods were developed to reduce the size of the model. The modal reduction techniques, the static condensation and the dynamic substructuring.

The modal reduction technique changes the problem to a frequency domain and decoupled the system of ordinary differential equations. The result is a system of equation in which every equation is orthogonal to the others. The system is solved by adding the contribution of the solution for each equation separately. The idea of this reduction technique is to use only the equations which are important to describe the system and neglect the small contributions to the solution of the other equations.

The equations are usually selected based on two criteria, the high value for the projection of the spectral content of the excitation on the eigenmode of the decoupled

equation or the excitation frequency is closer to the eigenfrequency of the decoupled equation (Natural frequency of the model). The idea is to solve only the important decoupled equations for the dynamic of the system doing the solution procedure faster.

The static condensation reduces the model by using an approximate displacement for some nodes. The different variants of this method differs only in how the method approximate the

displacement in some nodes. The most common approach of this method is the Guyan's static condensation. The Guyan's static condensation method uses the static solution of the problem and computes the displacement for the nodes. When is known the static displacement for the nodes the user selects on which nodes he want to impose this displacement and then the system is solved for the left degree of freedom. This algorithm is convenient because the error on the solution is only because the system do not consider the dynamical part of the solution of some nodes, from the static point of view the system is solved exactly.

The dynamic substructuring is a method to split structures into smaller ones. The idea is to express the behavior of the body based only on a few degrees of freedom. The most common method is the Craig Bampton which uses the static solution for the boundary nodes plus the internal vibration modes for the structure as a basis for the displacements. This method is exact for static response of the interface nodes.

2. Seismic analysis of wind turbines: general aspects

This chapter will provide a preliminary introduction to the relevant issues involved in the seismic assessment of horizontal axis wind turbines (HAWTs). Hence, detailed prescriptions of existing International Standards (ISs) and Certification Guidelines (CGs) will be reported.

2.1. Introduction

With the continuous increase of wind power production, the search for optimal design is facing new and challenging tasks. The design of HAWTs has been traditionally driven by high wind speed conditions. However, following the introduction of new technologies such as variable pitch and active control in larger, lighter and cost-effective HAWTs, in some cases the design-driving considerations have been changed, with fatigue and turbulence being considered in addition to high wind speed conditions. For these lighter HAWTs, especially when installed in seismically active areas, a question has soon arisen as to whether seismic loads shall be considered among design loads. On the other hand, the need to investigate the potential importance of seismic loads has been corroborated by the damage occurred to land-based HAWTs, following the 1986 North Palm Springs Earthquake, USA, and the 2011 Kashima City Earthquake, Japan. Post-earthquake surveys in the wind farms nearest the epicenter of North Palm Springs Earthquake documented that 48 out of 65 HAWTs were damaged, generally due to buckling in the walls of the supporting tower (photographs are available in the report by Swan and Hadjian [36]). Earthquake-induced failure may occur also at the foundation level, as for the case of the footing of a HAWT in the Kashima wind farm (photographs are available in the paper by Umar and Ishihara [37]). In this context, the seismic assessment of HAWTs has drawn an

increasing attention in the last years and, as a result, seismic loading has been progressively included in ISs and CGs [15-17, 38-41].

The key points in the seismic assessment of HAWTs can be briefly summarized as:

- ✓ Definition of the structural model
- ✓ Use of a specific analysis method
- ✓ Selection of the load combinations

However, because a certain flexibility is allowed, especially in the definition of the structural model and the selection of an appropriate analysis method, it is important that engineers be aware of the potential options available, and how they may affect the reliability of the results.

2.2. Seismic assessment of HAWTs

This section explains the key points for the seismic assessment of HAWTs.

The first considerations aim to explain the structural models. A fundamental assumption of existing ISs and CGs, with regard to the structural model, is material linearity. This assumption is essentially justified by the fact that the primary intent is to ensure power production for the design life of the HAWT, usually 20 years, and that nonlinear deformation (damage) to the turbine would interrupt reliable operation. Material linearity means low operational stresses, and this provide some safety margins against failure [42]. Therefore material linearity will be, in general, a pre-requisite of ISs and CGs also when assessing the response to seismic excitations.

Starting from the assumption of material linearity, in general two types of structural modeling are feasible (see Figure 2.1):

- ✓ simplified models, which model the tower and consider the rotor-nacelle assembly (RNA) as a lumped mass at the tower top;
- ✓ full system models, which describe the whole turbine, including the nacelle and rotor with a certain level of detail.

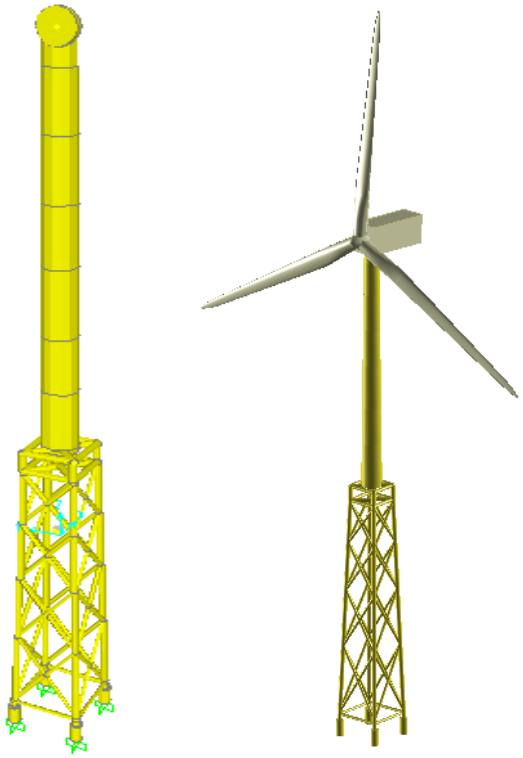

Figure 2.1: Simplified and full-system models of fixed offshore wind turbines.

Simplified models are appealing since the complexities involved in modeling the rotor are avoided. Full system models include the rotor blades and, in general, turbine components such as power transmission inside the nacelle, pitch and speed control devices, with a different degree of accuracy depending on the specific modeling adopted, for instance a finite-element (FE) or a rigid multi-body modeling.

Simplified or full system models can be used depending on the selected structural analysis method. In particular:

- ✓ fully-coupled time-domain simulations involve only full system models, as they require modeling the rotor aerodynamics, with the earthquake ground motion simultaneously acting at the tower base.
- ✓ decoupled analysis may be implemented using either a full system model, or a simplified model. If a simplified model is adopted, seismic loads are built considering the mass of RNA lumped at the tower top, while the other environmental loads are obtained by a dedicated software package, with no earthquake ground motion at the tower base, since the analysis is decoupled.

A fully-coupled time-domain simulation is the most desirable approach. The reason is that allows the actual wind loads on the blades to be evaluated correctly, taking into account that the oscillations of the tower top, induced by the earthquake ground motion, affect the rotor aerodynamics (in particular, the relative wind speed at the blades, depending on which lift and drag forces are calculated). However, for the implementation of fully-coupled time-domain simulations dedicated software packages are required, capable of solving the nonlinear motion equations of the structural system under simultaneous wind+wave loads and seismic excitations.

When performing a decoupled analysis, instead, the responses to wind, wave and seismic loading are built separately.

Decoupled analyses may be performed in time and frequency domain. Especially frequency-domain formulations have been awarded a considerable attention, because in this case the separate response to earthquake loading can be built by coded response spectra, a concept most engineers are familiar with.

The selection of appropriate load combinations for seismic assessment is a relevant issue addressed by ISs and CGs. In general, they are recommended based on the observations that follow.

At sites with a significant seismic hazard, there is a reasonable likelihood that an earthquake occurs while the HAWT is in an operational state, i.e. while the rotor is spinning; in this case, the HAWT is subjected to simultaneous earthquake loads and operational loads. It shall be considered, also, the possibility that the earthquake triggers a shutdown and that, as a result, the HAWT is subjected to simultaneous earthquake loads and emergency stop loads. Another possible scenario is that the earthquake strikes when the turbine is parked, i.e. not operating due to wind speeds exceeding the cut-off wind speed of the turbine; specifically, blades may be locked against motion (fixed pitch turbines) or feathered such that no sufficient torque is generated for the rotor to spin (active pitch turbines). In recognition of these observations, the load combinations generally suggested by ISs and CGs for the seismic assessment of HAWTs are:

- ✓ Earthquake loads and operational loads
- ✓ Earthquake loads and emergency stop loads
- ✓ Earthquake loads with environmental loads in a parked state

Both earthquake loads and wind loads are stochastic processes. The wind process is generally treated as a stationary process. Samples can be generated from well-established

power spectral densities (PSDs) in the literature (e.g., Von Karman PSD or Kaimal PSD, see [43]), with parameters to be set depending on site conditions. Wind acts on the blades of the rotor and along the tower. Obviously, wind loading on the blades varies significantly depending on whether the rotor is spinning or not; to generate wind loading on a spinning rotor concepts of classical aerodynamics are used, for instance those of Blade Element Momentum (BEM) theory and subsequent modifications [43]. The earthquake process is inherently non-stationary. Spectrum-compatible samples may be synthetized from site-dependent response spectra, or site-specific historical records may be used, according to the prescriptions of the adopted ISs and CGs.

2.3. International standards and Certification guidelines

Guidance for seismic loading on HAWTs can be found in the following ISs and CGs:

- ✓ IEC 61400-3. Wind turbine generator systems. Part 3: Design requirements for offshore wind turbines [15] (IEC 2007). Released by International Electrotechnical Commission (IEC);
- ✓ GL 2012: Guidelines for the certification of offshore wind turbines [16] (GL 2012). Released by Germanischer Lloyd (GL);
- ✓ DNV – OS – J101: Design of Offshore Wind Turbine Structures [17] (DNV 2013). Released by Det Norske Veritas (DNV).

2.3.1. IEC 61400-3 Standards

IEC 61400-3 Standards aim to specify essential design requirements to ensure structural integrity of wind turbines (IEC 2007). They have the status of national standards in all European countries whose national electrotechnical committees are CENELEC members (CENELEC = European Committee for Electrotechnical Standardization).

IEC 61400-3 no gives any requirements for seismic analysis of the offshore wind turbines; for consideration of earthquake conditions and effects see IEC 61400-1 [40]. In particular, recommends that in seismically active areas the integrity of the HAWT is demonstrated for the specific site conditions (Section 11.6), while no seismic assessment is required for sites already excluded by the local building code, due to weak seismic actions. The seismic loading shall be combined with other significant, frequently occurring

operational loads. In particular, IEC 61400-1 prescribes that the seismic loading shall be superposed with operational loads, to be selected as the higher of:

a) loads during normal power production, by averaging over the lifetime;

b) loads during emergency shutdown, for a wind speed selected so that the loads prior to the shutdown are equal to those obtained with a).

No explicit reference is made, however, to the load case of an earthquake loading striking in a parked state.

The safety factor for all load components to be combined with seismic loading shall be set equal to 1,0. The ground acceleration shall be evaluated for a 475-year recurrence period, based on ground acceleration and response spectrum requirements as defined in local building codes. If a local building code is not available or does not provide ground acceleration and response spectrum, an appropriate evaluation of these parameters shall be carried out.

Regarding the method of analysis, fully-coupled or decoupled analysis are possible (11.6). In time-domain analyses, sufficient simulations shall be undertaken to ensure that the operational load is statistically representative. It is prescribed that the number of tower vibration modes used in either of the above methods shall be selected in accordance with a recognized building code. In the absence of a locally applicable building code, consecutive modes with a total modal mass of 85 % of the total mass shall be used.

IEC 61400-1 gives no particular indications on the structural model for seismic analysis. In agreement with GL 2010, however, it is implicit that the structure shall be modeled as a MDOF system, since the use of consecutive modes with a total modal mass equal to at least 85% of the total mass is recommended. In general, the response should be linearly elastic, while a ductile response with energy dissipation is allowed only for specific structures, in particular for lattice structures with bolted joints.

Annex C of IEC 61400-1 presents a simplified, conservative method for the calculation of seismic loads. This procedure is meant to be used when the most significant seismic loads can reasonably be predicted on the tower, and shall not be used if it is likely that the earthquake ground motion may cause significant loading on the rotor blades or the structural components of the foundation. The principal simplifications in Annex C are ignoring the vibration modes higher than the first tower bending mode, and the assumption that the whole structure is subjected to the same acceleration. Upon evaluating or estimating the site and soil conditions required by the local building code, or adopting

conservative assumptions whereas detailed site data are not available, the simplified method can be applied as follows:

- ✓ The acceleration at the first tower bending natural frequency is set using a normalized design response spectrum and a seismic hazard-zoning factor. For this, a 1% damping ratio is assumed.
- ✓ Earthquake-induced shear and bending moments at the tower base are calculated by applying, at the tower top, a force equal to the total mass of the RNA + ½ the mass of the tower, times the design acceleration response.
- ✓ The corresponding base shear and bending moments are added to the characteristic loads calculated for an emergency stop at rated wind speed, i.e. the speed at which the limit of the generator output is reached.
- ✓ The results are compared with those obtained against the design loads or the design resistance for the HAWT. If the tower can sustain the resulting combined loading, no further investigation is needed. Otherwise, a thorough investigation shall be carried out on a MDOF structural model.

With regard to such a simplified method, described in Annex C, it shall be pointed out that ignoring the second mode is a significant non-conservative simplification (e.g., see [44] on the role of the second mode in the seismic response of HAWTs). This is somehow compensated for by incorporating ½ of the tower mass with the tower head mass, and prescribing superposition with the characteristic loads calculated for an emergency stop at rated wind speed, which represent quite conservative aerodynamic loads.

2.3.2. GL 2012 Guidelines

GL 2012 Guidelines aim to set a number of requirements for the certification of wind turbines (GL 2012). For this reason, they are quite prescriptive and provide detailed information on some particular aspects of seismic risk.

GL 2012 prescribes that seismic loading shall be taken into account in seismically-active areas (Section 4.2.4.7). Earthquake loading is included in a group of design load cases (Table 4.4.2) classified as load cases accounting for “extended” design situations, including special applications and site conditions. These design load cases are not mandatory for certification purposes, but may be chosen for the verification of the HAWT to complement the applicability in specific design situations. The response to seismic loading is to be

assessed both in the operational state and the parked state (Table 4.3.2), under normal wind loading. For the operational state it is also suggested to consider the activation of the emergency shutdown triggered by the earthquake. The safety factor for all the loads to be combined with seismic loading is equal to 1.0. (Section 4.4.9.2.3). A return period of 475 years is prescribed as the design level earthquake. To model the seismic loading, recommendations of the local building code should be applied or, in the absence of locally applicable regulations, those of either Eurocode 8 [45] or American Petroleum Institute [46].

Regarding the method of analysis, GL 2012 specifies that fully-coupled or decoupled analyses are possible, with at least 3 modes in both cases. Time domain simulations shall be carried out considering at least 6 simulations per load case. No guidance is provided on the damping ratio to be adopted when using the design response spectrum in a decoupled analysis. Again, because of the lack of guidance on this matter, it shall be kept in mind that the 5% damping ratio is appropriate only in the operational state, and that lower damping ratios shall be considered in the parked state.

GL 2012 gives no particular prescriptions on the structural model to be adopted. However, because at least 3 modes have to be included in the vibration response, the use of a multi-degree-of-freedom (MDOF) structural model is implicitly suggested. In general, a linear elastic behavior shall be assumed. A ductile response can be considered only whereas the support structure has a sufficient static redundancy, such as for instance a lattice tower. However, if ductile behavior is assumed, the structure shall be mandatorily inspected after occurrence of an earthquake.

2.3.3. DNV-OS-J101 Standards

DNV-OS-J101 Standards are meant to provide a basic introduction to the most relevant subjects in wind turbine engineering. Consistently with this general purpose, quite general suggestions are given to deal with seismic loading.

It is prescribed that earthquake effects should be considered for HAWTs located in areas that are considered seismically active based on previous records of earthquake activity (Section 4. E 700). For those areas known to be seismically active but with no sufficient information available for a detailed characterization of seismicity, an evaluation of the regional and local geology is recommended, to determine the location of the HAWT

relative to the alignment of faults, the epicentral and focal distances, the source mechanism for energy release, and the source-to-site attenuation characteristics. In this case, the evaluation should aim to estimate both the design earthquake and the maximum expectable earthquake, taking into account also the potential influence of local soil conditions on the ground motion.

No specific recommendations are given on the earthquake-wind and wave load combinations to be considered. However, since it is prescribed that in seismically active areas the HAWT should be designed so as to withstand earthquake loads, it is implicit that the three, typical load combinations described earlier (i.e. earthquake loads and operational environmental loads; earthquake loads and emergency stop loads; earthquake loads occurring in a parked state) shall be referred to.

As for what concerns the method of analysis, DNV-OS-J101 provides explicit suggestions only for the response spectrum method, as used in a decoupled analysis. In particular, the use of a single-degree-of-freedom (SDOF) system with a lumped mass on top of a vertical rod is suggested, with the rod length equal to the tower height, and the lumped mass including the mass of the rotor-nacelle assembly (RNA) and ¼ of the mass of the tower. It is prescribed that the fundamental period of the SDOF system is used in conjunction with a design acceleration response spectrum to determine the loads set up by the ground motion, by analogy with the simplified procedures used in building codes. Analyses shall be performed for horizontal and vertical earthquake-induced accelerations. However, no explicit recommendations are given on the criterion to translate the resulting spectral response acceleration into design seismic loads, as well as on the damping ratio to be used. Since, in the absence of specific guidance on this matter, a most intuitive choice of engineers could be using the typical procedures of the International Building Code (ICC 2012), it has to be remarked that the 5% damping ratio, embedded in the standard design response spectrum, is appropriate only for seismic loading acting during an operational state, but overestimates considerably the actual damping in a parked state. This aspect should be well kept in mind, when referring to DNV-OS-J101 for seismic assessment of HAWTs.

Regarding the structural model, attention is drawn to the need of including the actual stiffness of the structural component of the foundation and an appropriate model of the supporting or surrounding soil, the latter through a proper soil-structure interaction (SSI) modeling (Section 10 A 500). Although, for this purpose, nonlinear and frequency-

dependent models are recommended in principle, appropriate linearized models are allowed, depending on the expected strain level in the soil (typically, it may be up to 10-1 for earthquake loading and considerably larger than for other loading conditions). The linearized models consist of translational and rotational springs for circular footings and piles.

3. Seismic analysis of offshore wind turbines: coupled analysis

This chapter presents the study of seismic behavior of a horizontal axis wind turbine on two bottom-fixed support structures for transitional water depths (30-60 m). Fully-coupled, non-linear time-domain simulations on full system models are carried out under combined wind-wave-earthquake loadings, for different load cases, considering fixed and flexible foundation models. After a brief introduction about the earthquake response of offshore wind turbines and the description of the structural model, this chapter illustrates the results of time-domain simulations with the full earthquake set and the comparison with some IEC 61400-3 load cases [15].

3.1. Introduction

While an increasing number of offshore wind farms are being planned worldwide to satisfy a growing energy demand, the design of offshore horizontal axis wind turbines (HAWTs) is facing novel and challenging tasks. In this context, seismic assessment has become crucial for bottom-fixed offshore HAWTs in seismically active areas, especially since evidence exists that earthquakes can damage the support structure of land-based HAWTs, as in the case of the 1986 North Palm Springs Earthquake [36].

Seismic assessment of offshore HAWTs is prescribed by recent international guidelines and standards [15-17, 40]. In general, fully-coupled non-linear time-domain simulations [15-17, 40] or response spectra methods [15-17, 40] are suggested, on either simplified [15-17, 40] or full system models [16]. Fully-coupled non-linear time-domain simulations compute the response to earthquake and environmental loads acting simultaneously, considering interactions of aerodynamic, hydrodynamic and seismic responses [15-17, 40], while response spectra methods involve a linear superposition of

separately computed responses to earthquake and environmental loads [15-17, 40]. Simplified system models include the support structure only, with the rotor-nacelle assembly (RNA) modelled as a lumped mass at the tower top [17, 40]. Full system models involve the support structure and the whole turbine, i.e. nacelle, rotor blades and, in general, turbine components such as power transmission inside the nacelle, pitch and speed control devices, with a different degree of accuracy depending on the specific modelling adopted [16]. Fundamental load cases reflect the possible scenarios for an earthquake strike, and are generally chosen as: (1) earthquake loads with operational loads, i.e. earthquake striking while the rotor is spinning; (2) earthquake loads with emergency stop loads, i.e. earthquake triggering a shutdown; (3) earthquake loads with non-operational loads, i.e. earthquake striking when the turbine is parked (not operating), due to wind speeds exceeding the cut-off wind speed of the turbine.

Since seismic assessment of offshore HAWTs has been included in international guidelines and standards, there is a great interest in assessing to which extent stress demands are increased by earthquake loads, and whether numerical results may be significantly affected by the method of analysis and system modelling adopted.

Extensive research studies on these issues are not available yet. However, it is important to remark that earlier studies on land-based HAWTs have already addressed these issues, showing that accurate predictions of the seismic response can be obtained only by performing fully-coupled non-linear time-domain simulations, on full system models including support structure and the whole turbine [44, 47-51]. The main reasons substantiating these conclusions can be summarized as follows:

- ✓ a full system model allows loads acting on all system components to be estimated, including those on the rotor blades, whose integrity is crucial to ensure a reliable power production over the design life of the HAWT.
- ✓ higher rotor modes can be considered only in a full system model, and these modes may be important in the seismic response, as they may fall in the region of maxima spectral accelerations [48-50];
- ✓ non-linear time-domain simulations can capture how tower top oscillations due to the earthquake ground motion affect rotor aerodynamics, in particular the relative wind speed at the blades, depending on which the aerodynamic loading, i.e. lift and drag forces on the blades, are calculated. Also, important sources of non-

linearity have been found in soil response, especially when HAWTs are installed on relatively soft soils or loose soils containing alluvial deposits [52].

Within this theoretical framework, Zhao et al. [44, 47], Prowell et al. [48-51] have investigated the seismic response of land-based HAWTs of different rated power, by fully-coupled non-linear time-domain simulations on full system models of the HAWT, based on a hybrid multi-body system approach [44, 47] or a combined modal and multi-body dynamics formulation, as implemented in FAST software package [48-51]. Zhao et al. have found that force and bending moment at the tower base of a 1.5MW HAWT are affected considerably by an earthquake striking in the operational state, especially in the lateral direction where there are no wind loads, even for a weak earthquake intensity [44]. Prowell et al. have shown that, for the reference National Renewable Energy Laboratory (NREL) 5MW HAWT [53], the bending moment demand at the tower base is significantly above the demand from extreme wind events. This result has been obtained for parked, operational and emergency stop simulations under a large set of ground motions [9-10], showing that earthquake loads may be design driving for large turbines in regions of high seismic hazard.

It is apparent that the conclusions above, as drawn from the seismic analysis of land-based HAWTs, have general validity and shall be kept in mind also for seismic assessment of offshore HAWTs. On the other hand it is important to remark that, in this case, non-linearities arise also from the hydrodynamic loading and that, in general, interactions of aerodynamic, hydrodynamic and seismic responses shall be considered in fully-coupled, non-linear time-domain simulations.

Hacifiendoglu [54] has investigated the seismic response of a 3MW HAWT on a monopile, under a stochastic earthquake excitation occurring in the parked state. A simplified model of the HAWT has been used, with the RNA modelled as a lumped top mass and a full 3D model of sea water and soil, and motion equations of the coupled system water-structure-soil have been derived upon enforcing continuity of displacements in the normal direction to the interfaces. Sensitivity of displacement and stress responses to sea water level, soil conditions and presence of a surrounding ice sheet has been investigated. Kim et al. [55] have studied the seismic response of the NREL 5MW HAWT on a monopile, under real and artificial earthquake ground motions occurring in the parked state. A simplified model of the HAWT has been implemented, with the RNA modelled as a lumped top mass; non-linear springs have been introduced along the pile length to model

soil stiffness, considering also the variation of the earthquake ground motion through different soil layers. Important conclusions of this study are that fragility curves of the HAWT, built for a variety of peak ground accelerations (PGAs), can be predicted reasonably well by static pushover analyses and, also, that variation of earthquake ground motion through different soil layers plays an important role in the estimation of the fragility curves.

The purpose of this study is to investigate the seismic behaviour of bottom-fixed offshore HAWTs in transitional water depths (30-60 m). This subject appears of particular interest considering that wind farms are being planned far from near-shore shallow waters (< 30 m) to minimize visual impact, and there are transitional water depth sites with high wind speed resources and medium-to-high seismic hazard. Typical examples in the U.S. can be found in the Hawaiian islands [56-57]. In particular, the study is carried out on the NREL 5MW HAWT, as mounted on two typical steel support structures for transitional water depths, a tripod and a jacket resting on pile foundations. Wind and wave environmental states, water depth and soil profile are set in agreement with similar theoretical studies on offshore HAWTs [58-59]. Consistently with the approach followed for land-based HAWTs [49-51], the seismic response is investigated for a set of real earthquake records taken from existing databases [60-61], with different frequency content and intensity. Fully-coupled non-linear time-domain simulations are carried out on full system models including non-linear soil stiffness, using BLADED software package [35], certified by Germanischer Llyod for design of wind turbines. Simulations are run for earthquake striking in operational and parked states, and earthquake triggering an emergency stop, comparing stress resultant demands to those when no earthquake loads are considered, for fixed and flexible foundation models (FMs). For a further insight into the importance of seismic assessment, a comparison with demands from some typical design load cases prescribed by IEC 61400-3 is also provided [15].

3.2. Support structures

The turbine is the NREL 5MW three-bladed turbine, whose details can be found in ref. [53]. Two different steel support structures are considered, as shown in Figure 3.1: one with a centre column tripod, and the other with a jacket quattropod, both resting on pile foundations. The two support structures are designed according to current practice; in

particular, the one with the jacket quattropod is identical to that studied in ref. [62]. Details on the structural members are given in Figure 3.2. It is assumed that the water depth is 50 m, and the reference three-layer sandy soil of the OC3 project [58-59] is considered. In the following, the two support structures will be referred to as “Tripod” and “Jacket”, for simplicity.

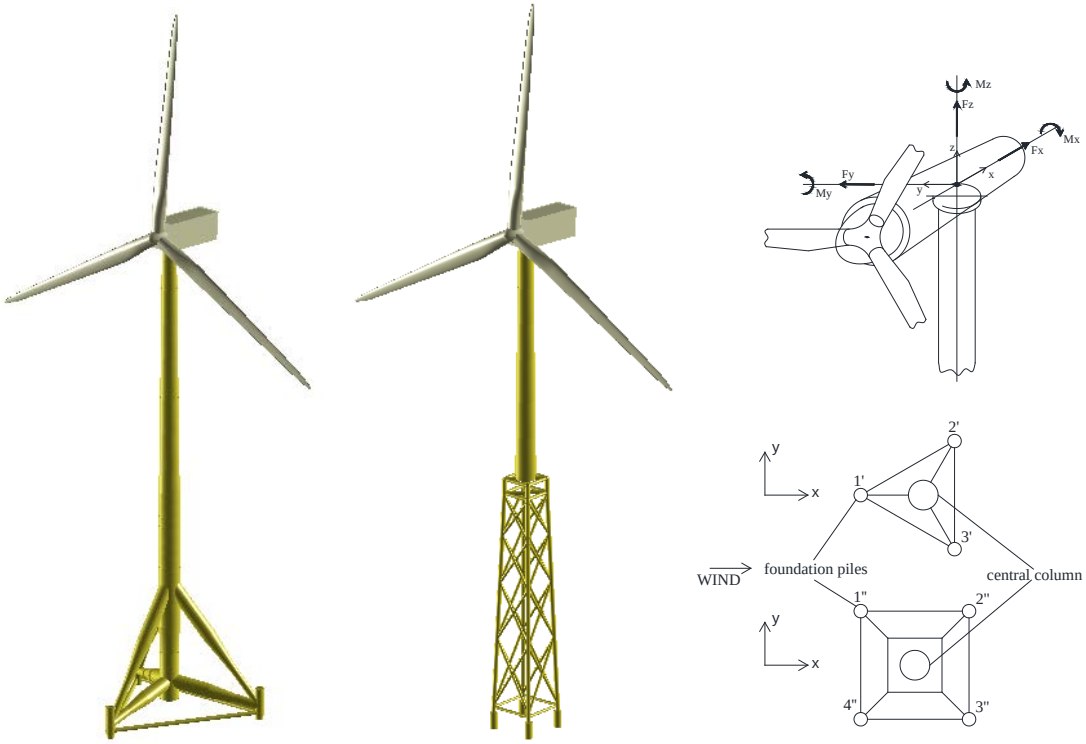

Figure 3.1: Tripod and jacket support structures, pile foundations and positive stress resultants.

The full system is implemented in BLADED [35], modelling nacelle, blades, drive train, control system, as given in ref. [53]. Beam elements with shear deformation are used for support structure structural members, piles and blades. Steel parameters are: Young’s modulus = 210 GPa, Poisson coefficient = 0.3, Mass density = 7850 kg m^{-3}. Two different FMs are considered: the first is fixed (clamped base), the second is flexible with lateral and vertical springs along the piles at a 1 m spacing, and a vertical spring at the piles tip, modelling soil stiffness [58-59, 63-64] (with respect to the reference system in Figure 3.1, lateral springs are in *x* and *y* directions, vertical springs in *z* direction). All springs are supposed to be uncoupled, with non-linear force-displacement laws set based on the *p-y*, *t-z* and *Q-z* curves in the API code [46], using the parameters of the OC3 project three-layer

sandy soil [58-59] and following the prescriptions for layered soils given in ref. [59] (detailed examples can be found also at the NREL website: https://wind.nrel.gov/forum/wind/viewtopic.php?f=3&t=880&start=0).

For completeness, *p-y*, *t-z* curves at various depths along the piles, and the *Q-z* curve at the piles tip, are reported in the Appendix A.

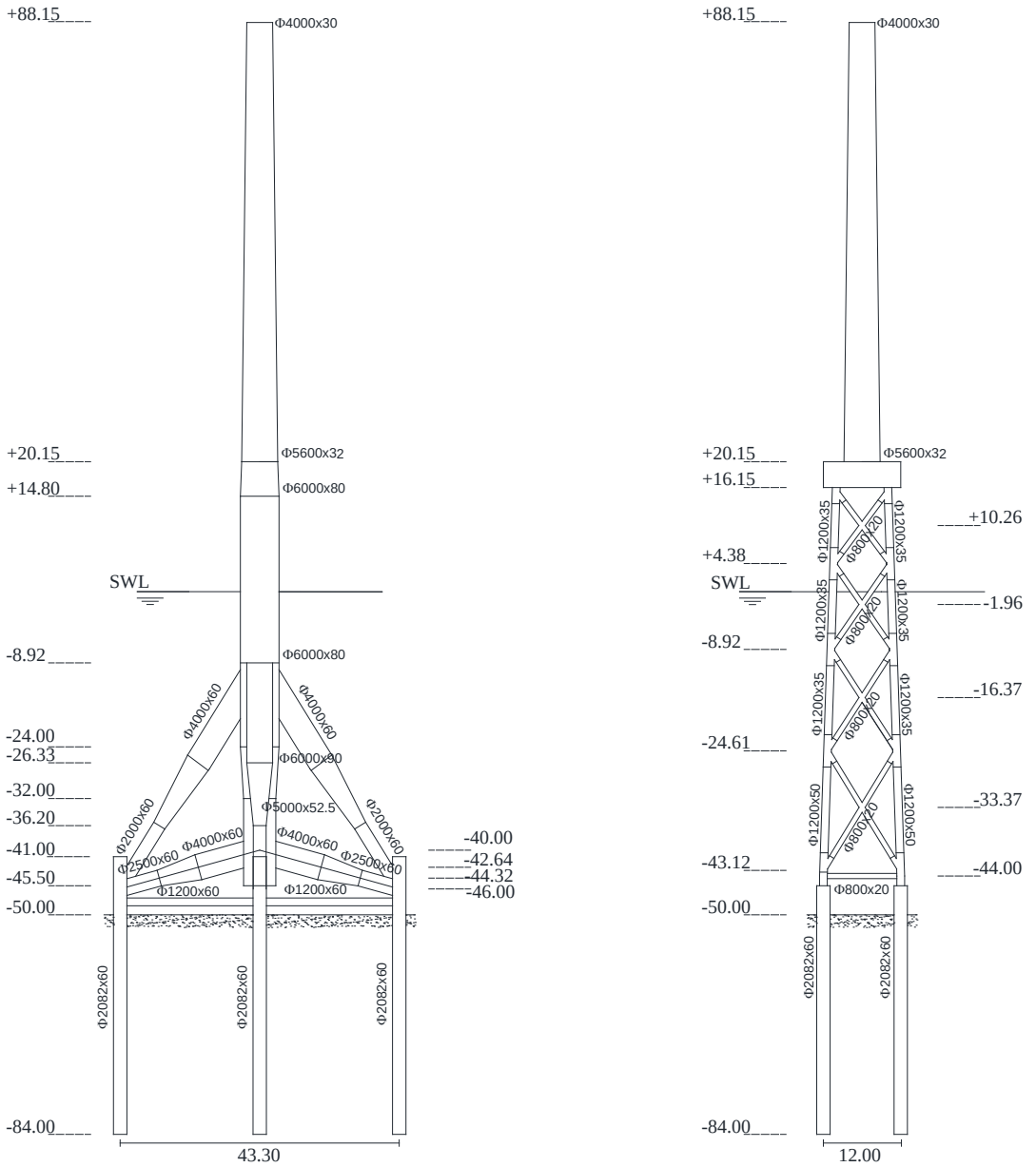

Figure 3.2: Geometry of Tripod and Jacket (dimensions of structural members in mm; heights and depths in m).

Table 3.1 shows the frequencies of support structure modes and blades modes, in a parked state (no rotational speed) at 0° azimuth angle (one blade upward and two blade downward), for fixed and flexible FMs, the latter with force-displacement laws of the soil springs linearized to the initial tangent stiffness.

For the fixed FM, the frequencies of the first fore-aft (FA) and side-to-side (SS) support structure modes, as well as the frequencies of the blades modes, are almost the same for Tripod and Jacket, while a substantial difference exists in the second FA and SS support structure modes (FA and SS directions correspond to *x* and *y* directions in Figure 3.1; "yaw" and "pitch" means that the blades modes are coupled with yaw and pitch motion of the rotor [47, 58]).

Table 3.1: Tripod and Jacket natural frequencies for fixed and flexible FMs.

	Tripod Frequencies (Hz)		Jacket Frequencies (Hz)	
Mode description	Fixed FM	Flexible FM	Fixed FM	Flexible FM
1st Tower Side-to-Side	0.309	0.306	0.314	0.300
1st Tower Fore-Aft	0.311	0.309	0.317	0.302
1st Blade Asymetric Flapwise Yaw	0.645	0.645	0.640	0.634
1st Blade Asymetric Flapwise Pitch	0.677	0.676	0.675	0.671
1st Blade Collective Flap	0.710	0.709	0.708	0.705
1st Blade Asymetric Edgewise Pitch	1.081	1.081	1.080	1.082
1st Blade Asymetric Edgewise Yaw	1.097	1.097	1.092	1.105
2nd Blade Asymetric Flapwise Yaw	1.749	1.735	1.714	1.721
2nd Blade Asymetric Flapwise Pitch	1.848	1.863	1.937	1.924
2nd Blade Collective Flap	1.996	1.996	2.003	2.009
2nd Tower Fore-Aft	2.206	1.277	1.219	0.984
2nd Tower Side-to-Side	2.277	1.279	1.241	0.990

As for the flexible FM, it can be observed that the frequencies of the first FA and SS support structure modes, and the frequencies of the blades modes, are practically identical to the corresponding ones for fixed FM, while the frequencies of the second FA and SS support structure modes are decreased. All these results are in agreement with findings of similar studies [63, 65]. For design purposes, it is important to remark that the frequencies of the first FA and SS support structure modes are almost the same for Tripod and Jacket, even when foundation flexibility is accounted for.

Stiffness and mass parameters are reported in Table 3.2, for fixed and flexible FMs, with non-linear laws of soil springs linearized to the initial tangent stiffness.

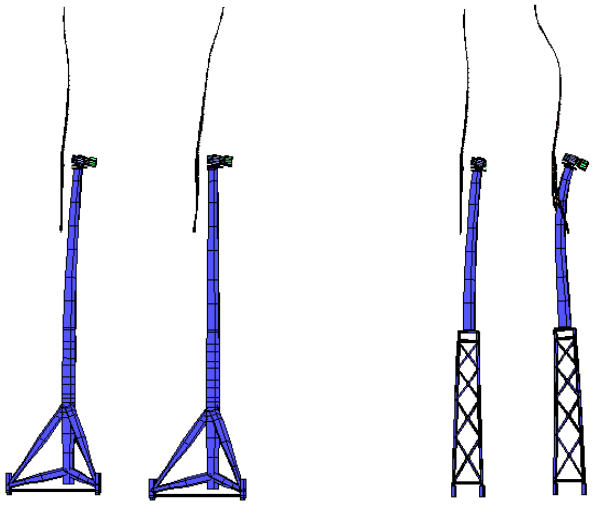

Figure 3.3: First and second FA support structure modes of Tripod and Jacket.

Table 3.2**:** Tripod and Jacket stiffness and mass parameters for fixed and flexible FMs**.**

	Tripod		Jacket	
Stiffness	Fixed FM	Flexible FM	Fixed FM	Flexible FM
K_{Fx} (Nm^{-1})	$1.74 \cdot 10^6$	$1.69 \cdot 10^6$	$1.65 \cdot 10^6$	$1.58 \cdot 10^6$
K_{Fy} (Nm^{-1})	$1.74 \cdot 10^6$	$1.69 \cdot 10^6$	$1.65 \cdot 10^6$	$1.58 \cdot 10^6$
K_{Mx} (Nm)	$3.07 \cdot 10^9$	$3.07 \cdot 10^9$	$2.86 \cdot 10^9$	$2.86 \cdot 10^9$
K_{My} (Nm)	$3.07 \cdot 10^9$	$3.07 \cdot 10^9$	$2.86 \cdot 10^9$	$2.86 \cdot 10^9$
Total Mass (ton)	2844	3175	1800	2238
RNA Mass (ton)	350	350	350	350
Tower Mass (ton)	646	646	290	290

3.3. Load cases

The earthquake set for seismic assessment includes 49 real records listed in Table 3.3, taken from ref. [60-61]. Each record has two horizontal components. Figure 4a shows the 5% damped acceleration response spectrum, computed as the maximum square root of the sum of the squares (SRSS) of the acceleration responses under the two horizontal components [50]. It can be seen that many frequencies of Tripod and Jacket, reported in Table 1, fall within the range of significant spectral accelerations (for reference, Figure 3.4

(a) includes only the periods of the first and second FA support structure modes, for fixed FM: T1 = 1/0.311 = 3.215, T2 = 1/2.206 = 0.453 for the Tripod; T1 = 1/0.317 = 3.155, T2 = 1/1.219 = 0.820 for the Jacket).

Table 3.3: Earthquake set from ref. [60-61].

ID No.	Year	Earthquake	Station	PGA	ID No.	Year	Earthquake	Station	PGA
1	1992	Cape Mendocino	P.	6.12	26	1989	Loma Prieta	APEEL 2	2.44
2	1999	Chi Chi Taiwan	TCU065	6.80	27	1989	Loma Prieta	F. C. – A. 1	2.75
3	1999	Chi Chi Taiwan	TCU102	2.17	28	1989	Loma Prieta	F. C. – M. C.	1.03
4	1999	Duzce-Turkey	D.	4.23	29	1989	Loma Prieta	G. A. #02	3.44
5	1992	Erzincan-Turkey	E.	4.43	30	1989	Loma Prieta	G. A. #03	4.84
6	1979	Imperial Valley-06	A. M.	3.06	31	1989	Loma Prieta	G. H. B.	2.66
7	1979	Imperial Valley-06	A.	2.76	32	1989	Loma Prieta	G. G. C.	3.42
8	1979	Imperial Valley-06	A. A.	1.79	33	1989	Loma Prieta	Larkspur	1.21
9	1979	Imperial Valley-06	EC C. C.	1.96	34	1989	Loma Prieta	S. –A.	3.62
10	1979	Imperial Valley-06	EC M. O.	3.11	35	1989	Loma Prieta	S.-W V.	3.15
11	1979	Imperial Valley-06	El C. A. #3	2.44	36	1989	Loma Prieta	T. I.	1.36
12	1979	Imperial Valley-06	El C. A. #4	4.04	37	1984	Morgan Hill	G. A. #06	2.75
13	1979	Imperial Valley-06	El C. A. #5	4.36	38	1986	North Palm Spring	N. P. S.	6.30
14	1979	Imperial Valley-06	El C. A. #6	4.12	39	1994	Northridge	J. F. P.	7.29
15	1979	Imperial Valley-06	El C. A. #7	3.86	40	1994	Northridge	N. F. S.	6.73
16	1979	Imperial Valley-06	El C. A. #8	5.16	41	1994	Northridge	N. W P. C.	3.38
17	1979	Imperial Valley-06	El C. A. #10	1.96	42	1994	Northridge	P. D. d.	3.43
18	1979	Imperial Valley-06	El C. A. #11	3.67	43	1994	Northridge	R.	5.95
19	1979	Imperial Valley-06	El C. D. A.	4.22	44	1994	Northridge	S. C. S.	6.74
20	1979	Imperial Valley-06	H. P. O.	2.40	45	1994	Northridge	S. C. E.	6.32
21	1979	Imperial Valley-07	El C. A. #3	1.40	46	1994	Northridge	S. S. O. V.	6.48
22	1980	Irpinia	S.	2.61	47	1987	Superstition Hills	P. T. S.	3.72
23	1995	Kobe-Japan	KJMA	6.71	48	1987	Superstition Hills	El C. I.	2.57
24	1999	Kocaeli	Ambarli	2.10	49	1987	Whittier Narrows	C. – W. S.	1.11
25	1989	Landers	L.	7.41					

Following the approach by Prowell et al. [49-50], who have extensively studied the seismic response of a land-based NREL 5MW HAWT, seismic effects are investigated in different scenarios, considering three load cases:

LC1 = Earthquake loads and operational wind-wave loads, for a wind speed at hub height V_{hub} = 11.4 ms^{-1}, a wave period T_p = 9.5 s and a significant wave height H_s = 5.0 m.

LC2 = Earthquake loads and emergency stop loads, for a wind speed at hub height V_{hub} = 11.4 ms^{-1}, a wave period T_p = 9.5 s and a significant wave height H_s = 5.0 m. It is assumed that the emergency stop is activated as the nacelle acceleration exceeds 1 ms^{-2}. This value is well higher than the nacelle accelerations due to the considered environmental state, and is in agreement with the emergency stop nacelle acceleration used for land-based HAWTs [49-50].

LC3 = Earthquake loads and wind-wave loads in a parked state, for a wind speed at hub height V_{hub} = 40 ms^{-1}, a wave period T_p = 11.5 s and a significant wave height H_s = 7.0 m.

Wind and wave parameters have been chosen based on the following criteria. In load cases LC1 and LC2, V_{hub} = 11.4 ms^{-1} is the rated wind speed of the 5MW turbine, i.e. the minimum wind speed at which the turbine generates its designated maximum power [40]; since turbines are generally designed to provide maximum power for wind speeds with high probability of occurrence at the site, V_{hub} = 11.4 ms^{-1} can reasonably be assumed as a most likely operational wind speed. In load case LC3, V_{hub} = 40 ms^{-1} is a very high wind speed, at which the turbine will certainly be parked, i.e. not operating. Consistently with similar studies [58], wave periods T_p and significant heights H_s have been chosen as those associated with the selected wind speeds V_{hub} in typical offshore environmental states, as for instance some encountered in the Pacific Ocean [66].

It is assumed that wind and waves act both in x direction (Figure 3.1). Samples are generated in BLADED based on pertinent power spectra [35]. The Kaimal spectrum is used for the wind process [40, 67]:

$$S_k(f) = \frac{4\sigma_k^2 L_k / V_{hub}}{\left(1 + 6 f L_k / V_{hub}\right)^{5/3}} \tag{3.1}$$

where f is the frequency (Hz), k is the index referring to the velocity component (1 = x direction, 2 = y direction and 3 = z direction), σ_k is the standard deviation and L_k is the integral scale parameter of each velocity component. Assuming medium turbulence characteristics [65], all parameters in Eq.(3.1) are set according to IEC 61400-1 prescriptions for a normal turbulence model [40]. The JONSWAP spectrum is used for the wave process [68]:

$$S_{JS}(f) = \alpha_2 H_s^2 T_p \left(\frac{f}{f_p}\right)^{-5} \exp\left[-1.25\left(\frac{f}{f_p}\right)^{-4}\right] \cdot \gamma^{\beta} \tag{3.2}$$

where $f_p = 1/T_p$, γ is the JONSWAP peakedness parameter [15]

$$\gamma = \begin{cases} 5 & T_p/\sqrt{H_s} \le 3.6 \\ \exp\left(5.75 - 1.15 T_p/\sqrt{H_s}\right) & 3.6 \le T_p/\sqrt{H_s} \le 5.0 \\ 1 & T_p/\sqrt{H_s} \le 5.0 \end{cases} \tag{3.3}$$

and

$$\alpha_2 = \frac{0.0624}{0.230 + 0.0336\gamma - \frac{0.185}{1.9+\gamma}} \quad \beta = \exp\left[-\frac{0.5}{\sigma^2}\left(\frac{f}{f_p} - 1\right)^2\right] \quad \sigma = \begin{cases} 0.07 & f \le f_p \\ 0.09 & f > f_p \end{cases} \tag{3.4}$$

The Kaimal and JONSWAP spectra for the considered environmental states are reported in Figure 3.4 (b), along with the rotor frequency band (1P) and blade passing frequency band (3P) of the 5MW HAWT [69]. It can be observed that the frequencies of the first FA support structure modes of both Tripod and Jacket fall within the interval 1P-3P, corresponding to a typical soft-stiff design.

Fully-coupled non-linear time-domain simulations are carried out in BLADED by numerical integration of motion equations built dynamic wake model for the axial inflow, in conjunction with classical BEM model for the tangential inflow [43], considering interactions of aerodynamic, hydrodynamic and seismic responses, and including non-linear soil stiffness as modelled in paragraph 3.2. The dynamic wake model takes into account that changes in the blade loads change the vorticity trailed into the rotor wake, and that the effect of these changes takes indeed a finite time to change the induced flow field, depending on which lift and drag forces acting on the blades are calculated [35]. The hydrodynamic loading on the structural members is computed based on Morison's equation [70], with drag and inertia coefficients set according to DNV recommendations [17]. Wind

loads acting along the tower are included. For both Tripod and Jacket, modal damping ratios are set equal to 10^{-2} for support structure modes, and 4.775×10^{-3} for the blades modes [53]. The simulation length is 800 sec, with the earthquake ground motion starting 400 seconds into the simulation, to ensure that the earthquake occurs as the structural response has already attained a steady state [49-50].

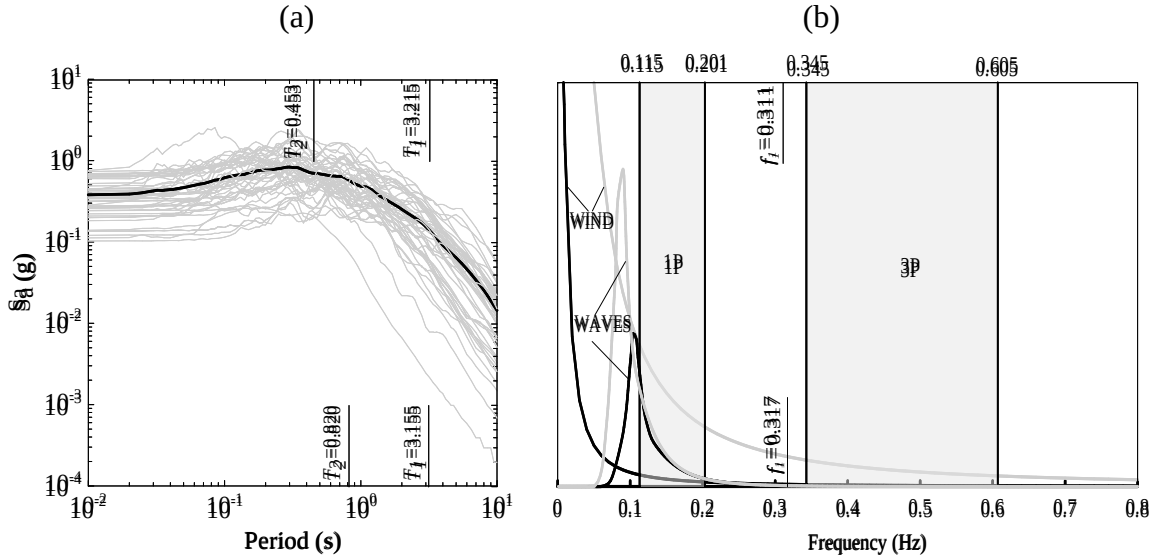

Figure 3.4: (a) 5% damped SRSS acceleration response spectrum for the earthquake set (black line: mean value); (b) wind and wave power spectral densities (black line: load cases LC1/LC2; grey line: load case LC3).

3.4. Response to a single earthquake record

To gain a preliminary insight into the response of Tripod and Jacket under combined wind, wave and earthquake loading, the response to a single earthquake is discussed. Specifically, the Northridge earthquake is considered (ID No. 44 in Table 3.3), a 40 second duration near fault ground motion [61]. Results are obtained assuming that the fault normal and fault parallel components act in x and y directions, respectively (see Figure 3.1).

The response is computed for load cases LC1, LC2 and LC3 in paragraph 3.3. For each load case, one sample of the wind process and one sample of the wave process are generated based on the spectra given in Eq.(3.1) and Eq.(3.2). For load case LC3, 0° and 180° azimuth angles are considered for the parked rotor (180° = two blades upward and one blade downward). Tower top deflection and maxima accelerations along the support structures are given in Figure 3.5-Figure 3.6 for fixed and flexible FMs.

3.4.1. Response for fixed foundation model

Figure 3.5Figure 3.5a-b and Figure 3.6a-b show the tower top deflection in *x* and *y* directions, for fixed FM. For both Tripod and Jacket, it is observed that:

- ✓ If the earthquake occurs in the operational state, the tower top deflection increases significantly starting from the earthquake strike (time history above *t*=400 sec), reducing progressively to the operational deflection once the earthquake has expired (time history above *t*=440 sec).
- ✓ As a result of an emergency stop triggered at a 1 ms^{-2} nacelle acceleration, the tower top deflection deviates from the operational deflection and, after a transient, attains a parked state, where the deflection is due only to wave loads, and wind loads acting on the parked rotor and along the tower.
- ✓ If the earthquake occurs in a parked state, the tower top deflection increases starting from the earthquake strike reducing progressively to the parked deflection. Differences between the 0° and 180° parked states are not noticeable. It can be argued that, although the geometry of the two rotor positions is different, the difference in terms of mass distributions along the height is relatively small, with a consequent relatively small effect on the seismic response. Notice that, once the earthquake has expired, the final parked deflections in load cases LC2 and LC3 are different, due to the fact that load case LC2 and load case LC3 involve different wind speeds V_{hub}, wave periods T_p and significant wave heights H_s.

Figure 3.5c-Figure 3.6c show the maxima accelerations along the support structures, in *x* and *y* directions. The acceleration profile in *x* direction shows that combined wind-wave-earthquake loadings activate first and second FA support structure modes, in both Tripod and Jacket, in all three load cases under investigation. The same observation can be made based on the acceleration profile in *y* direction. The activation of the second FA and SS support structure modes is confirmed by the fact that the acceleration profiles exhibit significant values at approximately 2/3 of the support structure height, and this result is consistent with analogous results for land-based HAWTs under earthquake loading [51].

TRIPOD

FIXED FM FLEXIBLE FM

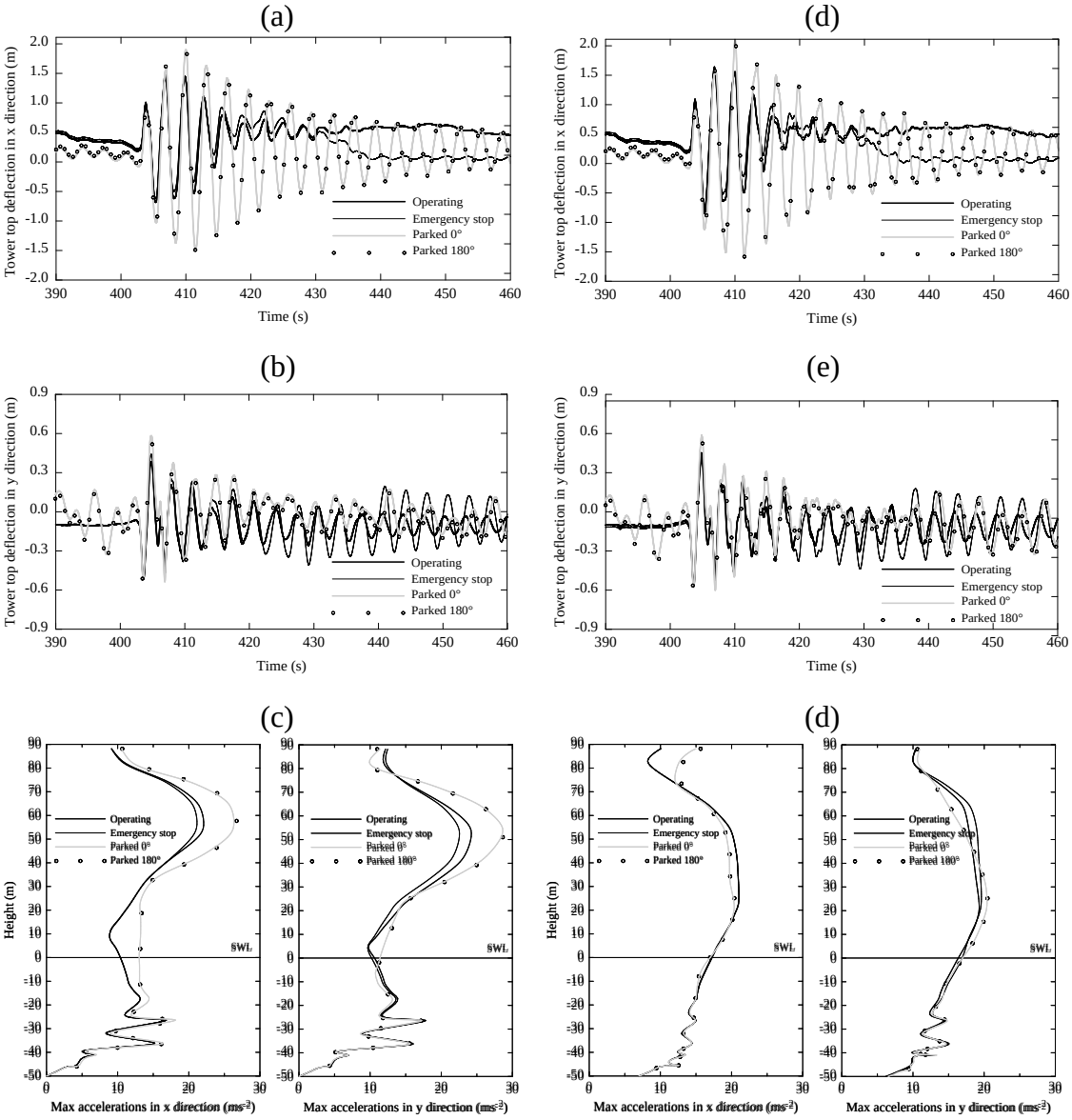

Figure 3.5: Tripod: tower top deflection and maxima acceleration profiles in *x* and *y* direction for fixed and flexible FMs.

JACKET

FIXED FM FLEXIBLE FM

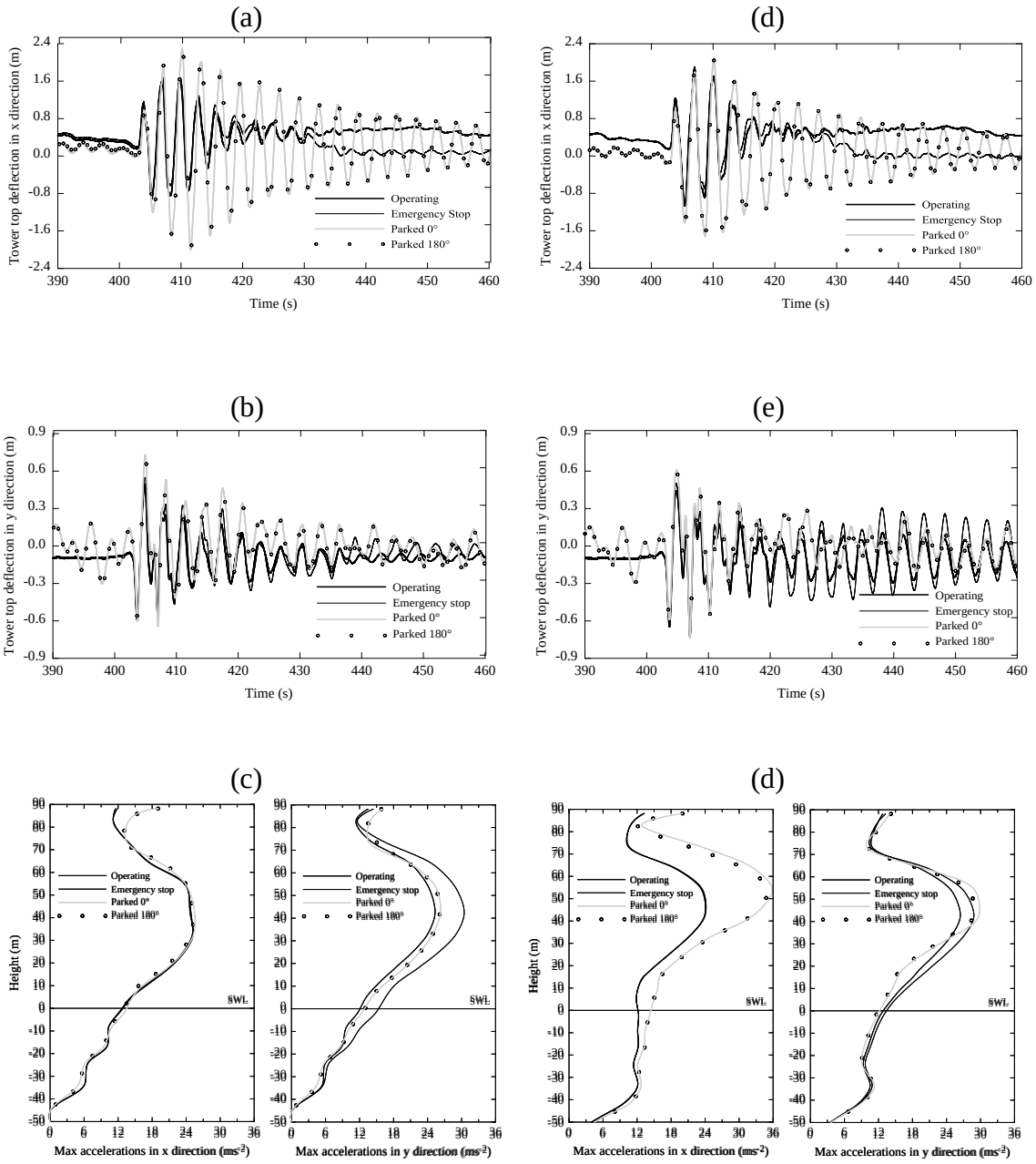

Figure 3.6: Jacket: tower top deflection and maxima acceleration profiles in *x* and *y* direction for fixed and flexible FMs.

3.4.2. Response for flexible foundation model

Figure 3.5d-e-f and Figure 3.6d-e-f show the tower top deflection and maxima accelerations along the support structures, in *x* and *y* directions, for flexible FM. Results appear in agreement with the corresponding ones for fixed FM. That is, the tower top deflection is significantly affected by the earthquake strike, with a considerable increase with respect to the operational deflection in load case LC1, a deviation from the operational deflection and subsequent transient in load case LC2, an increase with respect to the parked deflection in load case LC3, with no noticeable differences between 0° and 180° parked states. The acceleration profiles show contributions from first and second support structure modes. Also, it is seen that deflections and accelerations of the tower top are slightly larger, in most cases, than those for fixed FM.

3.5. Response to an earthquake set

Next, the seismic response of Tripod and Jacket is investigated using the full earthquake set in Table 3, for load cases LC1-LC2-LC3 introduced in paragraph 3.3. In particular, considering that the results of load case LC3 do not seem affected by the rotor position, a 0° parked state is assumed. For a given load case, two simulations are carried out for each earthquake, in agreement with the studies by Prowell et al. [49-50] on land-based HAWTs. The two simulations differ as the two horizontal components of the earthquake are rotated 90 degrees, in order to reduce bias from the orientation of the earthquake components relative to the wind direction [49-50]. Therefore, each load case involves 98=49×2 simulations.

For each simulation, some results of particular interest are considered as measures of the earthquake demand: maximum resultant bending moment at the tower base (= maximum SRSS of the bending moments in *x* and *y* directions); maximum axial force at the pile head, for pile #1' of the Tripod and pile #3" of the Jacket (see Figure 3.1); maximum resultant bending moment at the blade root (= maximum SRSS of the bending moments in orthogonal planes of the blade local coordinate system); maximum resultant acceleration at the tower top (= maximum SRSS of the accelerations in *x* and *y* directions). It is noticed that pile #1' of the Tripod and pile #3" of the Jacket are selected since, according to the simulation results, they undergo slightly higher demands with respect to the other piles. However, variability of results is very limited and, from an engineering point of view,

demands in all piles can be considered within the same range, in all load cases LC1-LC2-LC3. For completeness, results for all piles are reported in the Appendix B.

Results are reported in Figure 3.7-Figure 3.8 assuming the peak ground acceleration (PGA) as earthquake intensity measure, for fixed and flexible FMs. In total, 588=2×3×98 simulations have been run for each structure.

3.5.1. Stress resultant and tower top acceleration demands for fixed foundation model

In Figure 3.7-Figure 3.8, stress resultant and tower top acceleration demands for fixed FM are denoted by symbol "×". Black vertical lines indicate the corresponding demands due to wind and wave loads only, i.e. without earthquake loads, for the environmental states considered in load cases LC1-LC2-LC3 (see paragraph 3.3).

Firstly, some relevant comments are in order on the stress resultant demands at the tower base and pile head. For both Tripod and Jacket it can be seen that, as a result of the earthquake strike, stress resultant demands increase significantly, in all load cases LC1-LC2-LC3. In particular, considering that in both Tripod and Jacket the maxima stress resultant demands without earthquake loads are attained in the operational state (black vertical lines in load case LC1 of Figure 3.7-Figure 3.8), maxima stress resultant demands due to earthquake loads increase by a factor of 2-3 at the tower base and by a factor of 8-9 at the pile head of the Tripod (Figure 3.7), by a factor of 3-4 at the tower base and by a factor of 4-5 at the pile head of the Jacket (Figure 3.8). Further important observations are that significant stress resultant demands are encountered not only for high, but also for moderate PGA, and that stress resultant demands in load cases LC1-LC2-LC3 can be considered to be practically within the same range (100-400 MNm at the tower base and 10-80 MN at the pile head of the Tripod; 50-400 MNm at the tower base and 15-80 MN at the pile head of the Jacket). In this regard, it is worth noticing that stress resultant demands in the parked state (load case LC3) falling within the same range of stress resultant demands in the operational state (load case LC1) have been observed also in the seismic response of land-based HAWTs [48-50]. This result can be explained considering that, when the turbine is parked, the only damping is the structural damping of the support structure, usually low in steel structures, while in the operational state the structural response experiences an additional aerodynamic damping, whose source is essentially the

spinning rotor aerodynamics, and that depends on the oscillations of the tower top due to earthquake loading [71-72]. It is also worth noticing that the significant stress resultant demands found in case of an emergency stop (load case LC2), shown in Figure 3.7-Figure 3.8, mean that triggering a shutdown does not provide substantial benefits and that, therefore, load case LC2 shall generally be considered in the seismic assessment. In this context, it is pointed out that in all simulations of load case LC2 earthquake loads do trigger an emergency stop, i.e. the nacelle acceleration exceeds 1 ms^{-2}.

Comments on stress resultant demands at the tower base and pile head hold also for the tower top accelerations. Figure 3.7-Figure 3.8 show indeed that the tower top acceleration demands are significantly higher than the corresponding values without earthquake loads, in all load cases LC1-LC2-LC3.

As for the moment demands at the blade root, Figure 3.7-Figure 3.8 show that in both Tripod and Jacket they are not affected by an earthquake strike in the operational state (load case LC1) and in case of an emergency stop (load case LC2), while increments are experienced in the parked state (load case LC3); considering that the maxima moment demands without earthquake loads are attained in the operational state (black vertical lines in load case LC1), maxima moment demands increase by a factor of 1.2 in the Tripod (Figure 3.7), and by a factor of 2 in the Jacket (Figure 3.8). This result is evidence that seismic-induced blade vibrations are damped by aerodynamic damping in the operational state, but become significant in the parked state due to very low structural damping of the blades, in agreement with similar findings for land-based HAWTs [50]. For completeness, a comment is in order on symbols "×" on the left of the vertical lines in load case LC2, that correspond to simulations in which the maximum blade root bending moment after the start of earthquake shaking is found to be smaller than the maximum due to the considered operational wind-wave loads. This may happen considering that: (i) on one hand, the emergency stop may be activated just a few seconds after the start of earthquake shaking, i.e. when not enough time has elapsed for earthquake loads to cause moments higher than the maximum moment due to the operational wind-wave loads; (ii) on the other hand, after the activation of the emergency stop the moments caused by the combined earthquake loads + emergency stop loads may not exceed the maximum moment due to the operational wind-wave loads. However, there are also simulations in load case LC2 (symbols "×" on the right of the vertical lines) in which after the start of earthquake shaking, either before or after the

activation of the emergency stop, the maximum moment slightly exceeds the maximum due to the operational wind-wave loads, especially for high PGAs.

Comparing the responses of Tripod and Jacket, it is worth recalling that the frequencies of the first FA and SS support structure modes, as well as the frequencies of the blades modes (Table 3.1), are almost identical for the two structures; stress resultant demands at the tower base and pile head are found approximately within the same range, but moment demands at the blade root are generally higher in the Jacket, with a maximum demand nearly equal to 40 MNm (Figure 3.8) vs. 20 MNm in the Tripod (Figure 3.7). It is evident that these differences shall be attributed to dissimilar stiffness and mass distributions along the two support structures (Table 3.2) and, also, to the activation of the second FA and SS support structure modes, whose frequencies are substantially different in the Tripod and Jacket (Table 3.1).

A final important comment is that, as shown in Figure 3.7-Figure 3.8, stress resultant and tower top acceleration demands generally increase with the PGA, thus meaning that the PGA can be taken as an acceptable indicator of demand for the structures under study. Because the PGA is typically related to the short period energy content of the earthquake, this result reflects the fact that the rotor modes and second support structure modes (Table 3.1) play an important role in the seismic response, as shown in Figure 4a (periods of the rotor modes and second support structure modes fall in the region of maxima spectral accelerations) and

Figure 3.5-

Figure 3.6 (activation of the second support structure modes), in agreement with similar findings for land-based HAWTs [48-50].

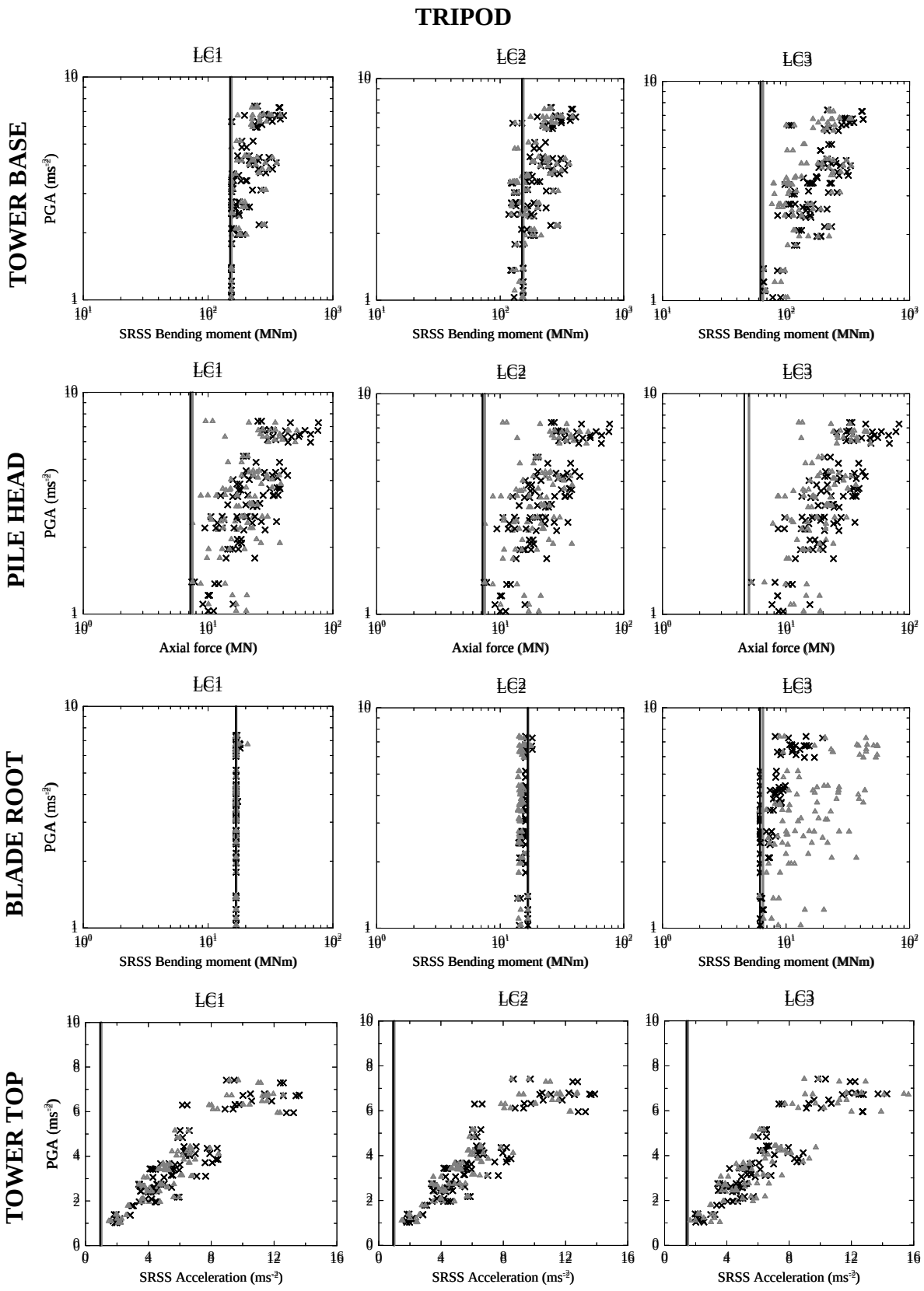

Figure 3.7: Tripod: stress resultant and tower top acceleration demands under the earthquake set for fixed and flexible FMs.

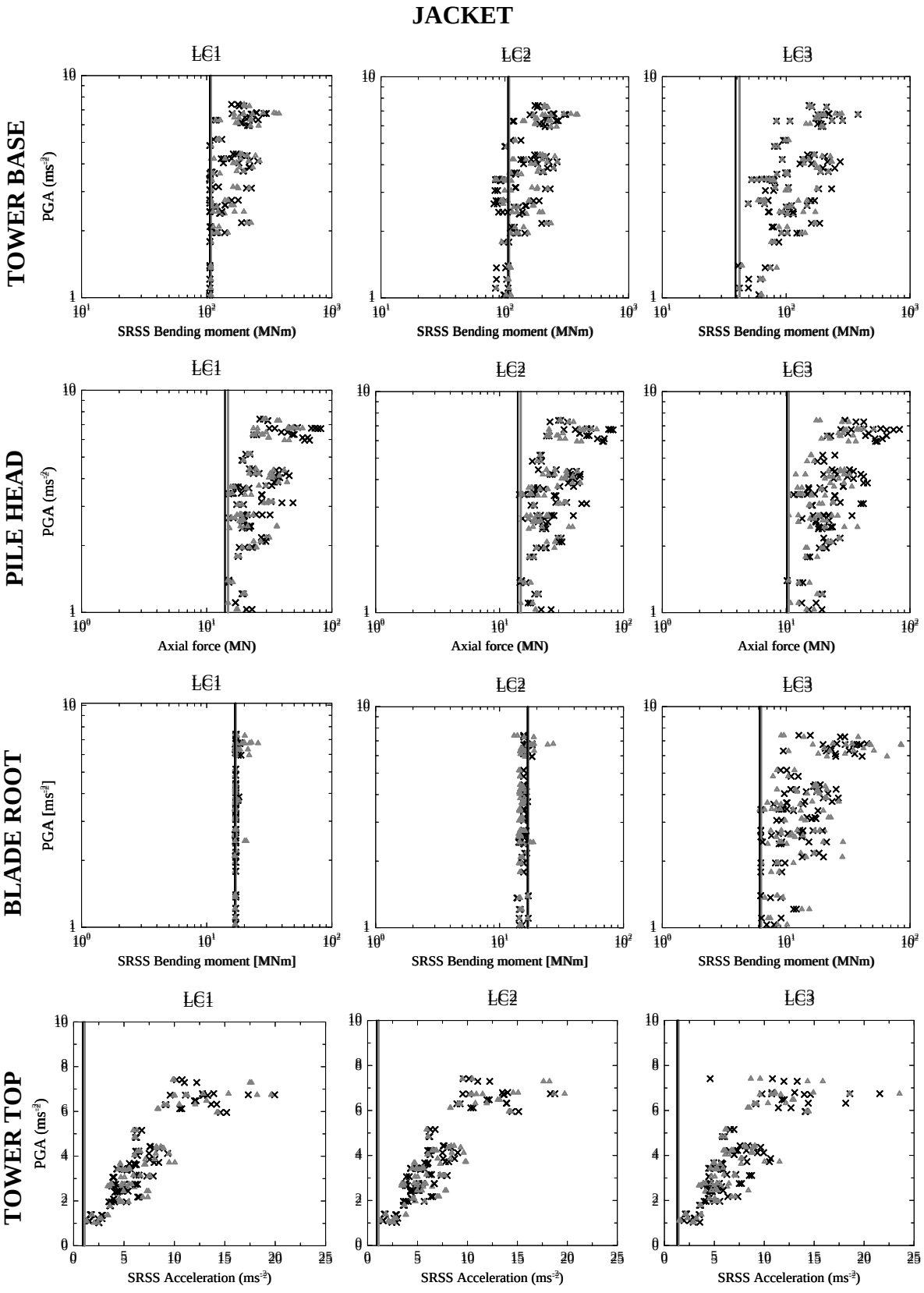

Figure 3.8: Jacket: stress resultant and tower top acceleration demands under the earthquake set for fixed and flexible FMs.

3.5.2. Stress resultant and tower top acceleration demands for flexible foundation model

In Figure 3.7-Figure 3.8, stress resultant and tower top acceleration demands for flexible FM are denoted by symbol "Δ", while grey vertical lines indicate the corresponding demands due to wind and wave loads only, for the environmental states in load cases LC1-LC2-LC3 (see Section 3).

At the tower base and pile head, in both Tripod and Jacket, stress resultant demands do not change significantly with respect to the corresponding demands for fixed FM, in all load cases LC1-LC2-LC3. This result may be explained considering that the frequencies of the first FA and SS support structure modes, as well as the frequencies of the blades modes, hold almost the same values for fixed and flexible FMs (Table 3.1), while the frequencies of second FA and SS support structure modes, although being reduced by the foundation flexibility (Table 3.1), still correspond to periods falling within the range of high spectral accelerations, as shown in Figure 3.4 (a) (for instance, for the second FA support structure modes: T_2 = 1/1.277 = 0.783 s in the Tripod, and T_2 = 1/0.984 = 1.016 s in the Jacket). The same observations can be made for the stress resultant demands at the tower base and pile head without earthquake loads (grey vertical lines in load cases LC1-LC2-LC3), which appear almost identical to the corresponding demands for fixed FM (black vertical lines), showing that frequencies of the second FA and SS support structure modes, although being reduced by the foundation flexibility, shift within a frequency range that is still relatively far from the excitation frequencies of wind and wave processes (Figure 3.4 (b)).

Figure 3.7-Figure 3.8 also show that, unlike the stress resultant demands at the tower base and pile head, moment demands at the blade root in the parked state (load case LC3) increase with respect to the corresponding demands for fixed FM, in both Tripod and Jacket. In particular, the maximum moment demand in the Tripod is found to be 60 MNm (vs. 20 MNm for fixed FM), while that in the Jacket is 90 MNm (vs. 40 MNm for fixed FM). It is interesting to remark that, as shown in Figure 3.7-Figure 3.8, such an increase of maximum moment demand at the blade root mirrors an increase of maximum tower top acceleration in the parked state (load case LC3) with respect to the corresponding maximum acceleration for fixed FM, and shall be considered, in this case, as a result of the additional flexibility introduced by the flexible FM [73].

Comparing Tripod and Jacket responses, it is observed that stress resultant demands at the tower base and pile head fall approximately within the same range, while the maximum

moment demand at the blade root is encountered in the Jacket (90 MNm). In these respects, results appear in a substantial agreement with those for fixed FM.

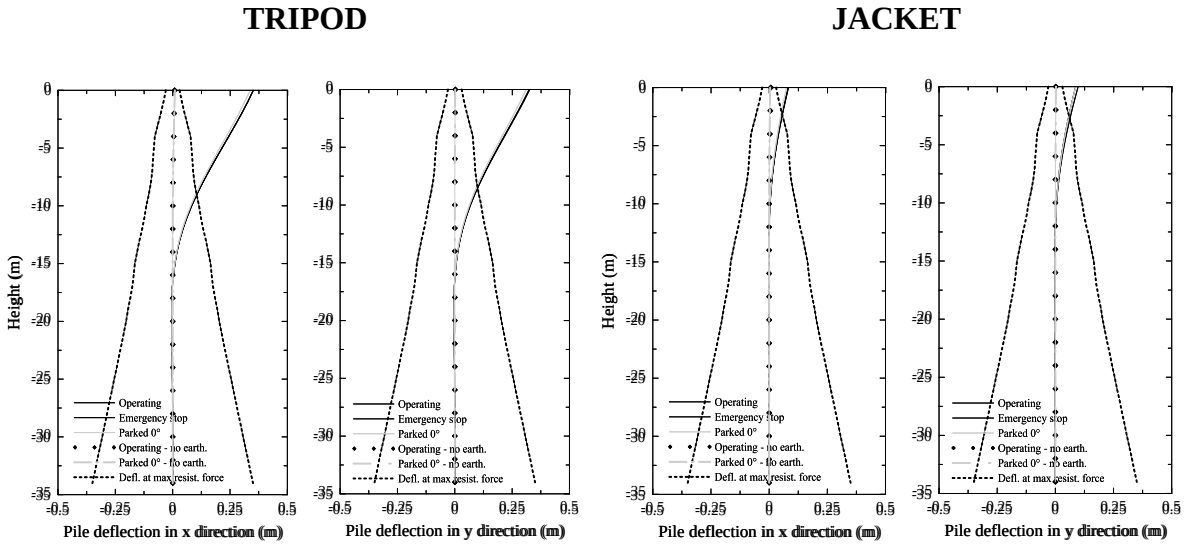

Figure 3.9: Tripod and Jacket pile maxima lateral deflections in *x* and *y* directions.

In order to have an indicator of non-linearity of the soil response, the maxima lateral *x*- and *y*-deflections obtained from all simulations of the earthquake set, at various depths along the piles, are reported in Figure 3.9 for load cases LC1-LC2-LC3. Here, the maximum deflection is intended as the maximum deviation from the initial vertical configuration of the pile and, as such, may be encountered in either the positive or negative direction of *x* and *y* axes. In particular, it has been found that the maxima lateral deflections at all depths are attained in the same simulation, and at the same time instant of the simulation, specifically as the pile head attains its maximum deflection. For example, in pile #1' of the Tripod, the maxima *x*-deflections at all depths are found in the simulation with the Northridge earthquake (ID No. 43 in Table 3.3), when its fault normal component acts in *x* direction, in all load cases LC1-LC2-LC3. It is observed that the profiles in Figure 3.9, with positive and negative deflections (the latter are slightly visible, for instance, in pile #1' of the Tripod), are in accordance with typical deflection profiles of flexible piles constrained by lateral springs and supporting structures under dynamic lateral loads [74]. For comparison, Figure 3.9 includes also: (i) the maxima lateral deflections due to wind-wave loads only (no earthquake loads), for the environmental states considered in load cases LC1-LC2-LC3; (ii) the lateral deflections at which the soil resistance forces attain, with a tolerance of 10^{-2}, the maxima asymptotic values given by the *p*-*y* API curves [46]

for the considered sandy soil [58-59], at various depths along the piles; notice that these lateral deflections can be taken as indicators of a significant non-linear soil response, because *p-y* curves deviate from linearity also for relatively small soil displacements [26]. Figure 3.9 shows that earthquake loads cause a considerable increase of lateral deflections with respect to corresponding values without earthquake loads. It is also seen that non-linear effects are significant, especially in the Tripod, where maxima lateral deflections are well above the lateral deflections corresponding to maxima soil resistance forces, over about one fourth of the total pile length. These results suggest that using linearized *p-y* curves, as for instance in simplified fatigue analysis of offshore HAWTs on bottom-fixed support structures [75], may not be appropriate for seismic assessment.

3.6. Comparison with the IEC 61400-3 load cases

In order to assess whether earthquake loads are design driving for the Tripod and Jacket under study, a full set of design load cases should be considered, as for instance those prescribed by IEC 61400-3 [15]. Analyses should be carried out for site-specific conditions, based on accurate joint statistics of wind and wave states, sea currents and water level, and on a proper description of local seismicity, as required by IEC 61400-3 [15].

Here it is of interest to compare the earthquake demands in Figure 3.7-Figure 3.8, obtained for earthquake loads combined with wind-wave loads in a typical operational state and a typical parked state, with demands from some IEC 61400-3 design load cases [15]. For this purpose, the load cases in Table 3.4 are selected as representative of operational and parked states [15], assuming environmental parameters that can reasonably be expected in offshore sites for wind turbines, in accordance with those in paragraph 3.3 (more details on the environmental parameters in Table 3.4 are reported in the Appendix C). Bearing in mind that a definitive answer as to whether earthquake loads are design driving can be given only for site-specific conditions, that the environmental parameters in Table 3.4 may not reflect particularly unfavourable site conditions, and that only a few environmental states are selected in Table 3.4 (e.g., DLC 1.3 and DLC 1.6 would require discrete values of the wind speed at the hub, V_{hub}, ranging from the cut-in speed V_{in} =3.0 ms^{-1} and the cut-out speed V_{out} = 25 ms^{-1} of the 5MW turbine [53] with intervals of 2 ms^{-1} [15]), it is believed that the load cases in Table 3.4 can provide at least a reasonable order of magnitude of

typical operational and parked state demands as prescribed by IEC 61400-3 [15], for comparison with the earthquake demands in Figure 3.7-Figure 3.8.

Table 3.4: IEC 61400-3 load cases [15], for comparison with earthquake load cases LC1-LC2-LC3.

Operational state	Wind	Waves	Sea currents	Water level
DLC 1.3_1	V_{hub}=10 ms^{-1}	H_s= 5.0 m T_p= 9.53 s	U_w(0)=0.069 ms^{-1}	MSL=50 m
DLC 1.3_2	V_{hub}=15 ms^{-1}	H_s= 5.5 m T_p= 10.0 s	U_w(0)=0.105 ms^{-1}	MSL=50 m
DLC 1.3_3	V_{hub}=20 ms^{-1}	H_s= 6.0 m T_p= 10.4 s	U_w(0)=0.139 ms^{-1}	MSL=50 m
DLC 1.3_4	V_{hub}=25 ms^{-1}	H_s= 6.5 m T_p= 10.9 s	U_w(0)=0.174 ms^{-1}	MSL=50 m
DLC 1.6a_1	V_{hub}=10 ms^{-1}	H_s=8.0 m T_p=12 s	U_w(0)=0.069 ms^{-1}	NWLR=52 m
DLC 1.6a_2	V_{hub}=15 ms^{-1}	H_s=8.0 m T_p=12 s	U_w(0)=0.105 ms^{-1}	NWLR=52 m
DLC 1.6a_3	V_{hub}=20 ms^{-1}	H_s=8.0 m T_p=12 s	U_w(0)=0.139 ms^{-1}	NWLR=52 m
DLC 1.6a_4	V_{hub}=25 ms^{-1}	H_s=8.0 m T_p=12 s	U_w(0)=0.174 ms^{-1}	NWLR=52 m
DLC 1.6a_5	V_{hub} =10 ms^{-1}	H_s=8.0 m T_p =12 s	U_w(0)=0.069 ms^{-1}	NWLR=48 m
DLC 1.6a_6	V_{hub}=15 ms^{-1}	H_s=8.0 m T_p =12 s	U_w(0)=0.105 ms^{-1}	NWLR=48 m
DLC 1.6a_7	V_{hub}=20 ms^{-1}	H_s=8.0 m T_p=12 s	U_w(0)=0.139 ms^{-1}	NWLR=48 m
DLC 1.6a_8	V_{hub}=25 ms^{-1}	H_s=8.0 m T_p=12 s	U_w(0)=0.174 ms^{-1}	NWLR=48 m

Parked state	Wind	Waves	Wave dir.	Sea currents	Water level
DLC 6.1a_1	V_{hub}=47.5 ms^{-1}	H_s=8.7 m T_p=12.6 s	+30°	U_w(0)=0.37 ms^{-1} U_{ss}(0)=3.0 ms^{-1}	EWLR=53 m
DLC 6.1a_2	V_{hub}=47.5 ms^{-1}	H_s=8.7 m T_p=12.6 s	0°	U_w(0)=0.37 ms^{-1} U_{ss}(0)=3.0 ms^{-1}	EWLR=53 m
DLC 6.1a_3	V_{hub}=47.5 ms^{-1}	H_s=8.7 m T_p=12.6 s	–30°	U_w(0)=0.37 ms^{-1} U_{ss}(0)=3.0 ms^{-1}	EWLR=53 m
DLC 6.1a_4	V_{hub}=47.5 ms^{-1}	H_s=8.7 m T_p=12.6 s	+30°	U_w(0)=0.37 ms^{-1} U_{ss}(0)=3.0 ms^{-1}	EWLR=47 m
DLC 6.1a_5	V_{hub} =47.5 ms^{-1}	H_s=8.7 m T_p=12.6 s	0°	U_w(0)=0.37 ms^{-1} U_{ss}(0)=3.0 ms^{-1}	EWLR=47 m
DLC 6.1a_6	V_{hub}=47.5 ms^{-1}	H_s=8.7 m T_p=12.6 s	–30°	U_w(0)=0.37 ms^{-1} U_{ss}(0)=3.0 ms^{-1}	EWLR=47 m

For each load case, six simulations are implemented in BLADED [35], with either 10 min or 1-hour length [15]. Maxima stress resultants at the tower base, pile head (pile #1' of the Tripod, pile #3" of the Jacket) and blade root are reported in Table 3.5-Table 3.6. Maxima axial forces in the other piles are found within the range of those in Table 3.5-Table 3.6 and, for completeness, are reported in the Appendix D.

Hence, according to IEC 61400-3 [15], the demands in Table 3.5-Table 3.6 should be multiplied by a load safety factor equal to 1.35 and, for the operational load cases involving a wind speed range (Section 7.5.4 in ref. [15]), a second multiplicative factor should be considered to extrapolate appropriate long-term characteristic demands, based on a site-specific joint probability distribution of wind and wave states. Although different approaches exist to compute such extrapolation factor, indicative values of 1.2÷1.3 may be derived from land-based HAWTs (see ref. [49-50] or Annex F in ref. [40] for the

characteristic moment at the blade root). Therefore, multiplying the values in Table 3.5-Table 3.6 by a 1.35 load safety factor and also by a 1.3 extrapolation factor for the operational load cases, it can readily be observed that the derived demands would be smaller than the earthquake demands obtained for the highest levels of PGA, as reported in Figure 3.7-Figure 3.8. It is also worth noticing that, at the pile head and blade root of the Tripod, earthquake demands would be higher also for moderate levels of PGA. In particular, at the blade root this holds true for the flexible FM (Figure 3.7).

Table 3.5: Tripod: IEC 61400-3 load cases [15], for comparison with earthquake load cases LC1-LC2-LC3.

TRIPOD

Operational state	**Tower base moment (MNm)**		**Pile #1′ head axial force (MN)**		**Blade root moment (MNm)**	
	Fixed FM	Flex. FM	Fixed FM	Flex. FM	Fixed FM	Flex. FM
DLC 1.3_1	122.72	120.80	6.85	7.63	17.57	16.59
DLC 1.3_2	111.62	101.49	7.04	7.66	14.34	15.42
DLC 1.3_3	110.42	110.19	7.10	7.68	15.22	15.26
DLC 1.3_4	118.00	112.62	7.20	8.32	15.01	15.18
DLC 1.6a_1	166.02	169.14	10.72	12.06	18.82	18.78
DLC 1.6a_2	130.46	136.66	7.38	7.90	16.34	16.72
DLC 1.6a_3	110.72	108.13	9.52	9.73	14.58	14.67
DLC 1.6a_4	116.29	114.43	9.97	9.02	13.86	13.98
DLC 1.6a_5	156.11	157.18	10.30	11.73	19.04	18.78
DLC 1.6a_6	125.46	132.96	7.79	7.58	16.66	16.86
DLC 1.6a_7	104.72	103.71	9.34	9.09	14.30	14.34
DLC 1.6a_8	115.74	110.98	9.66	8.80	13.78	13.74
Parked state	**Tower base moment (MNm)**		**Pile #1′ head axial force (MN)**		**Blade root moment (MNm)**	
	Fixed FM	Flex. FM	Fixed FM	Flex. FM	Fixed FM	Flex. FM
DLC 6.1a_1	184.06	182.57	9.06	10.32	16.72	16.60
DLC 6.1a_2	185.00	183.78	10.05	11.51	16.73	16.63
DLC 6.1a_3	186.20	185.54	9.06	10.35	16.76	16.66
DLC 6.1a_4	185.51	183.20	8.01	9.86	16.69	16.62
DLC 6.1a_5	185.79	183.69	8.96	10.65	16.69	16.65
DLC 6.1a_6	186.41	184.62	7.99	9.83	16.70	16.66

Although the considered operational and parked states are certainly not exhaustive, and other important loads shall be considered in design analyses, such as fatigue loads, the results discussed above substantiate the need for an accurate seismic assessment of offshore HAWTs, also in recognition of the fact that no load safety factor has been applied to

earthquake demands when compared to the demands from the IEC 61400-3 load cases. Analogous conclusions have been drawn in studies on a land-based NREL 5MW HAWT [49-50], showing that earthquake demands may be design driving in regions of high seismic hazard.

Table 3.6: Jacket: IEC 61400-3 load cases [15], for comparison with earthquake load cases LC1-LC2-LC3.

JACKET

Operational state	**Tower base moment (MNm)**		**Pile #3″ head axial force (MN)**		**Blade root moment (MNm)**	
	Fixed FM	Flex. FM	Fixed FM	Flex. FM	Fixed FM	Flex. FM
DLC 1.3_1	69.92	68.58	16.10	15.96	16.12	15.86
DLC 1.3_2	73.53	71.49	16.97	16.52	14.47	14.69
DLC 1.3_3	72.00	74.24	17.31	16.86	15.74	15.71
DLC 1.3_4	80.24	76.30	18.24	17.49	16.54	16.39
DLC 1.6a_1	111.64	113.19	20.01	20.57	20.49	20.03
DLC 1.6a_2	86.87	82.52	16.34	16.61	17.36	16.22
DLC 1.6a_3	73.36	68.41	17.83	17.73	15.57	15.08
DLC 1.6a_4	79.12	77.38	18.56	18.16	15.66	15.74
DLC 1.6a_5	110.26	112.78	20.03	20.23	20.32	20.18
DLC 1.6a_6	82.88	74.97	15.98	16.46	16.80	16.41
DLC 1.6a_7	74.72	69.90	17.70	17.26	15.05	14.99
DLC 1.6a_8	79.48	79.44	18.21	17.95	15.44	15.64
Parked state	**Tower base moment (MNm)**		**Pile #3″ head axial force (MN)**		**Blade root moment (MNm)**	
	Fixed FM	Flex. FM	Fixed FM	Flex. FM	Fixed FM	Flex. FM
DLC 6.1a_1	123.65	122.63	30.27	25.34	16.81	16.46
DLC 6.1a_2	123.98	123.14	25.49	23.18	16.81	16.42
DLC 6.1a_3	124.11	124.26	21.06	22.25	16.83	16.38
DLC 6.1a_4	123.41	122.33	28.04	24.39	16.81	16.41
DLC 6.1a_5	123.56	122.96	23.86	22.68	16.80	16.38
DLC 6.1a_6	123.54	124.04	21.21	22.27	16.81	16.37

3.7. Conclusion

The seismic behaviour of the NREL 5MW HAWT [53], mounted on a Tripod and a Jacket in transitional water depths, has been investigated by fully-coupled non-linear time-domain simulations on full system models implemented in BLADED [35], for fixed and flexible FMs. Some typical scenarios, i.e. earthquake striking in the operational state (load

case LC1) or parked state (load case LC3), and earthquake triggering an emergency stop (load case LC2) have been considered, selecting two typical wind-wave states for operational and parked states. The main results can be summarized as follows.

(i) For the fixed FM, in both Tripod and Jacket, moment demand at the tower base and axial force at the pile head in load cases LC1-LC2-LC3, as well as moment demand at the blade root in load case LC3, increase significantly with respect to the corresponding demands without earthquake loads, even for moderate PGA.

(ii) For the flexible FM, in both Tripod and Jacket, moment demand at the tower base and axial force demand at the pile head do not change significantly with respect to the corresponding demands for fixed FM, while maxima moment demands at the blade root increase significantly. This is consistent with the fact that, as a result of the foundation flexibility, maxima tower top accelerations increase with respect to corresponding maxima for fixed FM [72], while, in contrast, the natural frequencies are not significantly reduced.

(iii) For both fixed and flexible FMs, demands at the tower base and pile head of both Tripod and Jacket fall approximately within the same range, while maxima moment demands at the blade root are always encountered in the Jacket. These results are evidence that different mass and stiffness distributions, as well as activation of second FA and SS support structure modes, play a crucial role in the seismic response of the two structures.

The results of load cases LC1-LC2-LC3 suggest that fully-coupled non-linear time-domain simulations on full system models, i.e. including support structure, rotor blades and nacelle, as those implementable in BLADED [35] or similar software, are highly recommended for the seismic assessment of offshore HAWTs, while simplified models allowed by standards and guidelines [15, 44], that involve only the support structure and a lumped mass modelling the RNA at the tower top, would fail to capture relevant data. These conclusions can be drawn especially considering that simplified models could not provide any prediction on the response of the rotor blades, while the simulations run in the present study have revealed that, at the blade root, moment demands are significantly increased by earthquake loads, with maxima very sensitive to foundation flexibility, and that relevant differences may exist between maxima moment demands when different support structures are used, such as the Tripod and Jacket in Figure 3.2. Because rotor

blades are key components of the turbine, all these data are of crucial importance in the seismic assessment of offshore HAWTs. It is also recommended that full system models account for non-linear soil response, in recognition of the significant non-linear effects shown in Figure 3.9.

Further, the present study has shown that the stress resultant demands in load cases LC1-LC2-LC3 may be higher than demands from some typical design loads prescribed by IEC 61400-3 [15], in general for the highest levels of PGA. Although a definitive answer as to whether earthquake loads are design driving for the two structures under study can be given only considering site-specific conditions, these results substantiate the need for an accurate seismic assessment when installing offshore HAWTs in seismically active areas. In this context, refined seismic analyses should be carried out, considering vertical ground motion, variation of earthquake acceleration through soil layers [55], potential misalignment between wind and wave loads during earthquake shaking, and other important issues such as sensitivity to different models of *p-y* curves [74] and potential uncertainties in soil properties [76], alterations of the foundation stiffness due to strain-hardening or strain-softening soil behaviour [77-78]. Related effects shall accurately be investigated considering site-specific conditions.

4. Uncoupled analysis of offshore wind turbines

This chapter shows the results of time-domain uncoupled analysis for the support structures (tripod and jacket) adopted in the previous chapter. For different earthquake records, wind velocity and wave heights, comparison with fully-coupled show that the combination of uncoupled analysis implemented in time domain yields accurate results, provided that an appropriate level of *aerodynamic damping* is included in the model.

4.1. Introduction

Seismic assessment of bottom-fixed offshore horizontal-axis wind turbines (HAWTs) has become of particular interest considering that, while an increasing number of wind farm is being planned far from near-shore shallow waters (<30 m) to minimize visual impact, several transitional water depth (30-60 m) sites exist with high wind resources and medium-to-high seismic risk [79-81]. A few recent studies have investigated the seismic response of offshore HAWTs mounted on either monopiles [54-55] or support structures with a tripod or jacket [82].

In contrast, the seismic assessment of land-based horizontal-axis wind turbines has been the subject of several studies in the last decade. Investigations have been carried out adopting different system models, load combinations and methods of analysis [83,84]. Simplified models, or full models including support structure, rotor, as well as mechanical/electrical/control components of the turbine, have been used as system models. Combinations of earthquake loads with operational wind loads or emergency-stop loads, and earthquake loads acting in parked rotor conditions with or without wind loads, have been considered as typical loading conditions. Methods of analysis have been implemented in time or frequency domain, the latter based on the classical response spectrum approach.

Simplified finite element (FE) models have been implemented in ref. [42,85,52], under earthquake loads acting in parked rotor conditions without wind loads. Bazeos et al. [42] studied a 38 m high, 450 kW HAWT resting on a concrete square footing in a semi-rock soil, using shell or beam elements for the tower, a top lumped mass and a rigid block to model rotor-nacelle assembly (RNA) and square footing, respectively, springs/dashpots and added soil mass to account for soil-structure interaction [86]. Lavassas et al. [85] studied a 44 m high, 1 MW HAWT on a concrete circular footing in a rock soil, using shell elements for the tower, 3D-solid elements for the circular footing, and a top lumped mass to model the RNA. Stamatopolous [52] investigated a 53.95 m high HAWT resting on a circular footing, using beam elements for tower and blades, 3D-solid elements for the footing, nonlinear unilateral springs below the footing to model foundation flexibility. For the relatively low ground accelerations of the project sites under consideration, time-domain analyses in ref. [42] and frequency-domain analyses in ref. [42,85] found that earthquake loads acting in parked rotor conditions, without wind loads, induce low stress levels as compared to other design loads. On the other hand, time- and frequency-domain analyses in ref. [52] demonstrated that shear and bending moment demand at the tower base can be underestimated significantly by the Greek Design Code, when near fault ground motions are considered. Notice that, in ref. [52], the frequency-domain analysis was carried out by a response spectrum approach on a linearized model of the structure, where the nonlinear unilateral springs below the footing are replaced with an equivalent linearly-elastic rotational spring, whose stiffness is calibrated by an approximate iterative procedure. FE models under earthquake loads and operational wind loads have been investigated in ref. [87,88]. Sapountzakis et al. [87] have proposed a FE approach formulated by the boundary element method. They studied the National Renewable Energy Laboratory (NREL) 5 MW baseline HAWT [49,53] on either surface or monopile foundation, using beam elements for the tower, a top mass for the RNA, nonlinear springs/dashpots to model foundation flexibility, and including axial load effects.

Responses for surface and monopile foundations were compared under earthquake loads and a top force modeling wind loads, with the latter built by applying the combined blade element and momentum (BEM) theory on the rotor, taken as fixed on a rigid tower. A FE model accounting for flexibility of the blades in the flapping direction, bending and twisting flexibility of the tower, gyroscopic effects of the rotor, has been proposed by Diaz and Suarez [88]. They investigated the seismic response of a 76 m high, 1.65 MW HAWT,

modeling the tower by beam elements and the blades by rigid rods with rotational springs at the roots. Considering four strong ground motions with operational wind loads, they showed that stresses at some tower sections may exceed those from extreme winds.

Fully-coupled, nonlinear time-domain simulations on full system models have been implemented in ref.[44, 47-50]. Using FAST [90], a NREL simulation tool where motion equations of the system are derived by a combined multi-body dynamics and modal approach, Prowell et al. [48-50] showed that earthquakes may produce, in the NREL 5MW baseline HAWT, a bending-moment demand at the tower base well above the one from extreme wind events, in operational, emergency shutdown and parked simulations. Also, Prowell et al. [49] demonstrated that not only first but also second modes contribute significantly, in both fore-aft (FA) and side-to-side (SS) directions (i.e., parallel and perpendicular directions to the rotation axis of the rotor, respectively), in agreement with previous findings on the importance of the second modes in seismic response of large turbines [88,91]. Zhao et al. [44,47] developed a hybrid multi-body system (MBS) where nacelle and tower are discretized into an ensemble of rigid bodies coupled elastically by constraint joints and springs, the wind rotor is treated as a rigid disk, and a 3D set of uncoupled frequency-independent spring-damper devices, including translations and rotations, is used to model the foundation. Governing equations are derived using Lagrange's equations and no external calculation of component mode shapes is required. By the MBS approach, Zhao et al. [44] studied the seismic response of a 65 m high, 1.5 MW HAWT, showing that shear force and bending moment at the tower base are affected considerably by earthquake loads, both in the FA and SS directions. This result was found for operational conditions, with a weak real earthquake record. Studies in ref. [44, 47-50] demonstrated that earthquake loads may be design driving in regions of high seismic hazard.

Although fully-coupled, nonlinear time-domain simulations are certainly most indicated to build a numerical solution for seismic assessment, the main disadvantage is that computational costs may be significant, almost prohibitive when several analyses have to be implemented for different environmental states and system parameters, as in the early stages of design. For these reasons, a considerable attention has been devoted to assess whether the response to simultaneous wind and earthquake loads can be obtained by combining two uncoupled analyses, one under wind and another under earthquake only, instead of running a fully-coupled analysis. In this manner, the response to a given wind

state, once computed, could be combined with the response to different potential earthquake events or vice versa, with a significant reduction of computational costs with respect to fully-coupled time-domain simulations.

The implementation of uncoupled analyses is currently the subject of active research. Early investigations have been made by Witcher [71]. Using GH BLADED [35], a simulation tool where equations of motion are derived by a combined multi-body dynamics and modal approach, he studied a 2MW HAWT mounted on a 60 m high steel tower, showing that, if the separate earthquake moment demand at the tower base is computed from a 5% damped FA-response spectrum and then linearly combined with the separate wind moment demand computed by a time-domain simulation, a good matching is attained with the moment demand at the tower base computed from a fully-coupled, nonlinear time-domain simulation. Considering that steel structures can reasonably be given a 1% structural damping, using a 5% damped FA-response spectrum means that an additional 4% damping is included in the FA modes, when computing the separate earthquake response. The 4% additional damping has been named as aerodynamic damping, to point out that its source is essentially the aerodynamics of the spinning rotor. In a rather intuitive way, aerodynamic damping arises from the observation that forward/backward motion of a structure vibrating in a wind field induces a change in the aerodynamic forces that, in general, reduce the dynamic response of the structure [72]. Experimental tests run on a 65 kW HAWT by Prowell et al. [48], in operational state with earthquake shaking in FA and SS directions, confirmed that aerodynamic damping effects affect the FA response, and showed that are negligible in the SS direction. Recently, an analytical estimate of aerodynamic damping has been proposed by Valamanesh and Myers [72], based on BEM theory, under the assumption of laminar flow (no turbulence) and rigid rotor. The proposed estimate was found to depend on the wind velocity. Working on a FE model of the HAWT with beam elements along the tower and lumped masses at the element nodes and top, subjected to seven ground motions and a top thrust force built in steady-state laminar flow by FAST, the authors found a good agreement between top median drifts computed by combining separate wind and earthquake responses, when the earthquake response is built with either the proposed analytical estimate of aerodynamic damping depending on the wind direction [72].

International Standards such as IEC 61400-1 [40] and Guidelines as ASCE-AWEA RP2011 [41] allow combining uncoupled analyses, instead of performing fully-coupled,

nonlinear time-domain simulations. In Annex C, IEC 61400-1 [40] proposes a method to compute the response under earthquake and operational wind loads. It is based on the assumption that the whole structure is subjected to the same acceleration, computed from the first tower bending natural frequency using a 1% damped response spectrum. Stress resultants at the tower base are calculated by applying, at the tower top, a force equal to the total mass of the RNA + ½ the mass of the tower, times the design acceleration response. The corresponding base stress resultants are linearly combined with the separate wind demand, computed, in particular, from an emergency stop simulation at rated wind speed. Some prescriptions to compute the response under earthquake and operational loads are given also by ASCE-AWEA RP2011 [41]. It recommends that the separate earthquake demand is computed considering an acceleration response spectrum with 5% total damping, and combined with the operational wind demand using a combination load factor equal to 0.75. The 5% damped spectrum of ASCE-AWEA RP2011 [41] corresponds to consider 1% structural damping of steel structures + 4% aerodynamic damping, in agreement with findings of Witcher [71], Valamanesh and Myers [72].

Some insights into the uncoupled analyses prescribed by IEC 61400-1 [40] and ASCE-AWEA RP2011 [41] have been provided in ref. [50,92]. Considering the NREL 5MW baseline HAWT under a large database of earthquake records, Prowell [50] showed that the IEC method, if separate earthquake and wind demands are combined by a square root of the sum of the squared maxima (SRSS) instead of being linearly combined, can provide moment demands at the tower base that better match those obtained by fully-coupled, nonlinear time-domain simulations. He also showed that such SRSS combination of uncoupled analyses may predict either larger or smaller demands than those from fully-coupled simulations (see Figure 8.11 in ref. [50]). Again for the NREL 5MW baseline HAWT, Asareh and Prowell [92] proposed a combination of uncoupled analyses where a 0.75 combination factor, as in ASCE-AWEA RP2011, is used to combine the separate operational wind and earthquake demands, with the latter computed using a 4% aerodynamic damping in either time or frequency domain. The authors showed that, in this manner, the mean bending-moment demands along the tower, computed by averaging over a set of earthquake records [92], agree well with the mean demands from fully-coupled, nonlinear time-domain simulations. As in ref. [50], mean demands from the combination of uncoupled analyses were either larger or smaller than those from fully-coupled simulations. Notice that fixed foundation models were assumed in both ref. [50] and ref. [92].

In the uncoupled analyses allowed by IEC 61400-1 [40] and ASCE-AWEA RP2011 [41], the separate earthquake response is generally computed in the frequency domain, based on the acceleration response spectrum. When computing the earthquake response by a spectrum analysis, however, nonlinear foundation behaviour cannot be considered appropriately in the structural model, because periods T to be used in the response spectrum must be, indeed, periods of the structure assumed to behave linearly. To address these issues, uncoupled analyses where separate wind and earthquake responses are both computed in the time domain would be highly desirable, as they would allow nonlinearities, such as those deriving from foundation modelling, to be considered directly in the structural model. It is apparent, however, that the implementation of such uncoupled analyses requires an appropriate level of aerodynamic damping, on which, to the best of authors' knowledge, no data are available in the literature.

As for what concerns offshore HAWTs, however, neither numerical studies nor standards or guidelines recommendations exist on the appropriate aerodynamic damping to be adopted, when implementing uncoupled analysis for seismic assessment.

The purpose of this study is to investigate how uncoupled analyses, for fixed foundation model, can be implemented in the time domain, for the seismic assessment of offshore HAWTs. The study case is the NREL 5 MW baseline wind turbine [49,53], mounted on two different bottom-fixed support structures (tripod and jacket) introduced in chapter 3. For earthquake striking in operational state, fully-coupled and uncoupled analyses are implemented in the time domain using GH BLADED [35], on a full model of the system which includes support structure, rotor blades, mechanical/electrical/control components of the turbine, and nonlinear soil springs for foundation flexibility. Considering different wind velocities, sea states and ground motions, the response from fully-coupled simulation is compared with the linear combination of separate wind, wave and earthquake responses, the latter computed by adding different levels of aerodynamic damping in the first two FA support structure modes. The first step will be to assess whether there exists an aerodynamic damping level capable of minimizing a total error, which involves shear-force and bending-moment demands at the tower base, as computed by fully-coupled simulation and combination of uncoupled analyses. It will be found that such aerodynamic damping level cannot be obtained, for all the considered wind velocities, wave states and ground motions. However, it will be shown that errors in bending-moment and shear-force demands are within engineering margins, analogous to those encountered in

the combination of frequency-domain uncoupled analyses, if a 4% aerodynamic damping is assumed for all the considered wind velocities, wave states and ground motions. The results confirm that the 4% aerodynamic damping level, recommended by ASCE-AWEA RP2011 for the land-based wind turbine [41] and used in previous studies [71,72,92], can reasonably be used also in time-domain uncoupled analyses.

4.2. Structural models and environmental loads

The structural models adopted for the analysis are the tripod and jacket support structures introduced in chapter 3 , with fixed foundation model (clamped base).

The full system is implemented in GH BLADED [25] where rotor blades, nacelle, drive train, mechanical/electrical/control components are modelled according to parameters provided in ref. [53]. Shear-deformable 3D beam elements are used for support structure structural members, column and blades. Steel parameters are: Young's modulus = 210 GPa, Poisson coefficient = 0.3, Mass density = 7850 kg m^{-3}.

For a first insight, modal analysis is implemented in GH BLADED [35] considering the rotor in a parked state (no rotational speed) at 0° azimuth angle (one blade upward, two blades downward). Table 4.1 reports the frequencies of support structure modes and blades modes. For the time-domain simulations, structural damping is set assuming the following modal damping coefficients: 10^{-2} for support structure modes, and 4.775×10^{-3} for blade modes, consistently with previous studies [53].

The aerodynamic loads on the spinning rotor are generated, in GH BLADED [35], based on a dynamic wake model for the axial inflow, in conjunction with classical BEM model for the tangential inflow [43]. The dynamic wake model takes into account that changes in the blade loads change the vorticity trailed into the rotor wake, and that the effect of these changes takes indeed a finite time to change the induced flow field, depending on which lift and drag forces acting on the blades are calculated [35].

The Kaimal spectrum is used for the wind process [40]:

$$S_k(f) = \frac{4\sigma_k^2 L_k / V_{hub}}{\left(1 + 6 f L_k / V_{hub}\right)^{5/3}} \tag{4.1}$$

where f is the frequency (Hz), k is the index referring to the velocity component (1 = x direction, 2 = y direction and 3 = z direction), σ_k is the standard deviation and L_k is the integral scale parameter of each velocity component. Assuming medium turbulence characteristics [65], all parameters in Eq.(4.1) are set according to IEC 61400-1 prescriptions for a normal turbulence model [40].

Table 4.1: Tripod and Jacket natural frequencies.

Mode description	Tripod Frequencies (Hz)	Jacket Frequencies (Hz)
1st Tower Side-to-Side	0.309	0.314
1st Tower Fore-Aft	0.311	0.317
1st Blade Asymetric Flapwise Yaw	0.645	0.640
1st Blade Asymetric Flapwise Pitch	0.677	0.675
1st Blade Collective Flap	0.710	0.708
1st Blade Asymetric Edgewise Pitch	1.081	1.080
1st Blade Asymetric Edgewise Yaw	1.097	1.092
2nd Blade Asymetric Flapwise Yaw	1.749	1.714
2nd Blade Asymetric Flapwise Pitch	1.848	1.937
2nd Blade Collective Flap	1.996	2.003
2nd Tower Fore-Aft	2.206	1.219
2nd Tower Side-to-Side	2.277	1.241

The hydrodynamic loading on the structural members is computed based on Morison's equation [70], with drag and inertia coefficients set according to DNV recommendations [17]; the wave process is generated with the JONSWAP spectrum [68]:

$$S_{JS}(f) = \alpha_2 H_s^2 T_p \left(\frac{f}{f_p}\right)^{-5} \exp\left[-1.25\left(\frac{f}{f_p}\right)^{-4}\right] \cdot \gamma^{\beta} \tag{4.2}$$

where $f_p = 1/T_p$, γ is the JONSWAP peakedness parameter [15]

$$\gamma = \begin{cases} 5 & T_p \Big/ \sqrt{H_s} \le 3.6 \\ \exp\left(5.75 - 1.15 T_p \Big/ \sqrt{H_s}\right) & 3.6 \le T_p \Big/ \sqrt{H_s} \le 5.0 \\ 1 & T_p \Big/ \sqrt{H_s} \le 5.0 \end{cases} \tag{4.3}$$

and

$$\alpha_2 = \frac{0.0624}{0.230 + 0.0336\gamma - \dfrac{0.185}{1.9 + \gamma}} \quad \beta = \exp\left[-\frac{0.5}{\sigma^2}\left(\frac{f}{f_p} - 1 \right)^2 \right] \quad \sigma = \begin{cases} 0.07 & f \le f_p \\ 0.09 & f > f_p \end{cases} \tag{4.4}$$

Wind and waves are assumed to act in the *x* direction , and wind loads acting along the tower are included. Earthquake ground motion is modelled as an acceleration at the base with two horizontal components in *x* and *y* directions (see Figure 4.1).

In GH BLADED [35], the equations of motion are derived based on a multi-body dynamics approach combined with a modal representation of the flexible components, like blades and support structure. Within this framework, large displacements of the rotor with respect to the support structure are accounted for. The equations of motion are numerically integrated in the time-domain by the Runge-Kutta method, using a variable step size.

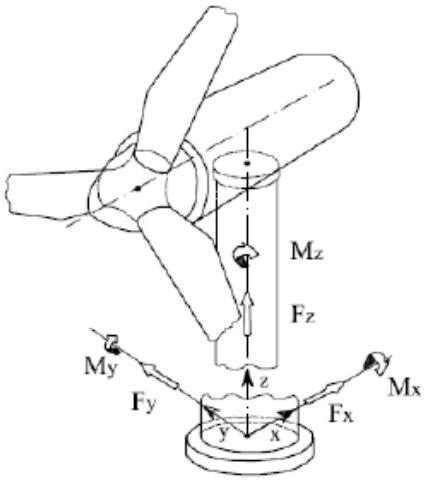

Figure 4.1: Sign convention for stress resultant at the tower base.

4.3. Comparison between uncoupled and fully-couple analysis

Comparisons between combination of uncoupled analyses and fully-coupled simulation are made for earthquake striking in operational conditions, i.e. while the rotor is spinning. Both coupled and uncoupled analyses are implemented in the time domain, using GH BLADED [35] as follows.

Fully-coupled, nonlinear time-domain simulations are carried out by numerical integration of motion equations, considering mutual interactions of aerodynamic, hydrodynamic and seismic responses.

That is, aerodynamic loads on the rotor blades are built taking into account blades motion due to global rotor motion and blades flexibility, as induced by wind loads, wave loads and earthquake shaking at the base, control system etc.. The total simulation length is 600 s, with the ground motion starting at t_0 = 400 s into the simulation, to ensure that the earthquake occurs as the system response has already attained a steady state [49,50].

In the uncoupled analyses, the separate responses to wind only, wave only and earthquake only are computed and then linearly combined. For wind excitation the rotor is spinning, while for wave and earthquake excitations the rotor is considered in a parked state. Aerodynamic damping is considered when computing the separate response to earthquake only. In particular, consistently with numerical evidence on the seismic response of land-based HAWTs [49,88], the additional aerodynamic damping is included in the first two FA support structure modes, by suitably increasing the structural modal damping, equal to 10^{-2}, assumed for the support structure modes (see paragraph 4.2).

The simulation length for wind and wave excitations is 600 s, i.e. identical to the length of the fully-coupled simulation, while the simulation length for earthquake excitation is 200 s, well longer than the duration of the earthquake records considered in this study. The three separate responses are linearly combined, summing the earthquake response, the wave response and the wind response from the time instant at which the earthquake occurs in the fully-coupled simulation, i.e. t_0 = 400 s. The maxima SRSS bending-moment and shear-force at the tower base, encountered after t_0 = 400 s, are computed from the combined response, and compared with the corresponding value from the fully-coupled, nonlinear time-domain simulation, estimating the following errors:

$$M_r \quad error = \left(\frac{M_r - \bar{M}_r}{M_r} \right) \qquad F_r \quad error = \left(\frac{F_r - \bar{F}_r}{F_r} \right) \tag{4.5}$$

$$Total \quad error = \left| \left(\frac{M_r - \bar{M}_r}{M_r} \right) \right| + \left| \left(\frac{F_r - \bar{F}_r}{F_r} \right) \right| \tag{4.6}$$

In Eqs.(4.5) – (4.6) , M_r and F_r are the maxima SRSS bending-moment and shear-force at the tower base obtained from the fully-coupled simulation, while $\bar{M}_r$ and $\bar{F}_r$ are the corresponding quantities from the combination of uncoupled analyses (subscripts *x* and *y* correspond to FA and SS directions in Figure 4.1, respectively):

$$M_r = \sqrt{M_x^2 + M_y^2} \qquad F_r = \sqrt{F_x^2 + F_y^2} \tag{4.7}$$

$$\bar{M}_r = \sqrt{\bar{M}_x^2 + \bar{M}_y^2} \qquad \bar{F}_r = \sqrt{\bar{F}_x^2 + \bar{F}_y^2} \tag{4.8}$$

Uncoupled analyses will be implemented for various potential values of aerodynamic damping, and the comparison with the fully-coupled simulation will be carried out considering either error (4.5) or error (4.6). Comparisons of demands along the tower will also be made, as explained next.

4.4. Numerical results

Three real earthquake records, three wind velocities at the hub and two sea state are considered, as in Table 4.2 .

The earthquake records are chosen as they feature different peak ground acceleration and quite different frequency content [93], see Figure 4.2 showing the pseudo spectral acceleration (PSA) spectrum as available in ref. [93]; horizontal components *x* and *y* coincide with first and second columns in the source files available in ref. [93].

The wind velocities are representative of potential operational states, within the cut-in-cut- out wind velocity range of the NREL 5MW HAWT, as reported in [53]. For each velocity, 5 wind samples are generated considering 5 different seeds, to account for the inherent stochastic nature of the wind process. Wind samples are generated based on the

Kaimal spectrum (4.1), assuming medium turbulence characteristics. In particular, all parameters in Eq.(4.1) are set according to IEC 61400-1 prescriptions for a normal turbulence model [40].

The wave periods T_p and significant wave height H_s have been chosen as those associated with the selected wind speeds V_{hub} in typical offshore environmental states, as for instance some encountered in the Pacific Ocean [66]. For each sea state, 3 samples are generated considering 3 different seed, to account the stochastic nature of the sea state process.

Table 4.2: Earthquake, wind velocities and sea state.

Wind, wave and earthquake loading			
Earthquake record	Year	Station	PGA
Cape Mendocino	1992	Petrolia	6.12
Imperial Valley-06	1979	E.C. #3	2.44
Northridge	1994	P. D. d.	3.43
Wind velocities at the hub, V	Number of wind samples #		
11.4 m/s	5		
15 m/s	5		
20 m/s	5		
Sea state	Number of sea state samples #		
H_s = 5m , T_p = 9.5 s	3		
H_s = 6m , T_p = 11.0 s	3		

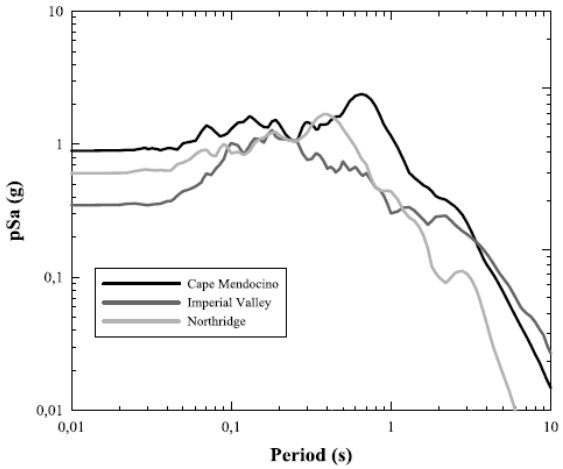

Figure 4.2: Pseudo Spectral acceleration of earthquake records in Table 4.2.

For the earthquake records, wind velocities *V* and significant wave height *Hs* in Table 4.2, Figure 4.3-Figure 4.5 show the errors (4.5)-(4.6) for tripod support structures while Figure 4.11-Figure 4.13 show the results for jacket support structures, as potential values of aerodynamic damping vary within the interval 0-6% at steps equal to 0.5%. In particular, 3x12=36 simulations have been run to compute the separate earthquake response for all potential aerodynamic damping values (3 ground motions, 12=6/0.5 potential aerodynamic damping values), 3x5=15 simulations to compute the separate wind response (5 samples for each of the 3 wind velocities), 2x3=6 simulations to compute the separate wave response (3 samples for each of the 2 sea states), 3x3x5x2x3= 270 fully-coupled simulations (3 ground motions, 5 samples for each of the 3 wind velocities and 3 samples for each of the 2 sea states), totaling 327 simulations for each support structures. Figure 4.3-Figure 4.5 reports the results of a few only, for brevity.

The results in Figure 4.3-Figure 4.5 vary with earthquake records, wind velocities and samples of wind simulation and sea state and sample of sea simulation. It is observed that, in most cases, an aerodynamic damping value capable of minimizing the total error (4.6) may be found. Typically, these are the cases in which either the "*Fr* error", or both "*Fr* error" and "*Mr* error", start from negative values for the lowest aerodynamic damping 0.5% and progressively tend to zero as the aerodynamic damping increases. That is, the combination of uncoupled analyses provides larger demands than the fully-coupled simulation for the lowest aerodynamic damping 0.5% ("*Mr* error" < 0 means $\bar{M}_r > Mr$, "*Fr* error" < 0 means $\bar{F}_r > Fr$), and progressively approaches the fully-coupled simulation with increasing aerodynamic damping. However, there may also be cases in which no minimum is found for the total error (4.6). In general, this occurs when both "*Mr* error" (4.5a) and "*Fr* error" (4.5b) start from positive values for the lowest aerodynamic damping 0.5%, and monotonically increase as aerodynamic damping increases. In these cases, $\bar{M}_r$ and $\bar{F}_r$ from the combination of uncoupled analyses are always smaller than *Mr* and *Fr* from fully-coupled simulation, regardless of the aerodynamic damping values. Such result is not surprising, since previous work in ref. [92] had already shown that the combination of separate wind and earthquake responses, the latter being computed with the inclusion of aerodynamic damping, may provide smaller bending-moment demands with respect to fully-coupled simulations [92] (no results are reported in ref. [92] on shear-force demands), and is explained considering that any aerodynamic damping based approach is, indeed, an approximate approach to account for the inherently nonlinear interaction between

aerodynamic and seismic responses (for instance, see Fig. 13 in ref. [92]). At any rate, based on the results in Figure 4.3-Figure 4.5, it can be concluded that an aerodynamic damping level minimizing the difference between fully-coupled simulation and combination of uncoupled analyses, in terms of the total error (4.6) involving both bending-moment and shear-force demands at the tower base, cannot exist for all ground motions and wind samples in Table 4.2.

Once it is established that such an aerodynamic damping value cannot exist, attention is focused on bending-moment and shear-force errors (4.5) at the tower base when, in the combination of uncoupled analyses, the separate earthquake response is built with a 4% aerodynamic damping. Figure 4.6-Figure 4.8 show that errors (4.5) are generally below 10%, with two maxima values almost equal to 15%, for the Cape Mendocino and Imperial Valley ground motions, wind and wave samples. For the Northridge earthquake, the errors (4.5) are generally around until 15%, for all environmental states, with three maxima values almost equal to 25%. The errors can be considered acceptable from an engineering point of view, and in agreement with errors encountered in alternative formulations of uncoupled analyses in the literature, as for instance the SRSS combination of separate wind and earthquake responses computed by the IEC method [50], which provide errors up to 20% depending on the PSA (see Figure 8.11 in ref. [50]). Also, as earlier mentioned, the fact that errors (4.5) may be negative or positive appears consistent with previous results in ref. [50, 92], which showed that the combination of uncoupled analyses does not necessarily provides always conservative results with respect to fully-coupled simulation (see Figure 8.11 in ref. [50] or Fig. 13 in ref. [92]).

For a further validation of the results obtained with a 4% aerodynamic damping, Figure 4.9-Figure 4.10 show the mean of SRSS bending-moment and shear-force demands along the tower, as computed by the combination of uncoupled analyses and fully-coupled simulation. For each wind velocity, wave height and ground motion, the mean is obtained by averaging the demands from all wind and wave realizations. Errors in Figure 4.9-Figure 4.10 can generally be considered within engineering margins along the whole tower. It is interesting to remark that the errors in the mean bending-moment demands in Figure 4.9-Figure 4.10 are similar to those obtained by Asareh and Prowell [92] for the land-based wind turbine, who used a 0.75 combination factor to combine the operational wind demand and the earthquake demand computed with a 4% aerodynamic damping.

TRIPOD

a)

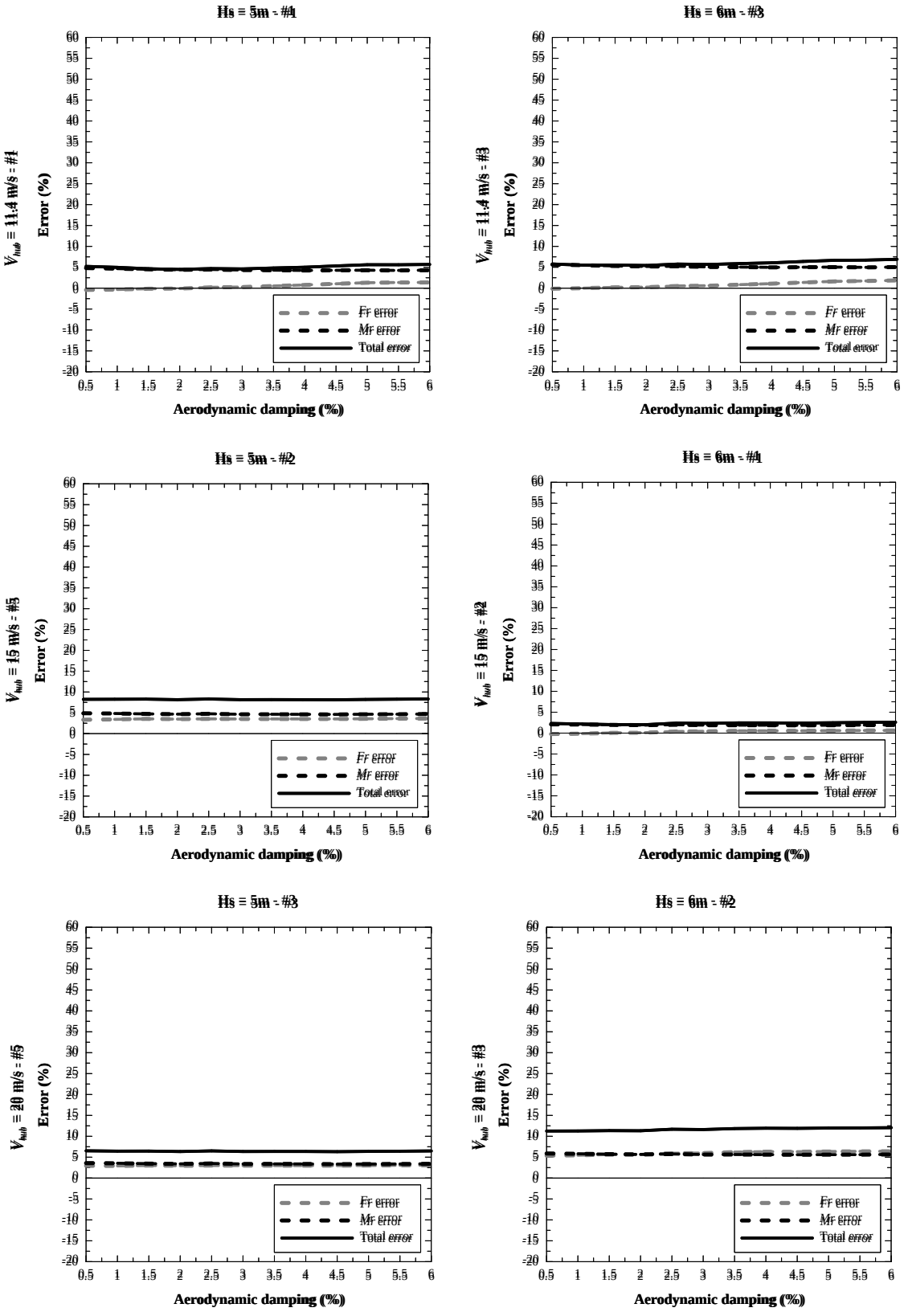
Hs = 5m - #1
Hs = 6m - #3
Hs = 5m - #2
Hs = 6m - #1
Hs = 5m - #3
Hs = 6m - #2
Vhub = 11.4 m/s - #1
Vhub = 11.4 m/s - #3
Vhub = 15 m/s - #5
Vhub = 15 m/s - #2
Vhub = 20 m/s - #5
Vhub = 20 m/s - #3
Error (%)
Aerodynamic damping (%)
Fr error
Mr error
Total error

TRIPOD

b)

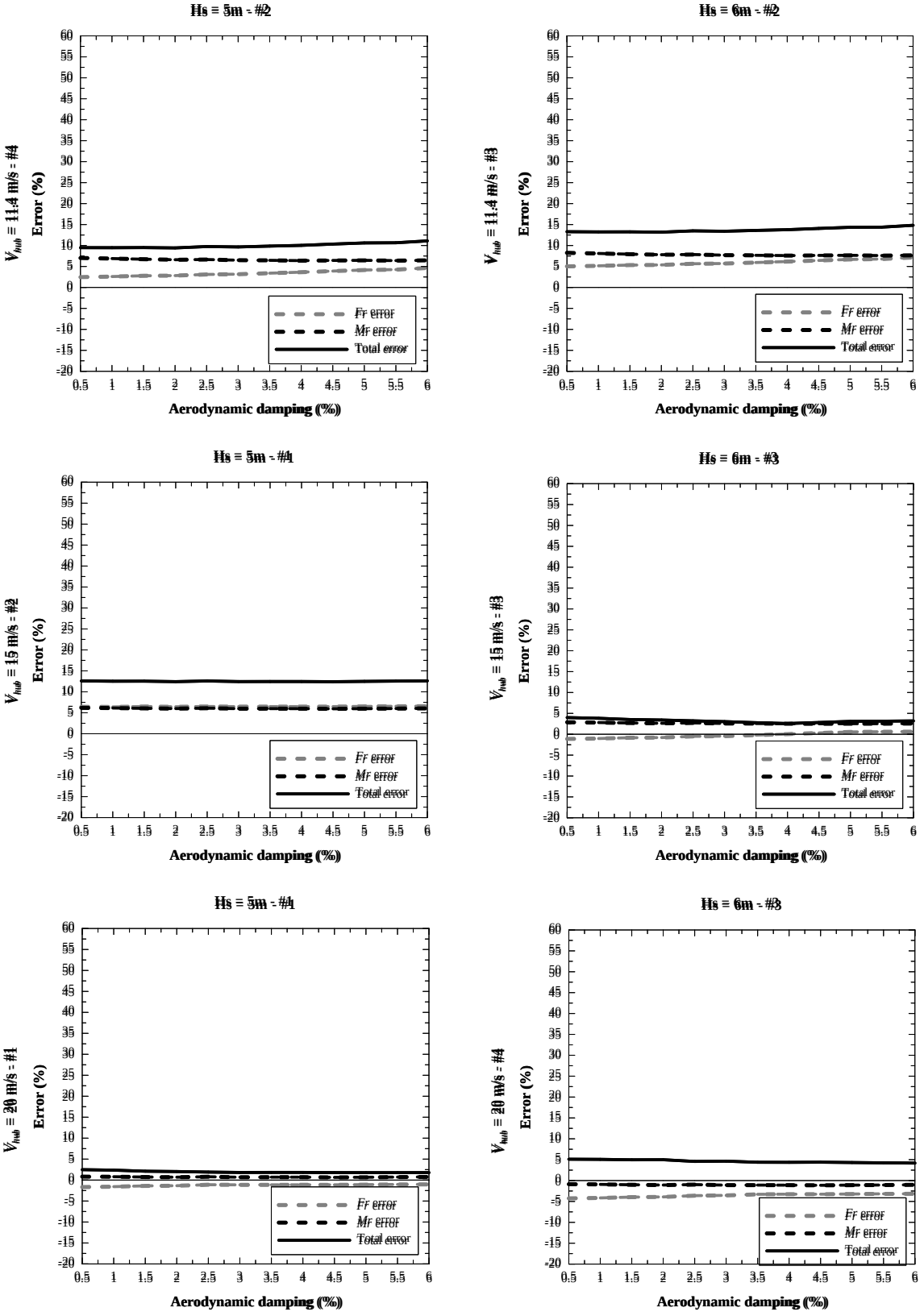

Figure 4.3 a)-b): Tripod: Errors (4.5)-(4.6) for various potential aerodynamic damping values, under Cape Mendocino earthquake.

TRIPOD

a)

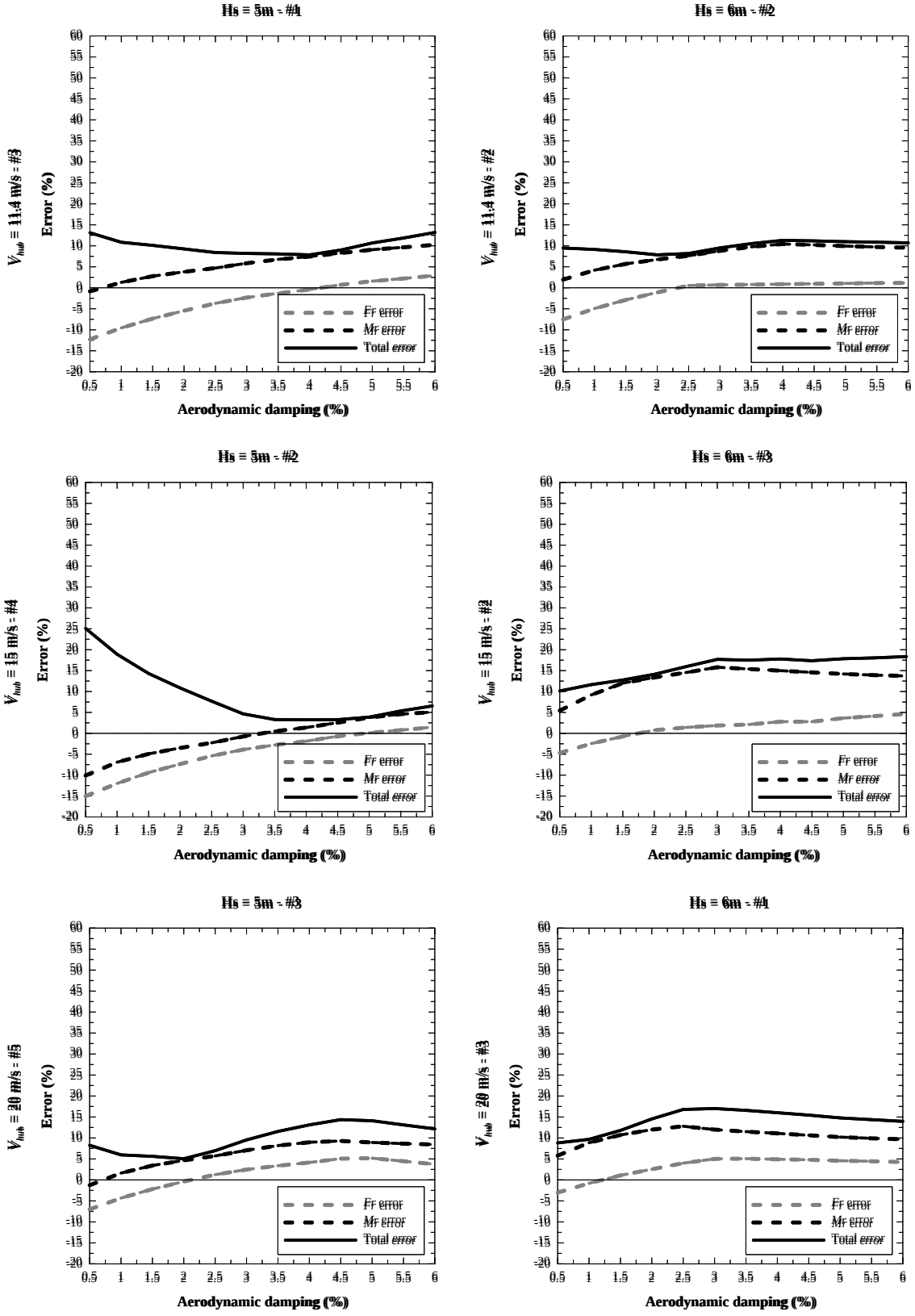
Hs = 5m - #1
Hs = 6m - #2
Hs = 5m - #2
Hs = 6m - #3
Hs = 5m - #3
Hs = 6m - #1
V_hub = 11.4 m/s - #3
V_hub = 11.4 m/s - #2
V_hub = 15 m/s - #4
V_hub = 15 m/s - #2
V_hub = 20 m/s - #5
V_hub = 20 m/s - #3
Error (%)
Aerodynamic damping (%)
Fr error
Mr error
Total error

TRIPOD

b)

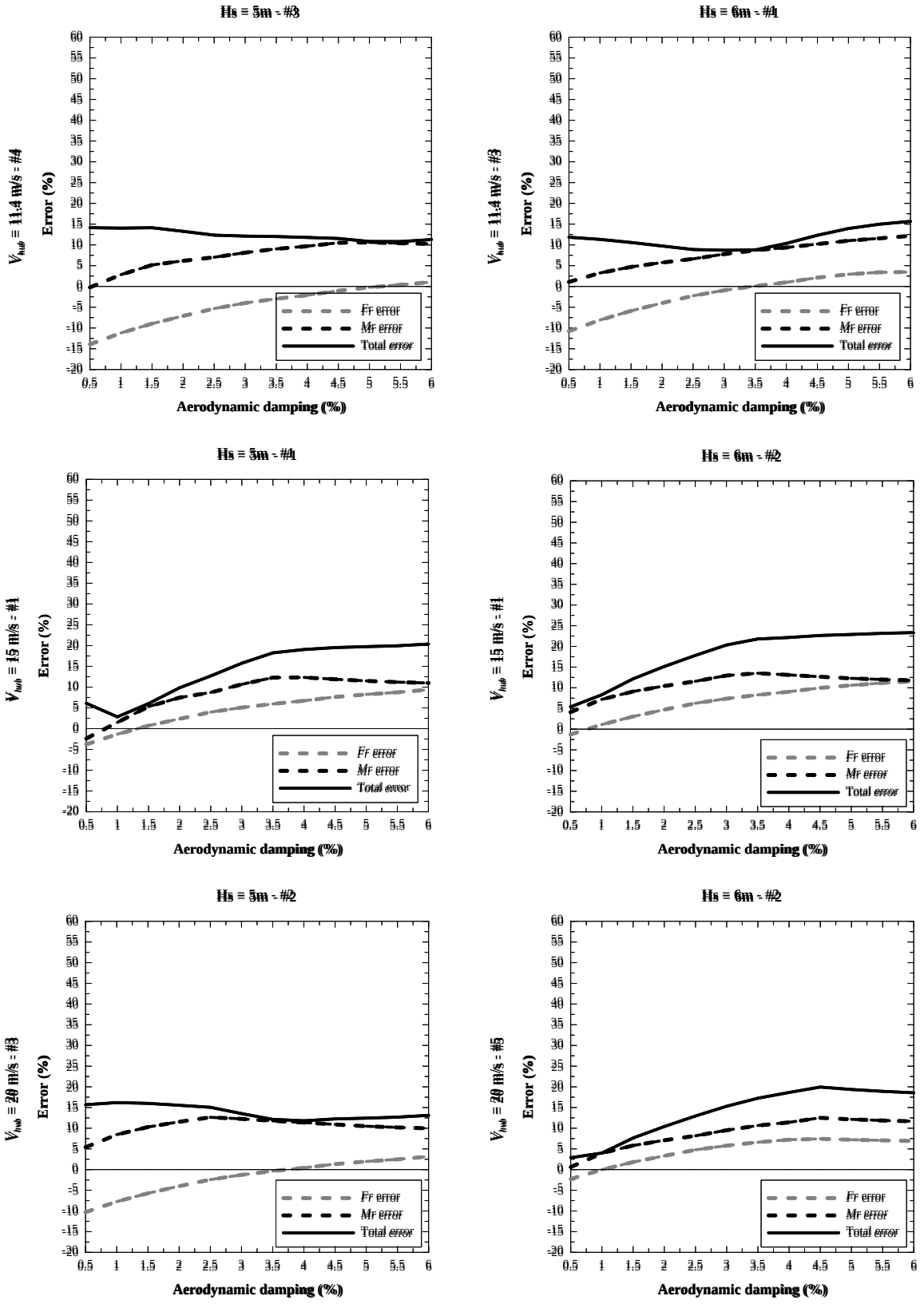

Figure 4.4 a)-b): Tripod: Errors (4.5)-(4.6) for various potential aerodynamic damping values, under Imperial Valley earthquake.

TRIPOD

a)

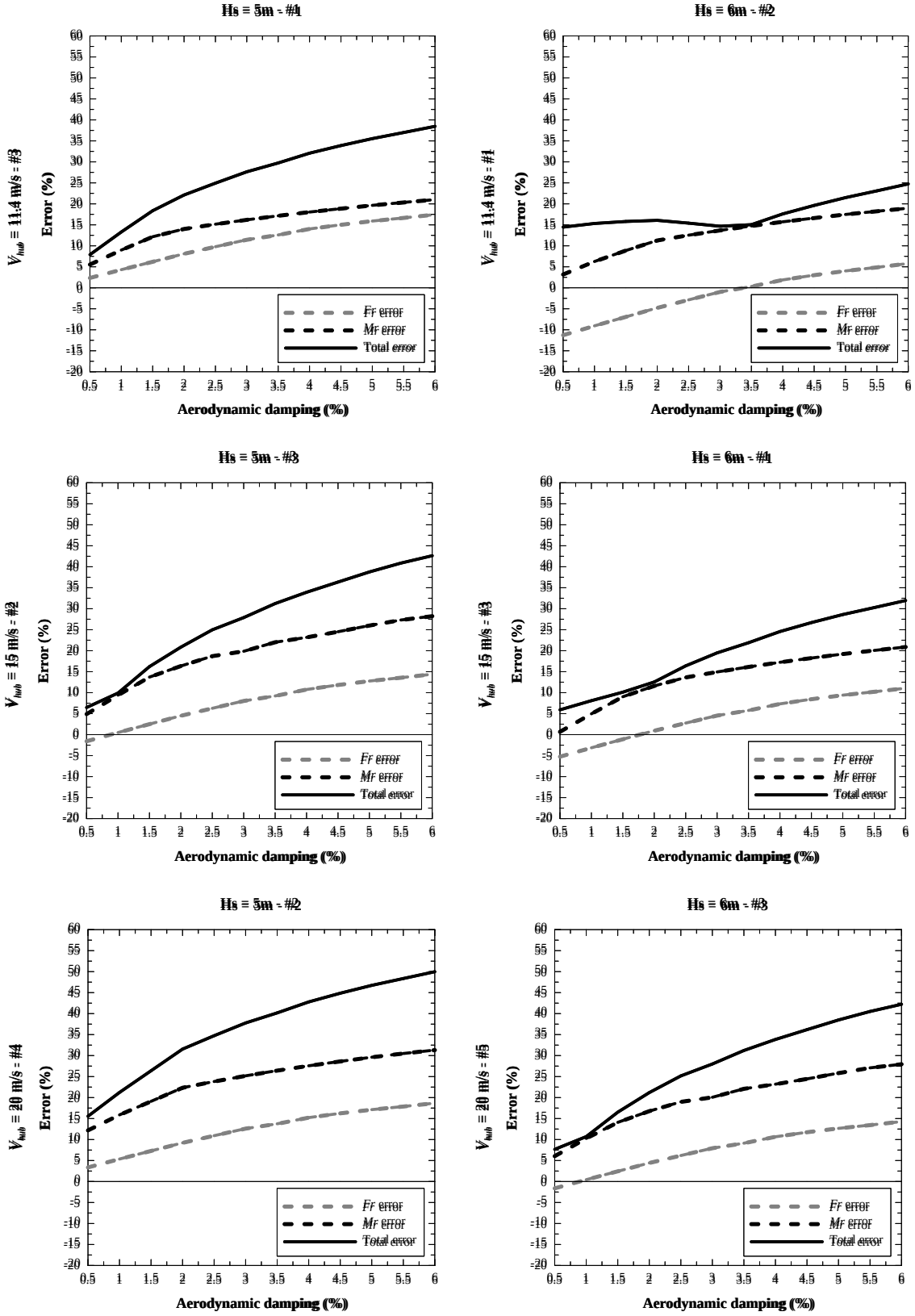
Hs = 5m - #1
Hs = 6m - #2
Hs = 5m - #3
Hs = 6m - #1
Hs = 5m - #2
Hs = 6m - #3
V_hub = 11.4 m/s - #3
V_hub = 11.4 m/s - #1
V_hub = 15 m/s - #2
V_hub = 15 m/s - #3
V_hub = 20 m/s - #4
V_hub = 20 m/s - #5
Error (%)
Aerodynamic damping (%)
Ff error
Mf error
Total error

TRIPOD

b)

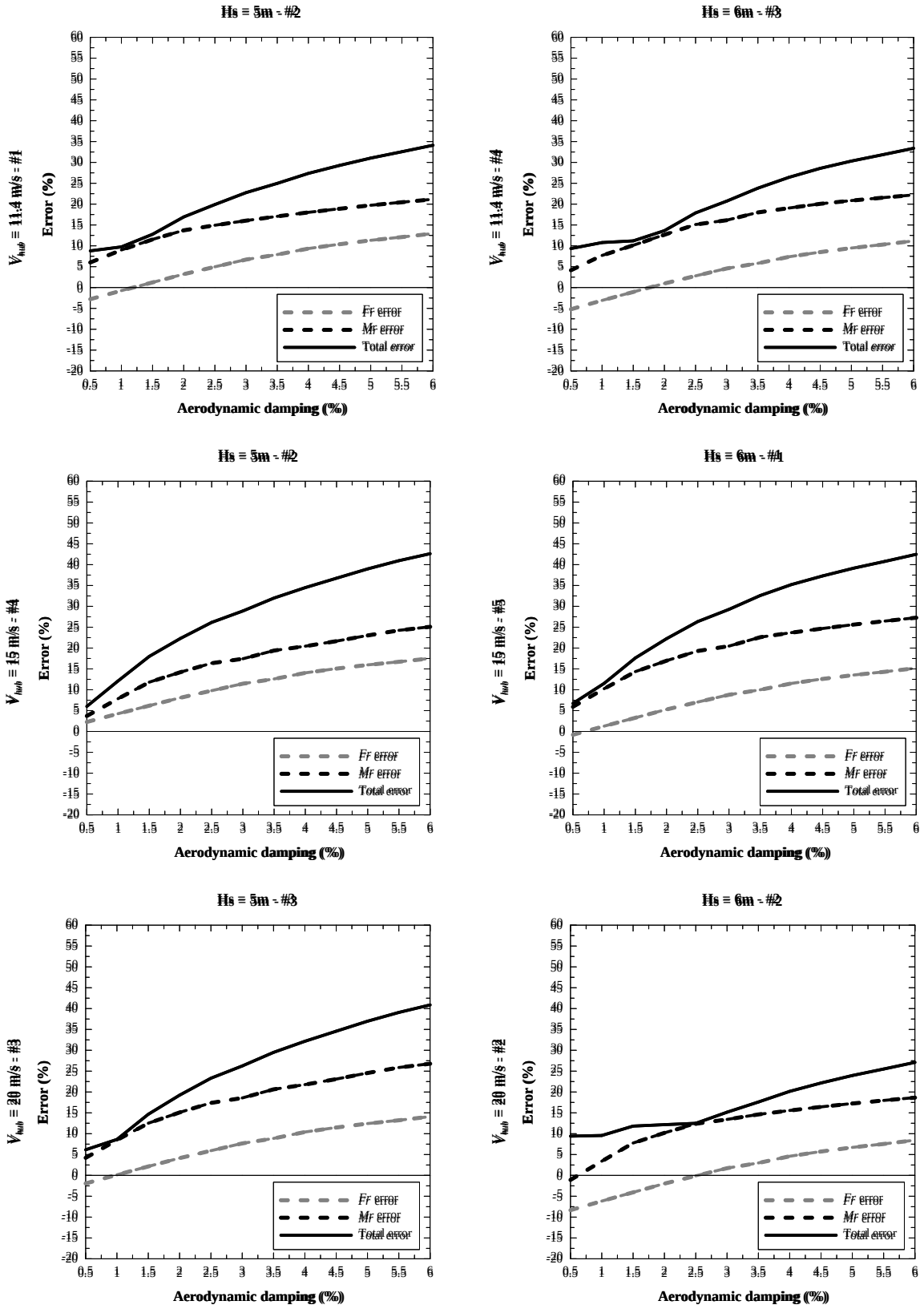

Figure 4.5 a)-b): Tripod: Errors (4.5)-(4.6) for various potential aerodynamic damping values, under Northridge earthquake.

TRIPOD

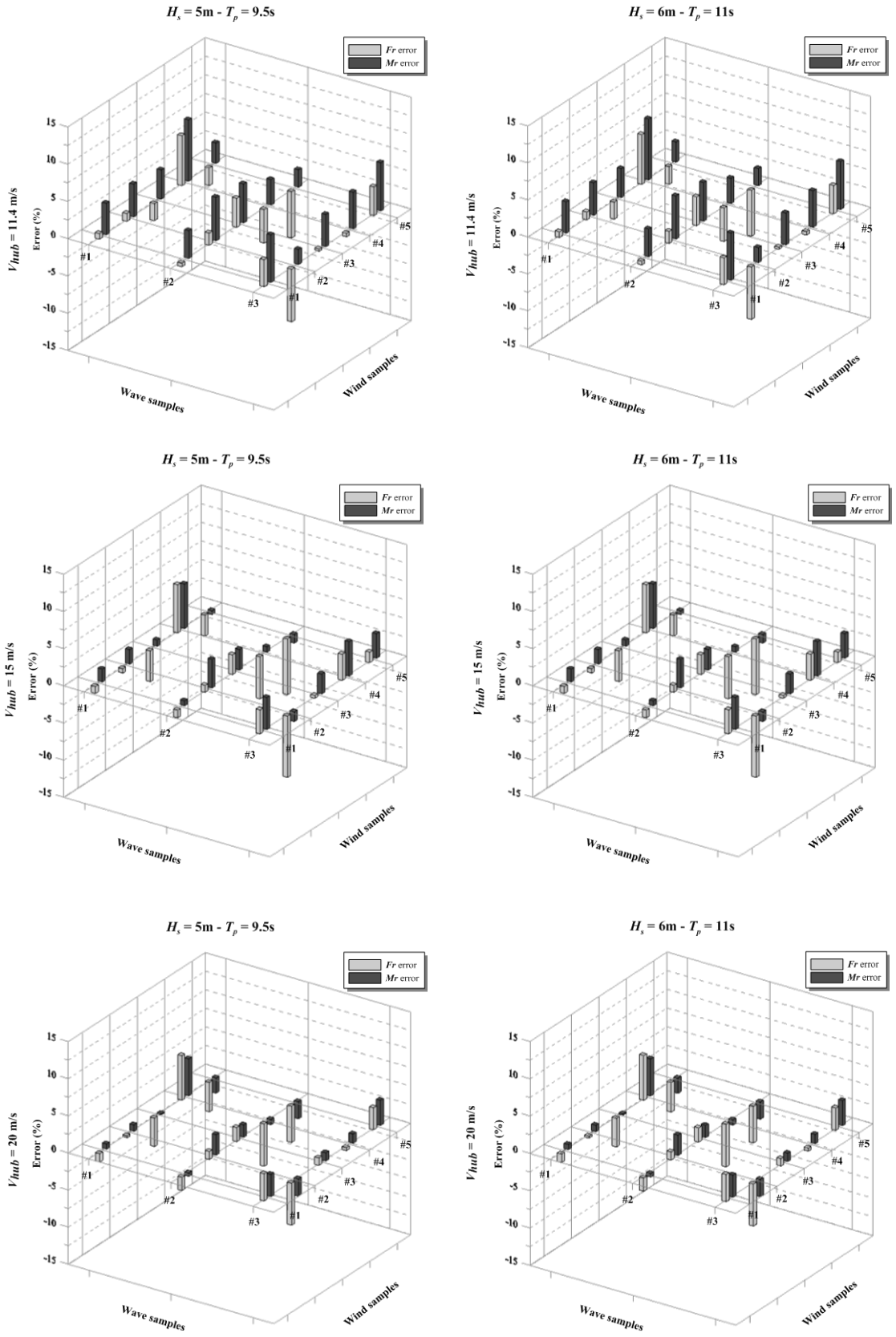

Figure 4.6: Tripod: Errors (4.5) for 4% aerodynamic damping, under Cape Mendocino earthquake.

TRIPOD

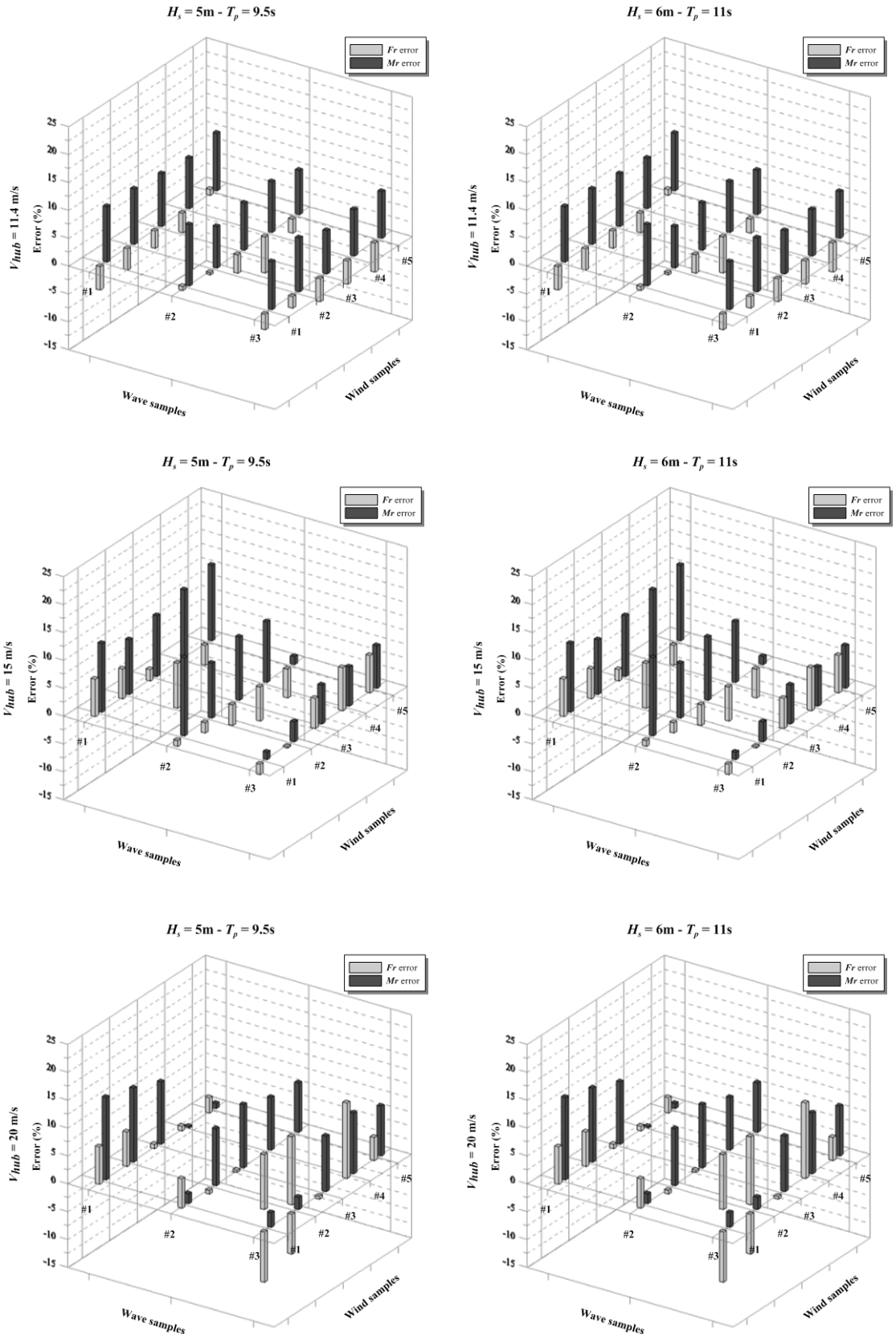

Figure 4.7: Tripod: Errors (4.5) for 4% aerodynamic damping, under Imperial Valley earthquake.

TRIPOD

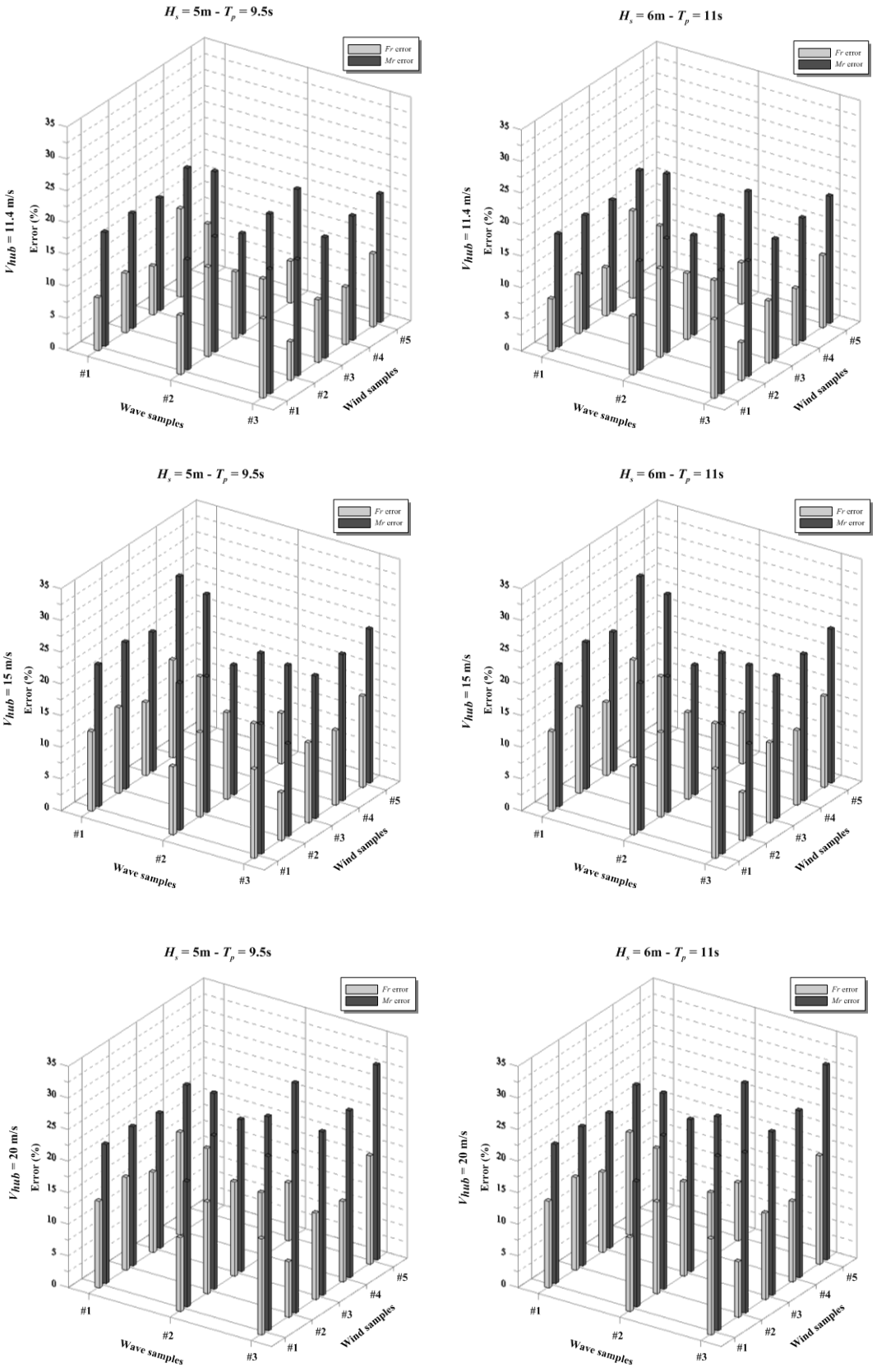

Figure 4.8: Tripod: Errors (4.5) for 4% aerodynamic damping, under Northridge earthquake.

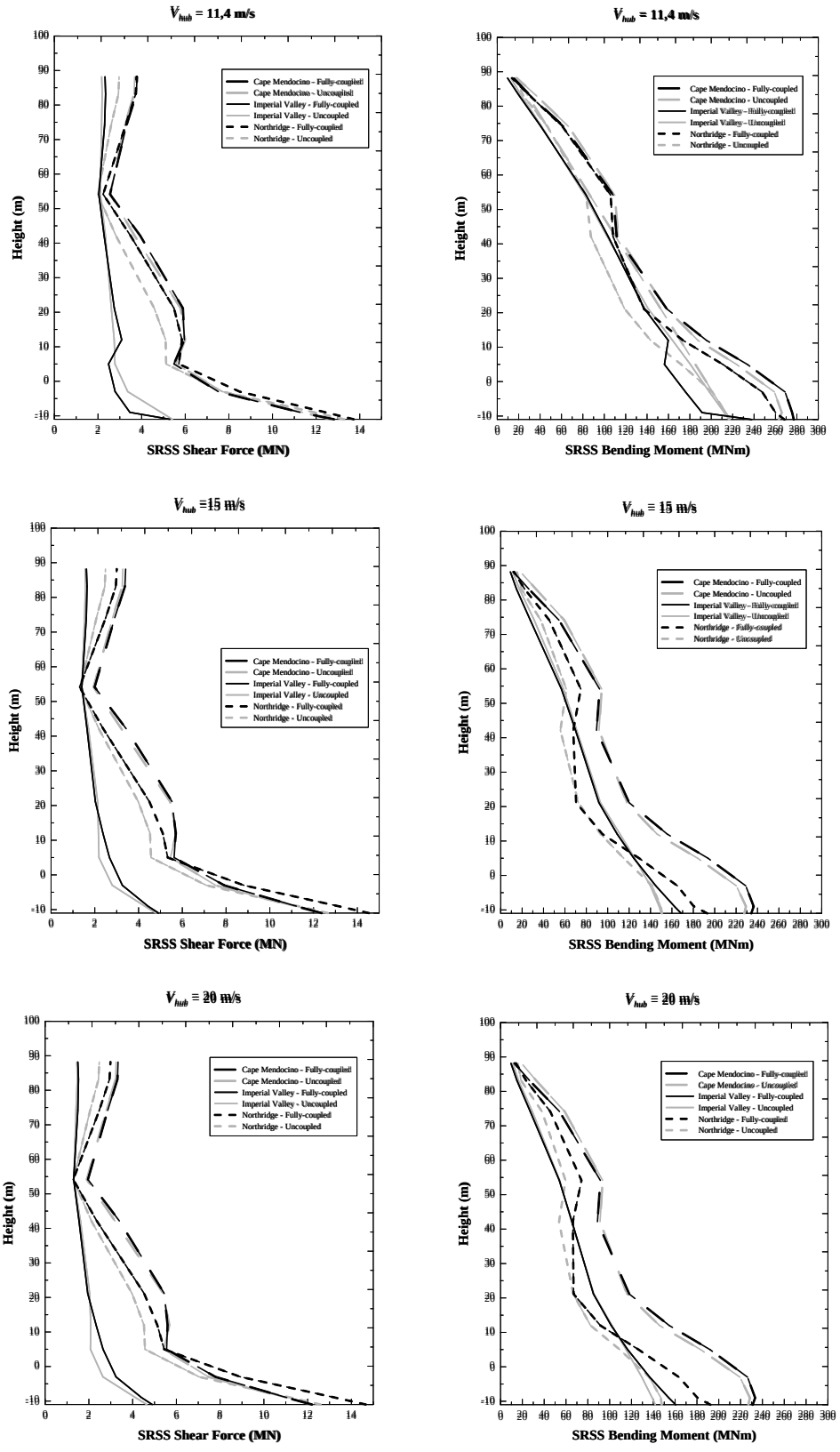

Figure 4.9: Tripod: mean demands along the tower H_s = 5m – T_p = 9.5s.

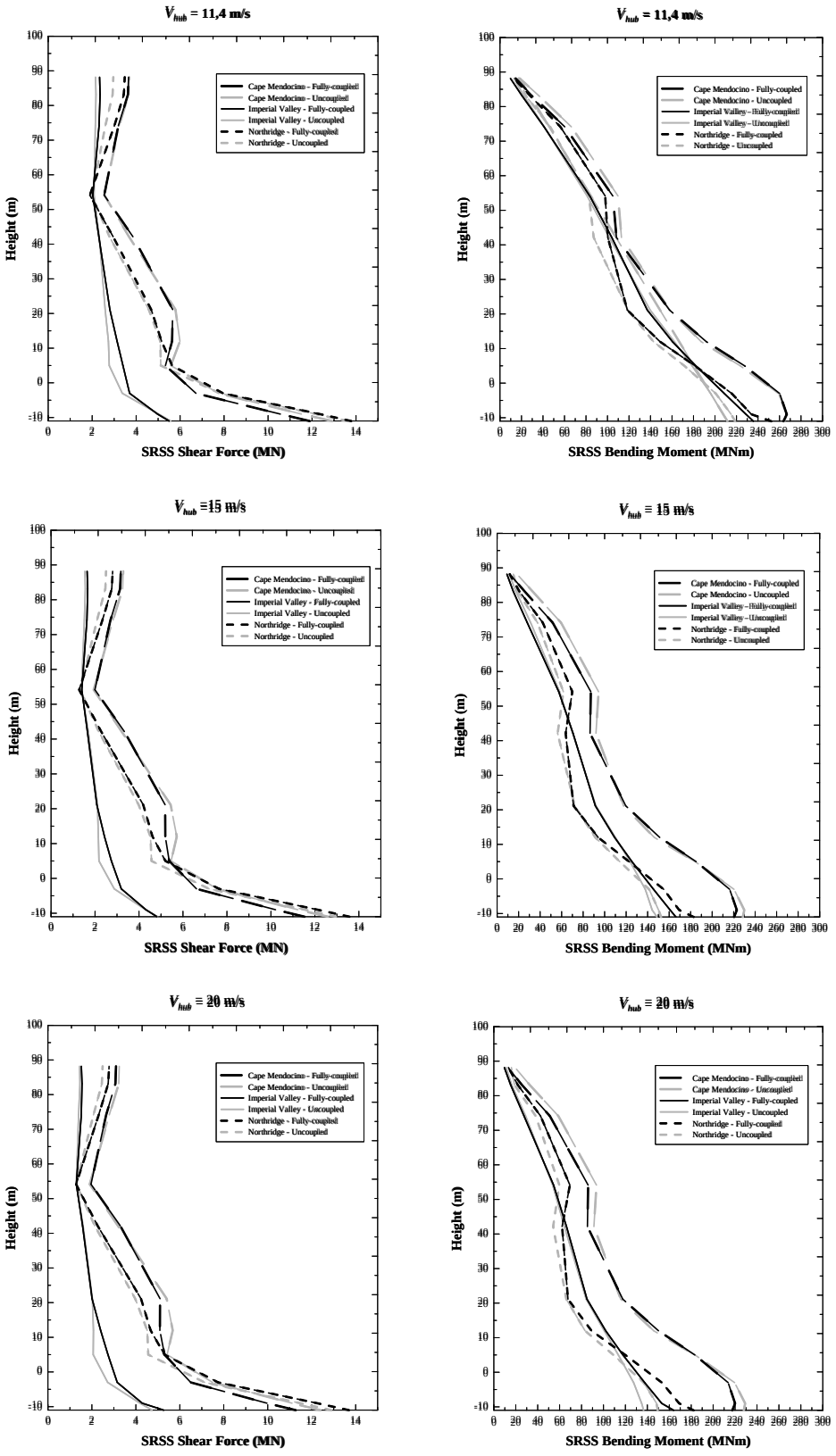

Figure 4.10: Tripod: mean demands along the tower for H_s = 6m – T_p = 11s.

As for the tripod, Figure 4.11-Figure 4.13 show errors (4.5)-(4.6) for the jacket support structures, as potential aerodynamic damping varies within the interval 0-6% at step 0.5%, for the environmental states in Table 4.2 (only few results are reported for brevity). Results mirror those in Figure 4.3-Figure 4.5. In most cases, an aerodynamic damping value minimizing the total error (4.6) may be found, typically when the combination of uncoupled analyses provide larger demands than the fully-coupled simulation for the lowest aerodynamic damping 0.5% (either "F_r error" < 0 means $\bar{F}_r > F_r$, or both "F_r error" and "M_r error" are negative being $\bar{F}_r > F_r$ and $\bar{M}_r > M_r$), and progressively approach the fully-coupled simulation as aerodynamic damping increases. In some cases, however, an aerodynamic damping value minimizing the total error (4.6) is not found, as the combination of uncoupled analyses provide smaller values than the fully-coupled simulation regardless of the aerodynamic damping value. As in the case of tripod support structures, therefore, it shall be concluded that an aerodynamic damping value capable of minimizing the total error (4.6) cannot exist.

Figure 4.14-Figure 4.16 show the shear-force and bending-moment errors (4.5), when a 4% aerodynamic damping is considered to compute the separate earthquake response. Again, results agree with those in Figure 4.6-Figure 4.8 for the tripod support structures. In most cases, errors are generally below 10%, with two maxima values almost equal to 15%, for the Cape Mendocino and Imperial Valley ground motions, wind and wave samples. For the Northridge earthquake, the errors (4.5) are generally around until 15%, for all environmental states, with three maxima values almost equal to 25%. Thus, errors are within the engineering margins encountered in existing combinations of uncoupled analyses, see the SRSS combination of separate wind and earthquake responses computed by the IEC method [50] (Figure 8.11 in ref. [50]). For a further validation, Figure 4.17-Figure 4.18 show the mean SRSS bending-moment and shear-force demands computed over all wind samples for each wind velocity, all wave samples for each sea state and ground motion, as obtained by combination of uncoupled analyses and fully-coupled simulation. Results appear quite accurate along the whole tower. In particular, errors in the mean bending-moment demands agree with those found by Asareh and Prowell in ref. [92] for onshore wind turbines, who used a 0.75 factor to combine the separate operational wind demand and the separate earthquake demand computed with a 4% aerodynamic damping.

At this stage, based on the results for both support structures, it can be concluded that the combination of time-domain uncoupled analyses, with 4% aerodynamic damping in the

separate earthquake response, can provide a reasonable estimate of maxima and mean demands from fully-coupled simulations. It is remarkable that such a level of aerodynamic damping agrees with that recommended by ASCE-AWEA RP2011 [41] for combining uncoupled analyses for land-based HAWTs, where the separate earthquake response is computed by a frequency-domain response spectrum approach. Notice that the same level of aerodynamic damping was also used in previous studies [71, 72, 92].

JACKET

a)

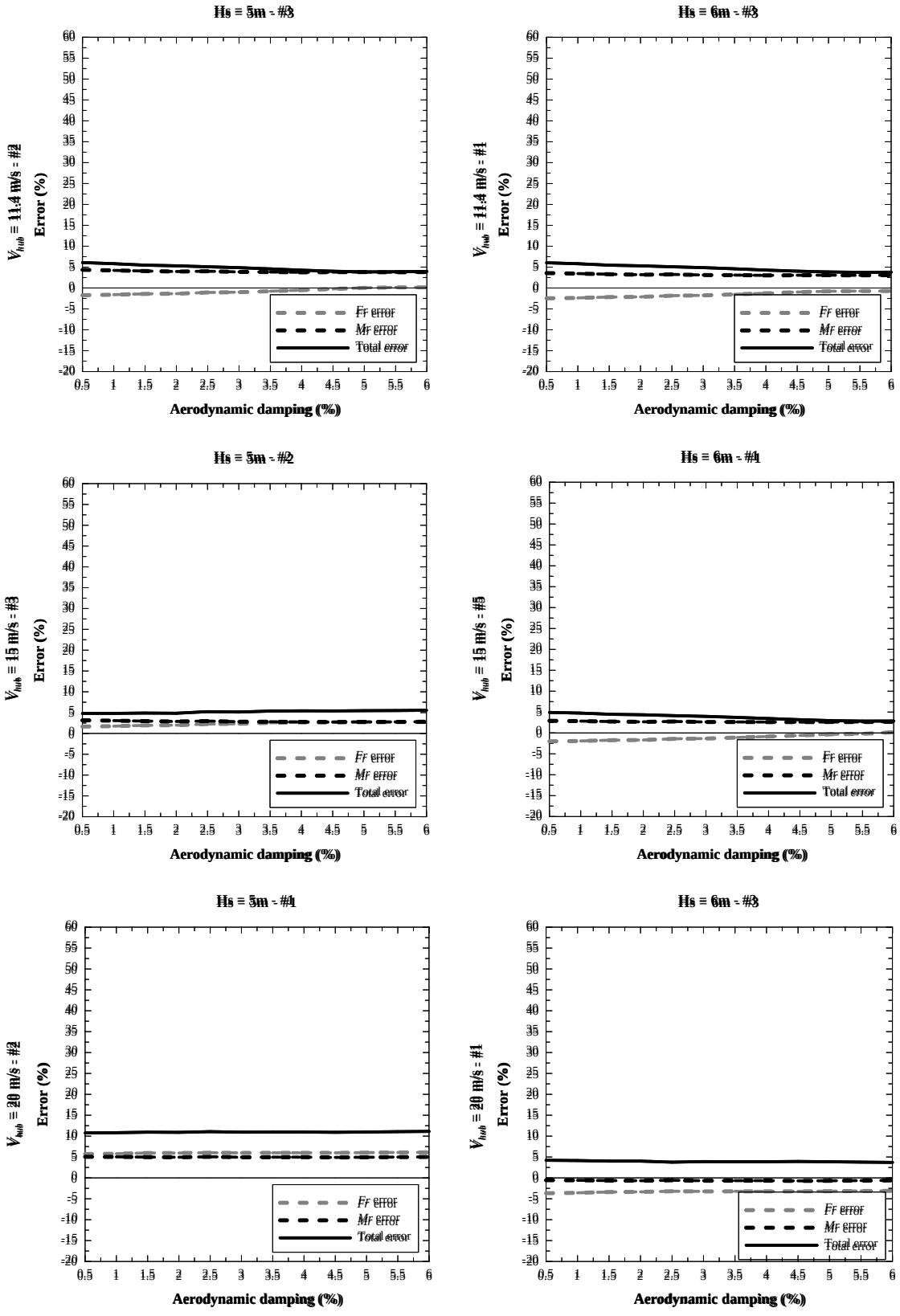
Hs = 5m - #3
Hs = 6m - #3
Hs = 5m - #2
Hs = 6m - #4
Hs = 5m - #1
Hs = 6m - #5
Vhub = 11.4 m/s - #2
Vhub = 11.4 m/s - #1
Vhub = 15 m/s - #3
Vhub = 15 m/s - #5
Vhub = 20 m/s - #2
Vhub = 20 m/s - #1
Error (%)
Aerodynamic damping (%)
Fr error
Mr error
Total error

JACKET

b)

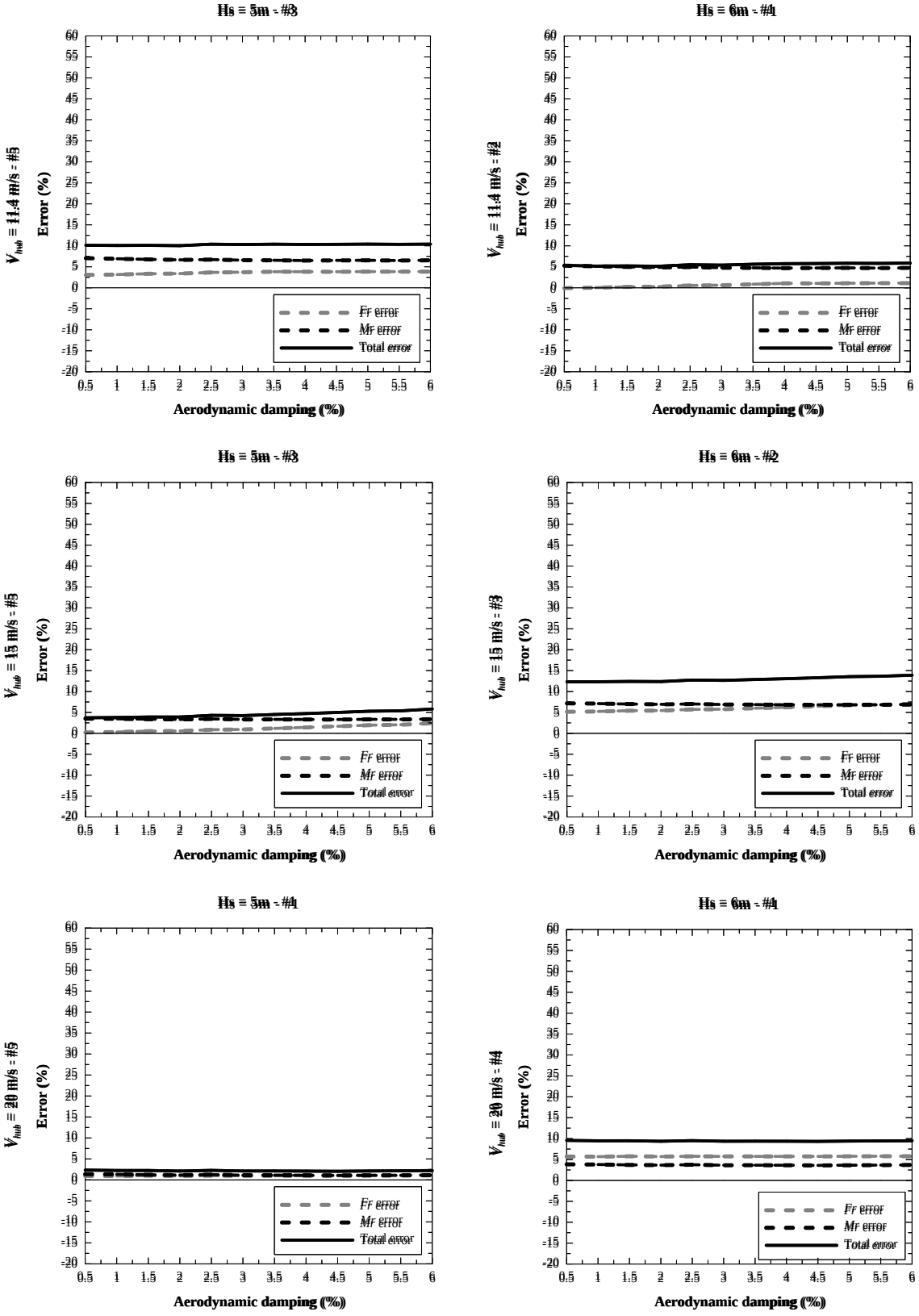

Figure 4.11 a)-b): Jacket: Errors (4.5)-(4.6) for various potential aerodynamic damping values, under Cape Mendocino earthquake.

JACKET

a)

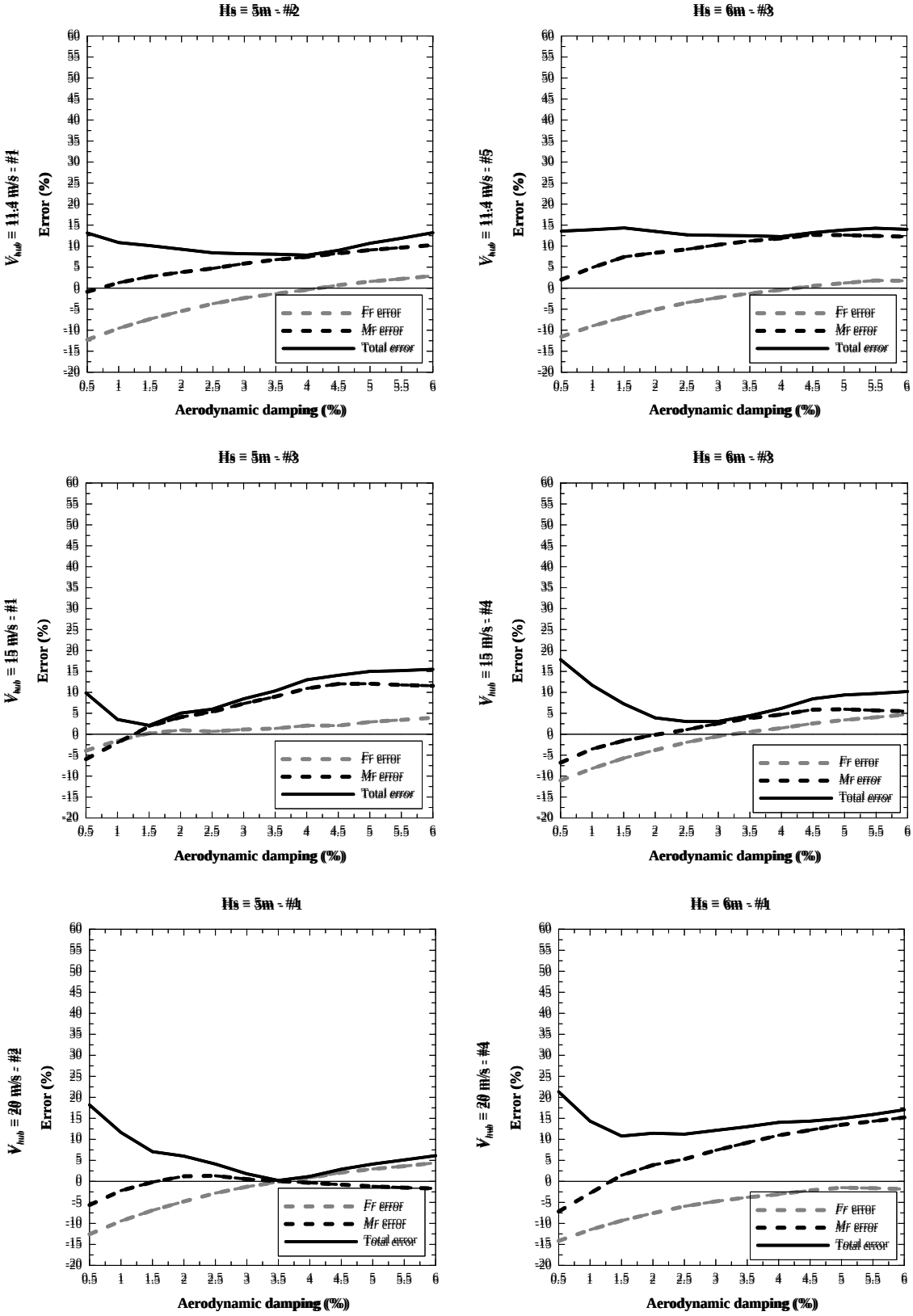
Hs = 5m - #2
Hs = 6m - #3
Hs = 5m - #3
Hs = 6m - #3
Hs = 5m - #1
Hs = 6m - #1
V_hub = 11.4 m/s - #1
V_hub = 11.4 m/s - #5
V_hub = 15 m/s - #1
V_hub = 15 m/s - #4
V_hub = 20 m/s - #2
V_hub = 20 m/s - #4
Error (%)
Aerodynamic damping (%)
Fr error
Mr error
Total error

JACKET

b)

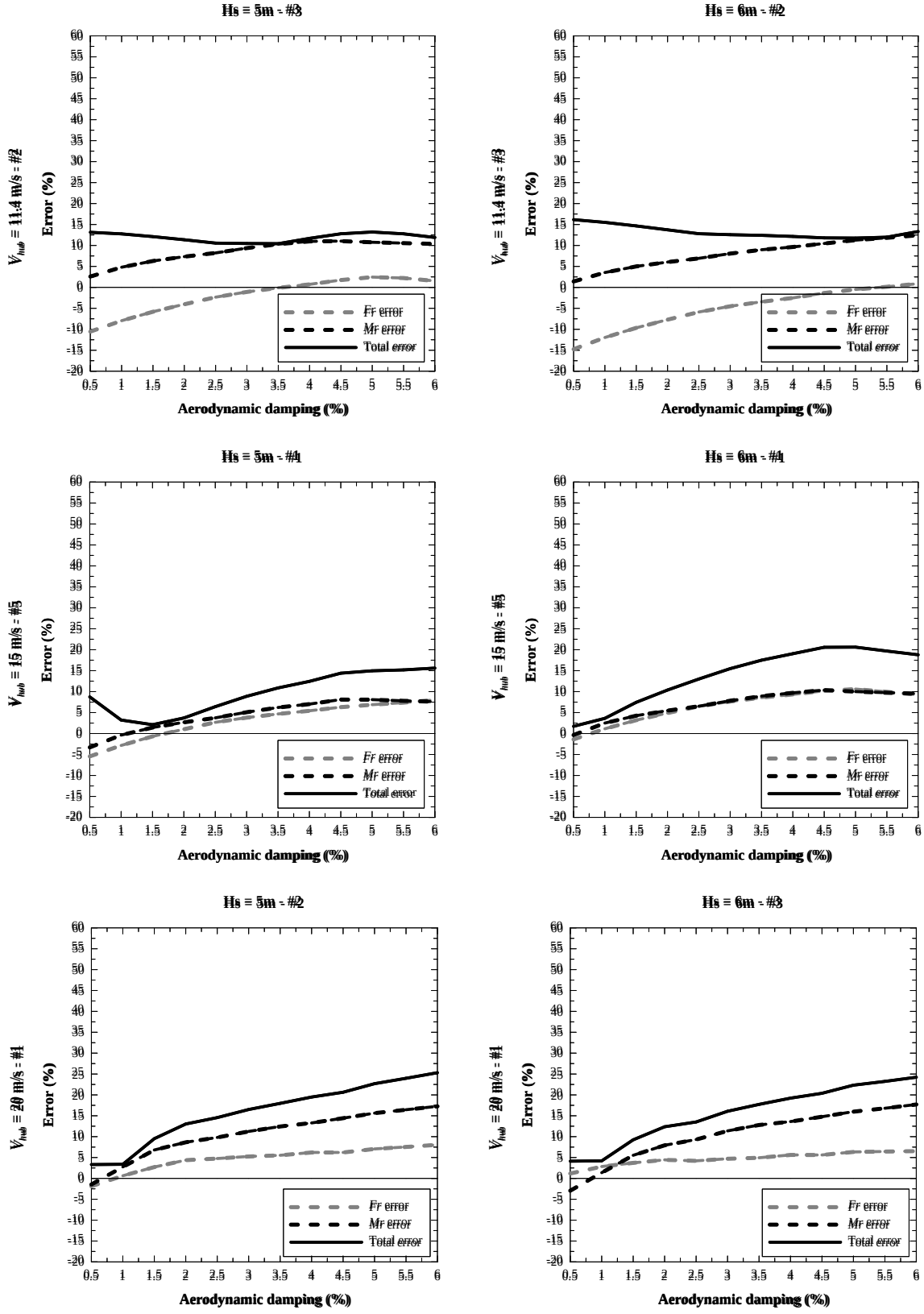

Figure 4.12 a)-b): Jacket: Errors (4.5)-(4.6) for various potential aerodynamic damping values, under Imperial Valley earthquake.

JACKET

a)

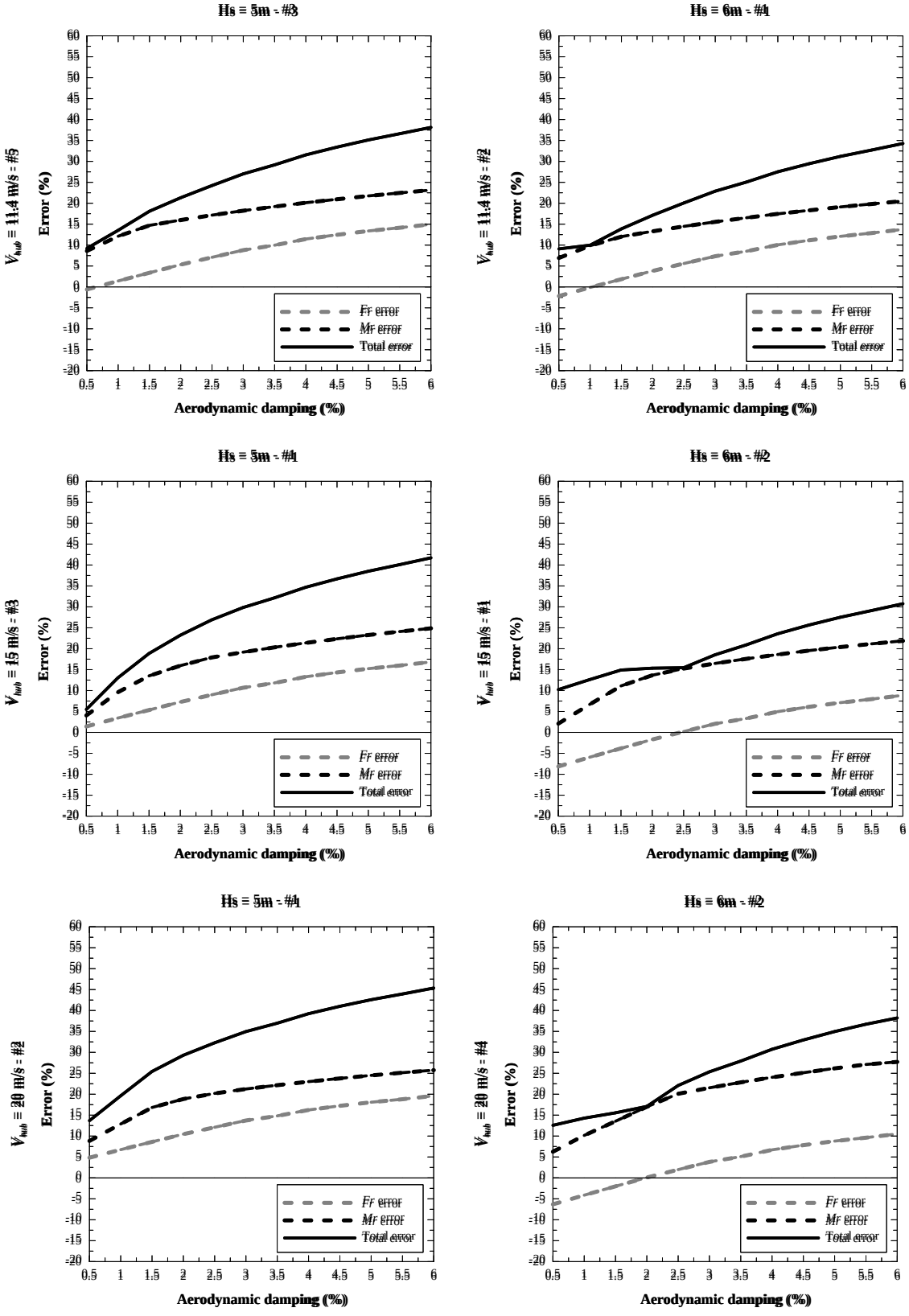
Hs = 5m - #3
Hs = 6m - #1
Hs = 5m - #4
Hs = 6m - #2
Hs = 5m - #1
Hs = 6m - #2
Vhub = 11.4 m/s - #5
Vhub = 11.4 m/s - #2
Vhub = 15 m/s - #3
Vhub = 15 m/s - #1
Vhub = 20 m/s - #2
Vhub = 20 m/s - #4
Error (%)
Aerodynamic damping (%)
Fr error
Mr error
Total error

JACKET

b)

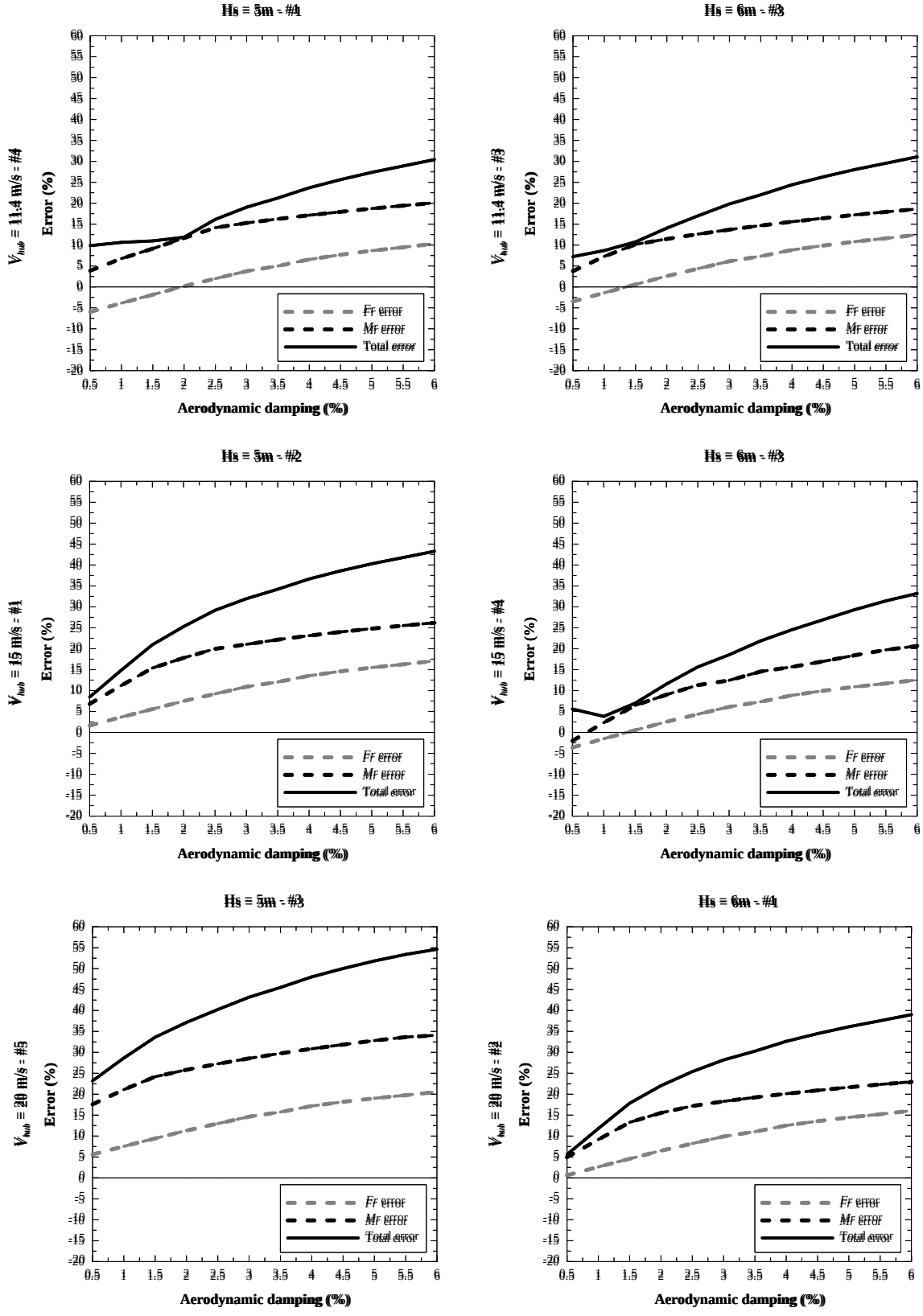

Figure 4.13 a)-b): Jacket: Errors (4.5)-(4.6) for various potential aerodynamic damping values, under Northridge earthquake.

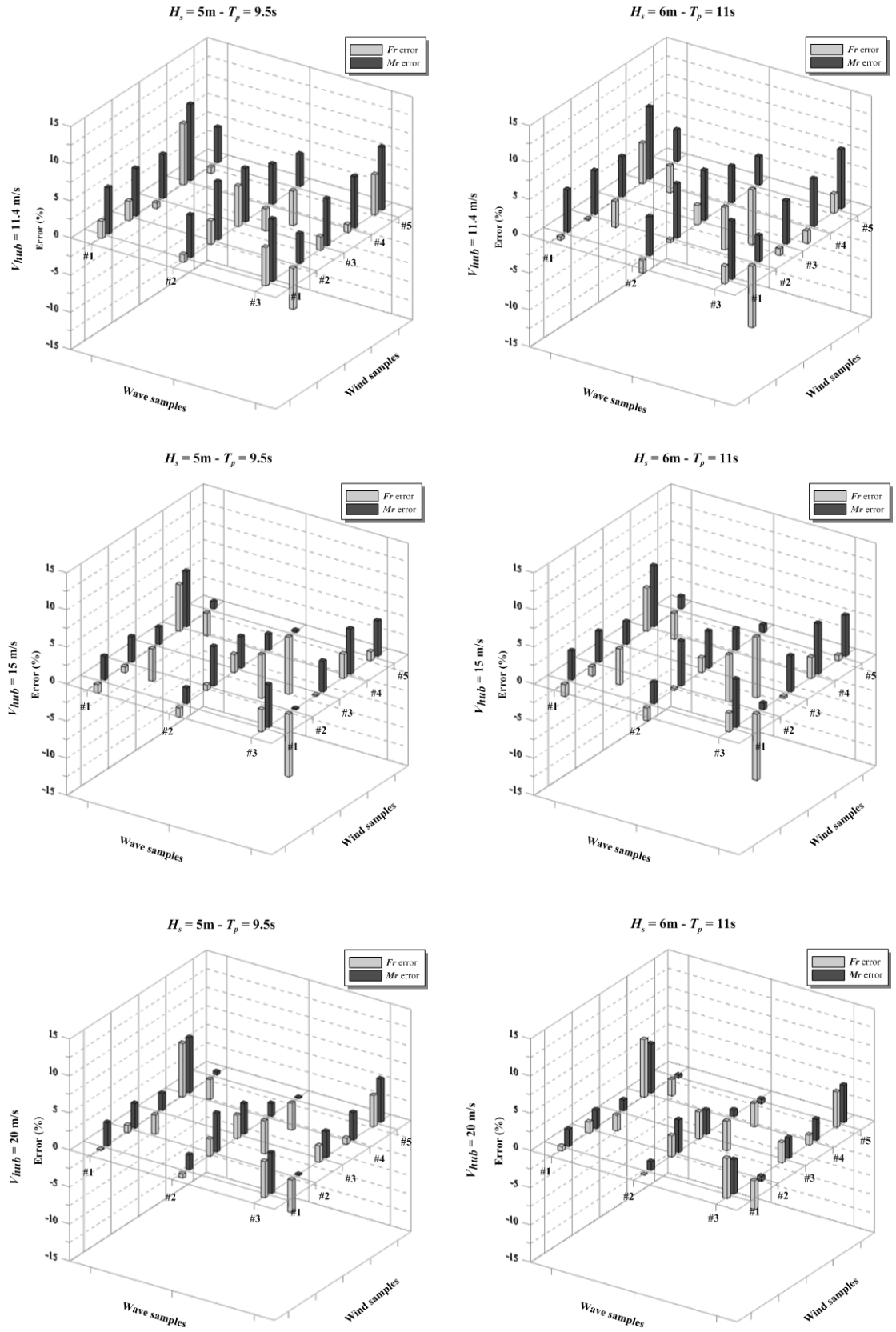

Figure 4.14: Jacket: Errors (4.5) for 4% aerodynamic damping, under Cape Mendocino earthquake.

JACKET

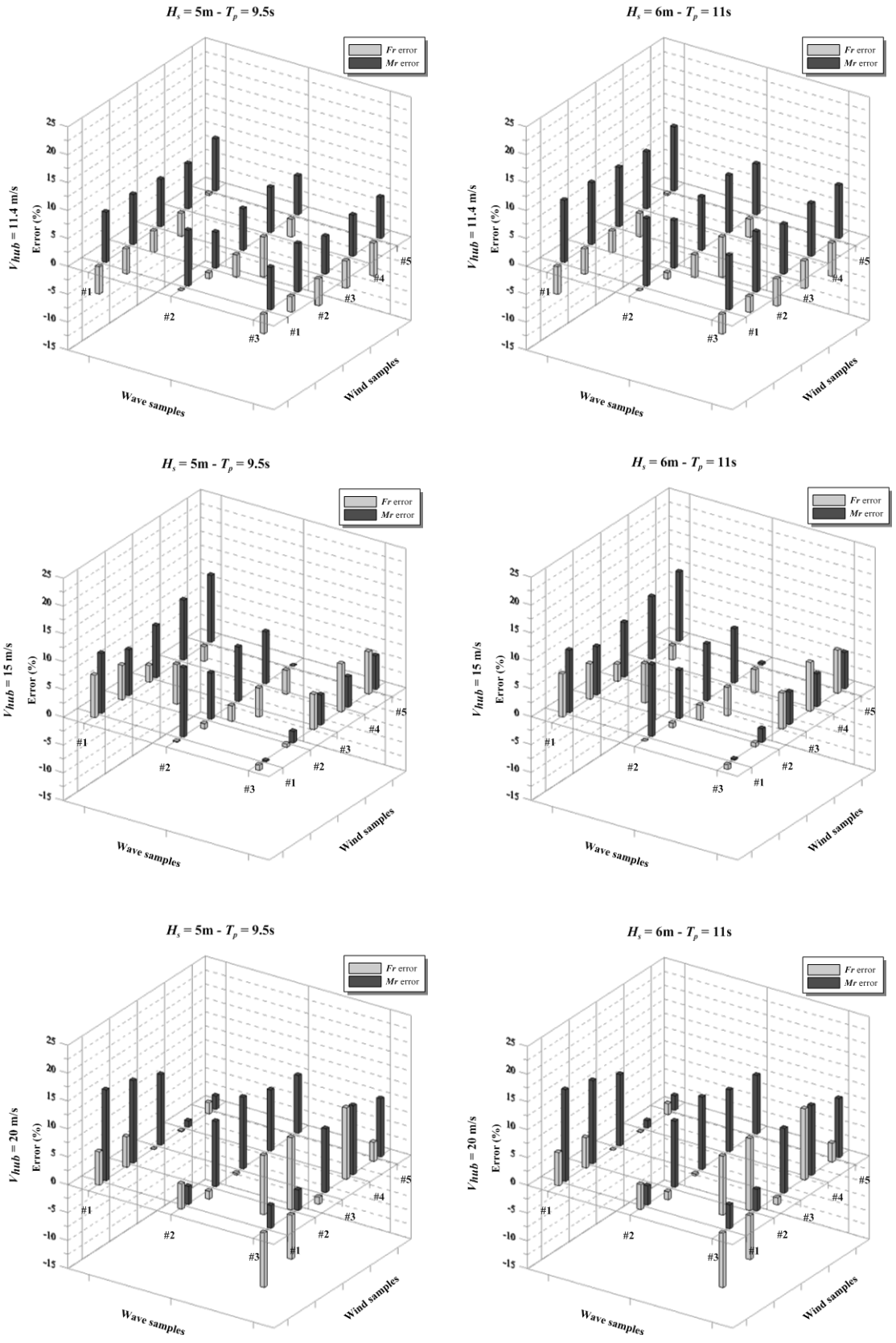

Figure 4.15: Jacket: Errors (4.5) for 4% aerodynamic damping, under Imperial Valley earthquake.

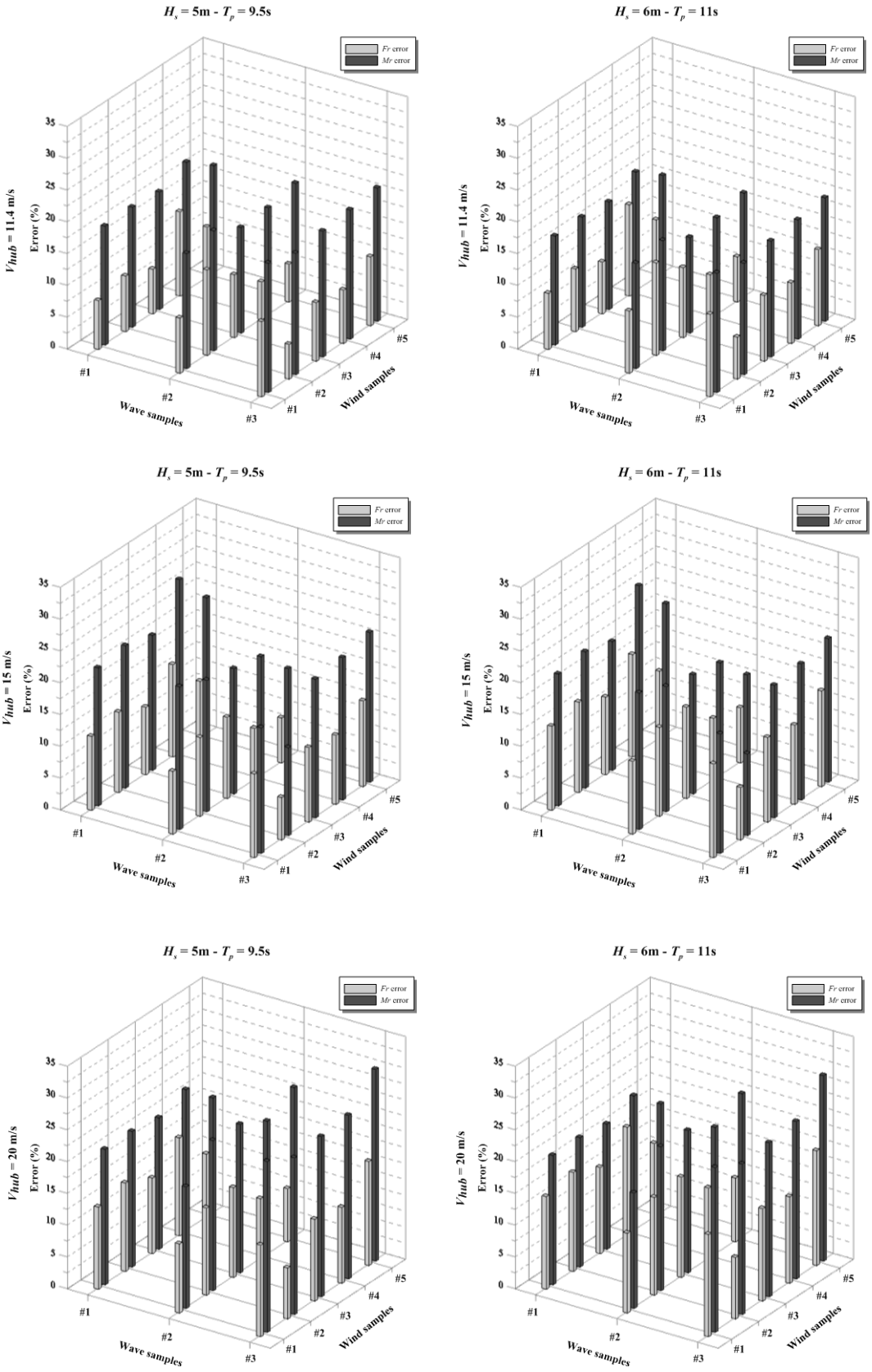

Figure 4.16: Jacket: Errors (4.5) for 4% aerodynamic damping, under Northridge earthquake.

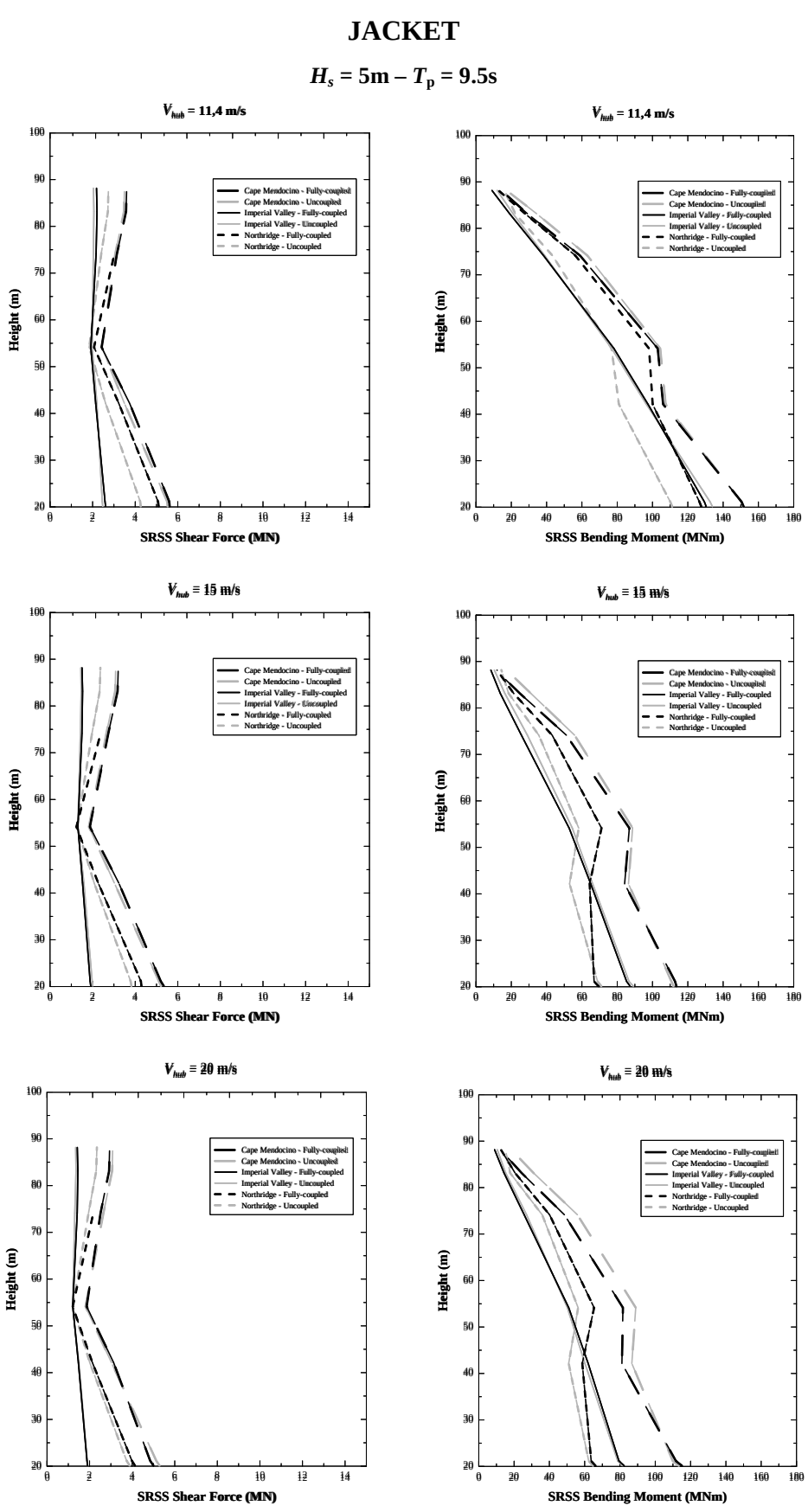

Figure 4.17: Jacket: mean demands along the tower H_s = 5m – T_p = 9.5s.

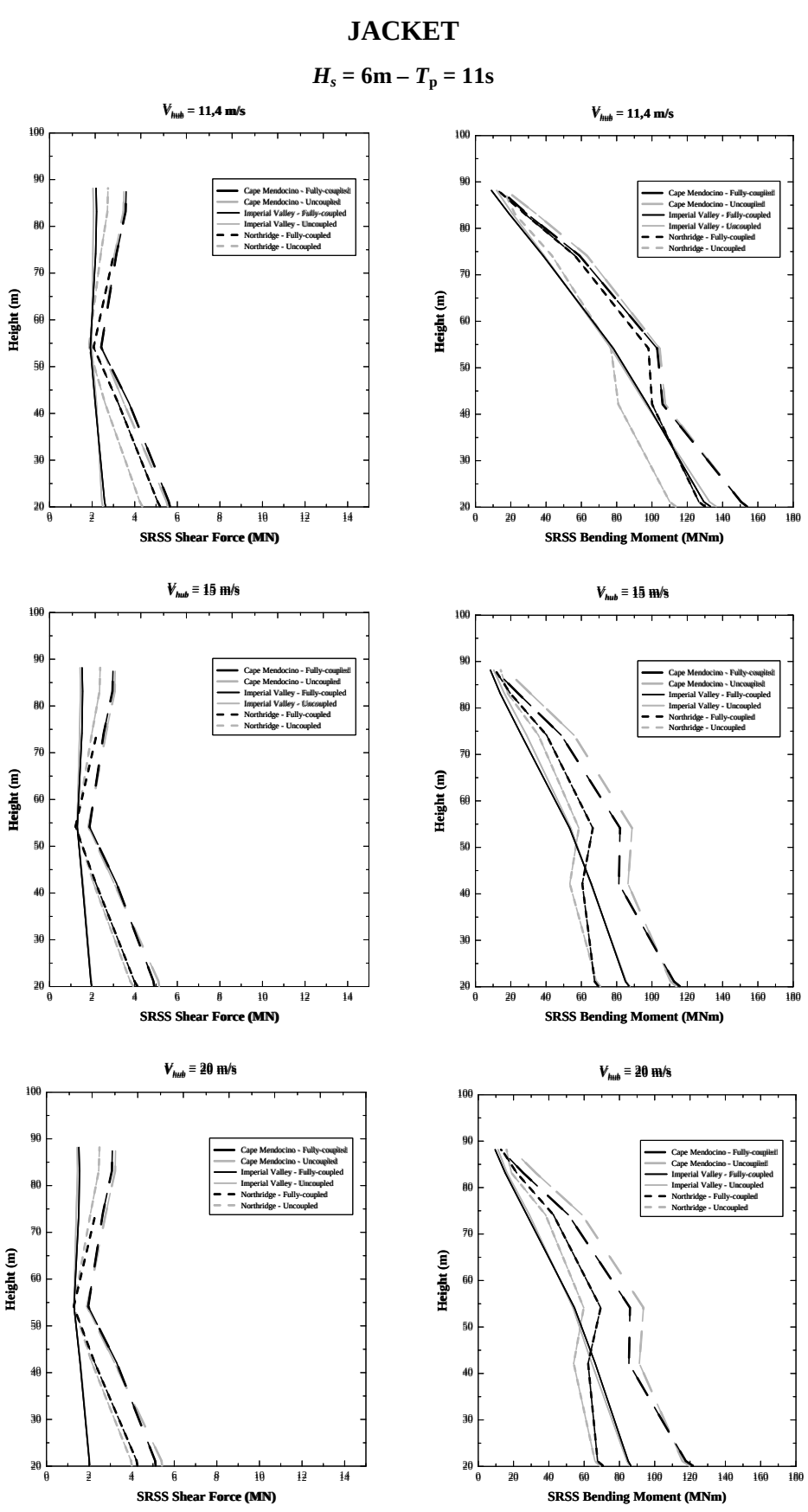

Figure 4.18: Jacket: mean demands along the tower H_s = 6m – T_p = 11s.

4.5. Conclusion

The present study has proposed a time-domain implementation of uncoupled analyses for seismic assessment of offshore HAWTs, for two different support structures in operating conditions. Wind, wave and earthquake responses are separately computed and linearly superposed, with the earthquake response computed from a structural model where additional aerodynamic damping is introduced, to account for mutual interactions between aerodynamic, hydrodynamic and seismic responses. This approach mirrors the existing formulation of uncoupled analyses in the frequency domain for land-based HAWTs, where the separate earthquake response is computed from the response spectrum method including an appropriate level of aerodynamic damping.

Numerical simulations have been run in GH BLADED [35], a simulation tool where the full system, i.e. support structure, nacelle, blades, drive train and control system, can be modeled. GH BLADED [35] has been used to implement both uncoupled analyses and fully-coupled simulations, for comparison.

First, it has been sought whether an aerodynamic damping value exists, capable of minimizing the difference between fully-coupled simulation and combination of uncoupled analyses, in terms of shear-force and bending-moment demands at the tower base. Numerical results for various wind velocities with different wind realizations, sea state with various wave sample and earthquake records have revealed that such an aerodynamic damping value cannot be found. However, it has been demonstrated that reasonably accurate results can be obtained when the separate earthquake response is computed using a 4% aerodynamic damping, for both support strucutres. In this case, errors in maxima and mean demands are similar to those obtained from the combination of uncoupled analyses existing in the literature [50,92]. It is remarkable that a 4% aerodynamic damping is, indeed, the one recommended by ASCE-AWEA RP2011 [41] for uncoupled analyses, where the separate earthquake response is computed by a frequency-domain response spectrum approach. Also, notice that a 4% aerodynamic damping has been used in previous studies [71, 72, 92].

The proposed uncoupled analyses allow a significant reduction of computational effort as compared to fully-coupled simulations. The advantage is that the wind and the wave responses, once computed for a given realization of the wind velocity at the hub and sea state, will apply for any potential earthquake record and, likewise, the response to a given earthquake record will apply for any potential wind and wave realizations. In the early

stages of design, when a considerable number of responses have to be compared for various wind-wave-earthquake realizations, a remarkable advantage can be attained with respect to fully-coupled simulations, which have to be re-run whenever wind or wave realizations or earthquake records change.

Further work is the feasibility of time-domain uncoupled analysis for seismic assessment of offshore HAWTs with flexible foundation model. This investigation is more important because the flexibility in the foundation is source of nonlinearity in the seismic response, as reported in the previous chapter. In addition, uncoupled analyses where the separate earthquake response is computed in the frequency domain by a response spectrum approach shall necessarily be computed from a linear or linearizes structural model.

References

[1] Global Wind Energy Council 2014 Global Wind Report - Annual market update 2013. Global Wind Energy Council Report, Brussels. (http://www.gwec.net)

[2] European Wind Energy Association 2011 Pure Power - Wind energy targets for 2020 and 2030. European Wind Energy Association Report, Brussels. (http://www.ewea.org)

[3] European Wind Energy Association 2013 Deep water: The next step for offshore wind energy. European Wind Energy Association Report, Brussels. (http://www.ewea.org)

[4] Manwell JF. 2013 Offshore wind energy technology trends, challenges, and risks. In: Encyclopedia of Sustainability Science and Technology (ed. R.A. Meyers), pp. 1306-1338. Berlin: Springer-Verlag. (doi: 10.1007/SpringerReference_308771)

[5] Islam MR, Guo Y, Zhu J. 2014 A review of offshore wind turbine nacelle: Technical challenges, and research and developmental trends. *Renew. Sustain. Energy Rev.* 33, 161-176. (doi: 10.1016/j.rser.2014.01.085)

[6] Negro V, López-Gutiérrez JS, Esteban MD, Matutano C. 2014 Uncertainties in the design of support structures and foundations for offshore wind turbines. *Renew. Energy* 63, 125-132. (doi: 10.1016/j.renene.2013.08.041)

[7] Lozano-Minguez E, Kolios AJ, Brennan FP. 2011 Multi-criteria assessment of offshore wind turbine support structures. *Renew. Energy* 36(11), 2831-2837. (doi: 10.1016/j.renene.2011.04.020)

[8] Jonkman JM, Matha D. 2011 Dynamics of offshore floating wind turbines-analysis of three concepts. *Wind Energy* 14, 557-569. (doi: 10.1002/we.442)

[9] Sclavounos P. 2008. Floating offshore wind turbines. *Mar. Technol. Soc. J.* 42(2), 39-43. (doi: 10.4031/002533208786829151)

[10] Butterfield S, Musial W, Jonkman JM, Sclavounos P. 2007 Engineering challenges for floating offshore wind turbines. NREL Report No. CP-500-38776, National Renewable Energy Laboratory, Golden, CO. (http://www.nrel.gov/docs/fy07osti/38776.pdf)

[11] Bachynski EE, Moan T. 2012 Design considerations for tension leg platform wind turbines. *Marine Struct.* 29, 89-114. (doi: 10.1016/j.marstruc.2012.09.001)

[12] Roddier D, Cermelli C, Aubault A, Weinstein A. 2010 WindFloat: A Floating Foundation for Offshore Wind Turbines. *J. Renew. Sustain. Energy* 2, 033104. (doi:10.1063/1.3435339)

[13] Skaare B, Nielsen FG, Hanson TD, Yttervik R, Havmøller O, Rekdal A. 2014 Analysis of measurements and simulations from the Hywind Demo floating wind turbine. *Wind Energy*, in press. (doi: 10.1002/we.1750)

[14] Jonkman JM, Buhl ML. 2007 Development and verification of a fully coupled simulator for offshore wind turbines. NREL Report No. CP-500-40979, National Renewable Energy Laboratory, Golden, CO. (http://www.nrel.gov/docs/fy07osti/40979.pdf)

[15] International Electrotechnical Commission 2009 Wind turbines. Part 3: Design requirements for offshore wind turbines. IEC 61400-3 (Ed. 1), Geneva.

[16] Germanischer Lloyd 2012 Guideline for the certification of offshore wind turbines. GL 2012, Hamburg.

[17] Det Norske Veritas 2013 Design of offshore wind turbine structures. DNV-OS-J101, Copenhagen.

[18] Alati N, Nava V, Failla G, Arena F, Santini A. 2014 On the fatigue behavior of support structures for offshore wind turbines. *Wind Struct.* 18(2), 117-134. (doi: 10.12989/was.2014.18.2.117)

[19] Haselbach P, Natarajan A, Jiwinangun RG, Branner K. 2013 Comparison of coupled and uncoupled load simulations on a jacket support structure. *Energy Procedia* 35, 244-252. (doi: 10.1016/j.egypro.2013.07.177)

[20] Karimirad M 2013 Modeling aspects of a floating wind turbine for coupled wave–wind-induced dynamic analyses. *Renew. Energy* 53, 299-305. (doi: 10.1016/j.renene.2012.12.006)

[21] Karimirad M, Moan T. 2012 A simplified method for coupled analysis of floating offshore wind turbines. *Marine Struct.* 27, 45-63. (doi: 10.1016/j.marstruc.2012.03.003)

[22] Agarwal P, Manuel L. 2011 Incorporating irregular non-linear waves in coupled simulation and reliability studies of offshore wind turbines. *Appl. Ocean Res.* 33, 215-227. (doi: 10.1016/j.apor.2011.02.001)

[23] Herbert GMJ, Iniyan S, Amutha D. 2014 A review of technical issues on the development of wind farms. *Renew. Sustain. Energy Rev.* 32, 619-641. (doi: 10.1016/j.rser.2014.01.055)

[24] Perveen R, Kishor N, Mohanty SR. 2014 Off-shore wind farm development: Present status and challenges. *Renew. Sustain. Energy Rev.* 29, 780-792. (doi: 10.1016/j.rser.2013.08.108)

[25] Hansen MOL, Madsen HA. 2011 Review paper on wind turbine aerodynamics. *J. Fluids Eng.* 133, 114001. (doi: 10.1115/1.4005031)

[26] Snel H. 2003 Review of aerodynamics for wind turbines. *Wind Energy* 6, 203-211. (doi: 10.1002/we.97)

[27] Rasmussen F, Hansen MH, Thomsen K, Larsen TJ, Bertagnolio F, Johansen J, Madsen HA, Bak C, Hansen AM. 2003. Present status of aeroelasticity of wind turbines. *Wind Energy* 6, 213-228. (doi: 10.1002/we.98)

[28] Matha D, Schlipf M, Cordle A, Pereira R, Jonkman J. 2011. Challenges in simulation of aerodynamics, hydrodynamics, and mooring-line dynamics of floating offshore wind turbines. NREL Report No. CP-5000-50544, National Renewable Energy Laboratory, Golden, CO. (http://www.nrel.gov/docs/fy12osti/50544.pdf)

[29] Sanderse B, van der Pijl SP, Koren B. 2011. Review of computational fluid dynamics for wind turbine wake aerodynamics. *Wind Energy* 14, 799-819. (doi: 10.1002/we.458)

[30] Sebastian T, Lackner MA 2012 Development of a free vortex wake method code for offshore floating wind turbines. *Renew. Energy* 46, 269-275. (doi: 10.1016/j.renene.2012.03.033)

[31] Matha D. 2010 Model development and loads analysis of an offshore wind turbine on a tension leg platform, with a comparison to other floating turbine concepts. NREL Report No. SR-500-45891, National Renewable Energy Laboratory, Golden, CO. (http://www.nrel.gov/docs/fy10osti/45891.pdf)

[32] Duarte T, Sarmento A, Jonkman J. 2014. Effects of second-order hydrodynamic forces on floating offshore wind turbines. NREL Report No. CP-5000-60966, National Renewable Energy Laboratory, Golden, CO. (http://www.nrel.gov/docs/fy14osti/60966.pdf)

[33] Westphalen J, Greaves DM, Williams CJK, Hunt-Raby AC, Zang J. 2012. Focused waves and wave-structure interaction in a numerical wave tank. *Ocean Eng.* 45, 9-21. (DOI: 10.1016/j.oceaneng.2011.12.016)

[34] Christensen ED, Hansen EA, Yde L, Tarp-Johansen NJ, Gravesen H, Damsgaard ML. Wave loads on offshore wind turbine foundations in shallow water: Engineering models vs. refined flow modelling. In: *Proc. Eur. Offshore Wind Conf. 2007.* December 4-6, Berlin.

[35] Bossanyi EA. 2000 Bladed for Windows User Manual. Garrad Hassan and Partners, Bristol.

[36] Swan, S., & Hadjian, A.H. 1988. The 1986 North Palm Springs earthquake: Effects on power facilities. NP-5607 Research Project 2848, Electric Power Research Institute (EPRI), Palo Alto, California.

[37] Umar, A.B., & Ishihara, T. 2012. Seismic load evaluation of wind turbine support structures considering low structural damping and soil structure interaction. Proceedings of the European Wind Energy Association Conference (EWEA), 16-19 April 2012, Copenhagen.

[38] DNV/Risø 2002. *Guidelines for Design of Wind Turbines*. Det Norske Veritas, Copenhagen and Wind Energy Department, Risø National Laboratory, Roskilde.

[39] GL 2010. *Guideline for the certification of wind turbines*. Germanischer Lloyd, Hamburg.

[40] IEC 2005. *Wind turbine generator systems. Part 1: Safety requirements*. IEC 61400-1 (Ed. 3). International Electrotechnical Commission, Geneva.

[41] ASCE/AWEA 2011. *Recommended practice for compliance of large land-based wind turbine support structures.* ASCE/AWEA RP2011. American Society of Civil Engineers, Reston, Virginia and American Wind Energy Association, Washington, DC.

[42] Bazeos, N., Hatzigeorgiou, G.D., Hondros, I.D., Karamaneas, H., Karabalis, D.L., Beskos, D.E. 2002. Static, seismic and stability analyses of a prototype wind turbine steel tower. *Engineering Structure*s, 24, 1015-1025.

[43] Manwell JF, McGowan JG, Rogers AL. 2010 Wind energy explained: Theory, design and application. Chichester, UK: John Wiley & Sons.

[44] Zhao, X., & Maisser, P. 2006. Seismic response analysis of wind turbine towers including soil-structure interaction. Proceedings of the Institution of Mechanical Engineers, Part K: Journal of Multi-body Dynamics, 220(1), 53-61.

[45] Eurocode 8 2004. *Design of structures for earthquake resistance. Part 1: General rules, seismic actions and rules for building*. EN 1998-1. European Committee for Standardization, Brussels.

[46] API 2000 *Recommended practice for planning, designing and constructing fixed offshore platforms – Working stress design*. API RP 2A-WSD (21st Ed.). American Petroleum Institute. Washington, DC.

[47] Zhao X, Maißer P, Wu, J. 2007 A new multibody modelling methodology for wind turbine structures using a cardanic joint beam element. *Renew. Energy* **32**, 532-546. (DOI:10.1016/j.renene.2006.04.010)

[48] Prowell I, Veletzos M, Elgamal A, Restrepo J. 2009 Experimental and numerical seismic response of a 65kW wind turbine. *J. Earth. Eng.* **13**(8), 1172-1190. (doi: 10.1080/13632460902898324)

[49] Prowell I, Elgamal A, Uang C, Jonkman J. 2010 Estimation of seismic load demand for a wind turbine in the time domain. In *Proc. Eur. Wind Energy Conf. Exhib.* (EWEC), Warsaw, 20-23 April.

[50] Prowell I. 2011 *An experimental and numerical study of wind turbine seismic behaviour*. PhD thesis, University of California, San Diego. (https://escholarship.org/uc/item/82b829mg)

[51] Prowell I, Elgamal A, Uang C, Luco JE, Romanowitz H, Duggan E. 2013 Shake table testing and numerical simulation of a utility-scale wind turbine including operational effects. *Wind Energy*, in press. (doi: 10.1002/we.1615)

[52] Stamatopoulos G. 2013 Response of a wind turbine subjected to near-fault excitation and comparison with the Greek Aseismic Code provisions. *Soil Dyn. Earth. Eng.* **46**, 77-84. (DOI: 10.1016/j.soildyn.2012.12.014)

[53] Jonkman J, Butterfield S, Musial W, Scott G. 2009 Definition of a 5-MW reference wind turbine for offshore system development. Report No. NREL/TP-500-38060, National Renewable Energy Laboratory, Golden, CO. (http://www.nrel.gov/wind/pdfs/38060.pdf)

[54] Haciefendioğlu K. 2012 Stochastic seismic response analysis of offshore wind turbine including fluid-structure-soil-interaction. *Struct. Design Tall Spec. Build.* **21**, 867-878. (doi: 10.1002/tal.646)

[55] Kim DH, Lee SG, Lee IK. 2014 Seismic fragility analysis of 5 MW offshore wind turbine. *Renew. Energy* **65**, 250-256. (DOI: 10.1016/j.renene.2013.09.023)

[56] Schwartz M, Heimiller D, Haymes S, Musial W. 2010 Assessment of offshore wind energy resources for the United States. Report No. NREL/TP-500-45889, National Renewable Energy Laboratory, Golden, CO. (http://www.nrel.gov/docs/fy10osti/45889.pdf)

[57] USGS 2008 Hazard map (PGA, 2% in 50 years). U.S. Geological Survey. (http://earthquake.usgs.gov/hazards/products)

[58] Jonkman J., Musial W. 2010 Offshore Code Comparison Collaboration (OC3) for IEA Task 23 Offshore Wind Technology and Deployment. Report No. NREL/TP-5000-48191, National Renewable Energy Laboratory, Golden, CO. (http://www.nrel.gov/docs/fy11osti/48191.pdf)

[59] Rendon EA, Manuel L. 2012 Long-term loads for a monopile-supported offshore wind turbine. *Wind Energy*. (DOI: 10.1002/we.1569)

[60] ATC 2009 *Quantification of building seismic performance factors*. Report No. FEMA-P695, Applied Technology Council, Redwood City, CA. (http://www.fema.gov/media-library-data/20130726-1716-25045-9655/fema_p695.pdf)

[61] Luco N. 2001 Probabilistic seismic demand analysis, smrf connection fractures, and near source effects. PhD thesis, Stanford University. (http://geohazards.cr.usgs.gov/staffweb/nluco/manuscripts/0206--Luco.pdf)

[62] Vorpahl F, Popko W, Kaufer D. 2013 Description of a Basic Model of the 'UpWind Reference Jacket' for Code Comparison in the OC4 Project under IEA Wind Annex 30. Technical report, Fraunhofer Institute for Wind Energy and Energy System Technology IWES, Bremerhaven, Germany.(http://www.iwes.fraunhofer.de/content/dam/iwes/en/documents/OC4%20Jacket%20Model%20Description.pdf)

[63] Zaaijer MB. 2006 Foundation modelling to assess dynamic behaviour of offshore wind turbines. *Applied Ocean Research* **28**, 45-57. (doi:10.1016/j.apor.2006.03.004)

[64] AlHamaydeh M, Hussain S. 2011 Optimized frequency-based foundation design for wind turbine towers utilizing soil–structure interaction. *Journal of the Franklin Institute* **348**(7): 1470-1487. (DOI: 10.1016/j.jfranklin.2010.04.013)

[65] Dong W, Moan T, Gao Z. 2011 Long-term fatigue analysis of multi-planar tubular joints for jacket-type offshore wind turbine in time domain. *Eng. Struct.* **33**, 2002-2014. (DOI:10.1016/j.engstruct.2011.02.037)

[66] Marine Innovation & Technology 2009 ClubStead Preliminary Analysis: Metocean Conditions. Report No. MI&T040-08_R2. Marine Innovation & Technology, Berkeley, CA. (http://www.seasteading.org/wp-content/uploads/2013/03/ClubStead-Metoceanv0a.pdf)

[67] ABS 2011 *Design Standards for Offshore Wind Farms*. American Bureau of Shipping, Corporate Offshore Technology, Renewables. Houston, TX.

[68] Hasselmann K, Barnett TP, Bouws E et al. 1973 Measurements of wind wave growth and swell decay during the Joint North Sea Wave Project (JONSWAP). *Deut. Hydrogr. Zeit*, A8, 1-95. (http://resolver.tudelft.nl/uuid:f204e188-13b9-49d8-a6dc-4fb7c20562fc)

[69] Van der Tempel J., Molenaar D.P. 2002 Wind Turbine Structural Dynamics – A Review of the Principles for Modern Power Generation, Onshore and Offshore. *Wind Eng.* **26**(4), 211-220. (DOI: 10.1260/030952402321039412)

[70] Chakrabarti SK. 1987 *Hydrodynamics of offshore structures*. Southampton, UK: WIT Press.

[71] Witcher D. 2005 Seismic analysis of wind turbines in the time domain. *Wind Energy* **8**, 81-91. (DOI: 10.1002/we.135)

[72] Valamanesh V, Myers AT. 2014 Aerodynamic damping and seismic response of horizontal axis wind turbine towers. *J. Struct. Eng.*, in press. (DOI: 10.1061/(ASCE)ST.1943-541X.0001018)

[73] Seidel M, Foss G. 2006 Impact of different substructures on turbine loading and dynamic behaviour for the DOWNVInD Project in 45m water depth. In: *Conf. Proc.* EWEC 2006. Athens 2006.

[74] Mostafa YE, El Naggar MH. 2004 Response of fixed offshore platforms to wave and current loading including soil–structure interaction. *Soil Dyn. Earth. Eng.* **24**, 357-368. (DOI:10.1016/j.soildyn.2003.11.008)

[75] Kuhn M. 2001 Dynamics and design optimisation of offshore wind energy conversion systems. Report no. 2001.002. Delft University Wind Energy Research Institute (DUWIND). (http://resolver.tudelft.nl/uuid:adc3b032-3dde-4e32-84c3-7b8e181e526)

[76] Carswell W, Arwade SR, DeGroot DJ, Lackner MA. 2014 Soil-structure reliability of offshore wind turbine monopile foundations. *Wind Energy*, in press. (DOI: 10.1002/we.1710)

[77] Bhattacharya S, Adhikari S. 2011 Experimental validation of soil–structure interaction of offshore wind turbines. *Soil Dyn. Earth. Eng.* **31**, 805-816. (DOI:10.1016/j.soildyn.2011.01.004)

[78] Bhattacharya S, Nikitas N, Garnsey J, Alexander NA, Cox J, Lombardi D, Muir Wood D, Nash DFT. 2013 Observed dynamic soil–structure interaction in scale testing of offshore wind turbine foundations. *Soil Dyn. Earth. Eng.* **54**, 47-60. (DOI: 10.1016/j.soildyn.2013.07.012)

[79] Failla G, Arena F. 2015. New perspectives in offshore wind energy. *Phil. Trans. R. Soc. A*, Vol. 373. (DOI: 20140228)

[80] Schwatrz M, Heimiller D, Haymes S, Musial W. 2010, Assessment of Offshore Wind Energy Resources for the United States. Report No. NREL/TP-500-45889, National Renewable Energy Laboratory, Golden, CO. (http://www.nrel.gov/docs/fy10osti/45889.pdf)

[81] U.S. Geological Survey, 2008, Hazard map (PGA, 2% in 50 years).

[82] Alati N, Failla G, Arena A. 2015 Seismic analysis of offshore wind turbines on bottom-fixed support structures. *Phil. Trans. R. Soc. A,* **Vol. 373** (DOI:20140086)

[83] Prowell I, Veers P. 2009 Assessment of wind turbine seismic risk: existing literature and simple study of tower moment demand. Technical Report No. SAND2009-1100. Albuquerque: Sandia National Laboratories

[84] Failla G. 2014 Seismic analysis of wind energy converters. In: Beer M, Kougioumtzoglou IA, Patelli E, Au IS-K, editors. Encyclopedia of earthquake engineering. Berlin-Heidelberg:Springer-Verlag

[85] Lavassas I, Nikolaidis G, Zervas P, Efthimiou E, Doudoumis IN, Baniotopoulos CC. 2003 Analysis and design of the prototype of a steel 1-MW wind turbine tower. *Eng Struct* , **25**(8), 1097-1106

[86] Mulliken JS, Karabalis DL. 1998 Discrete models for through-soil coupling of foundations and structures. *Earthq. Eng. Struct. Dyn.*, **27**,687-710.

[87] Sapountzakis EJ, Dikaros IC, Kampitsis AE, Koroneou AD. 2015 Nonlinear response of wind turbines under wind and seismic excitations with soil-structure interaction. *J. Comput. Nonlinear Dyn.*, **10**, 041007.

[88] Díaz O, Suárez LE. 2014 Seismic analysis of wind turbines. *Earthq. Spectra*, **30**(2), 743-765.

[89] Asareh MA, Schonberg W, Volz J. 2016, Effects of seismic and aerodynamic load interaction on structural dynamic response of multi-megawatt utility scale horizontal axis wind turbines. *Renew. Energy*, **86**, 49-58

[90] Jonkman JM, Buhl ML. 2005, FAST user's guide. Golden: National Renewable Energy Laboratory

[91] Haenler M, Ritschel U, Warnke I. 2006 Systematic modelling of wind turbine dynamics and earthquake loads on wind turbines. In: Proceedings of the European Wind Energy Conference & Exhibition (EWEC), Athens, Greece

[92] Asareh M-A, Prowell I. 2012, A simplified approach for implicitly considering aerodynamics in the seismic response of utility scale wind turbines. In: Proceedings of 53rd AIAA/ASME/ASCE/AHS/ASC Structures, Structural Dynamics and Materials Conference, Honolulu, Hawaii

[93] Pacific Earthquake Engineering Research Center (PEER) 2013 Peer ground motion database. University of California, Berkeley (http://ngawest2.berkeley.edu/).

APPENDIX A

p-y curves for soil springs in x and y dir. (see Figure 3.1 in the paper for x and y)

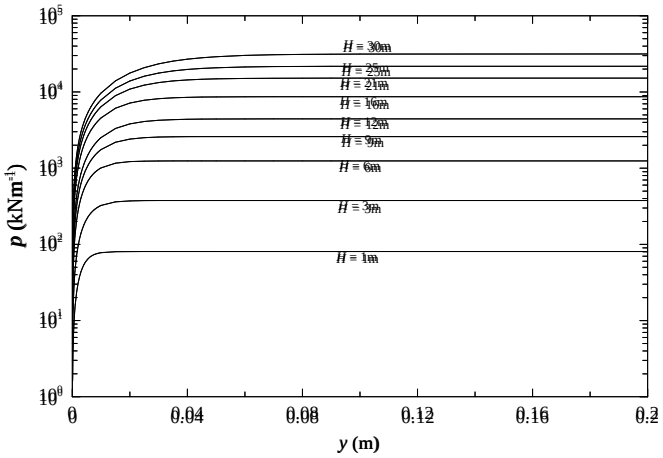

p-y law given in Section 6.8.7 of API code (ref. [46] in the paper) for cyclic loading (A=0.9)
H is the depth

t-z curves for soil springs in z dir. (see Figure 3.1 in the paper for z)

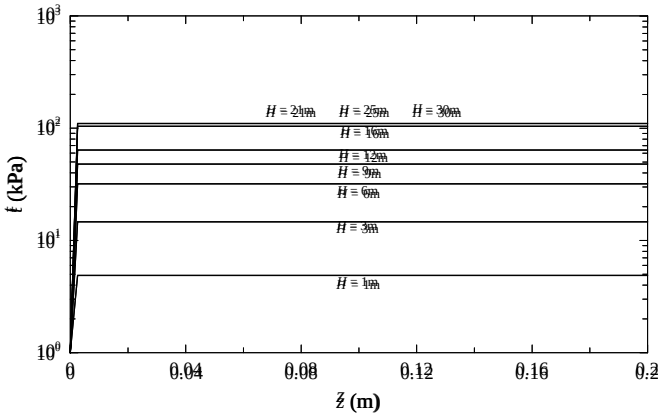

t-z law given in Section 6.7.2 of API code (ref. [46] in the paper)
H is the depth

Q-z curve for soil spring at the piles tip in z dir. (see Figure 3.1 in the paper for z)

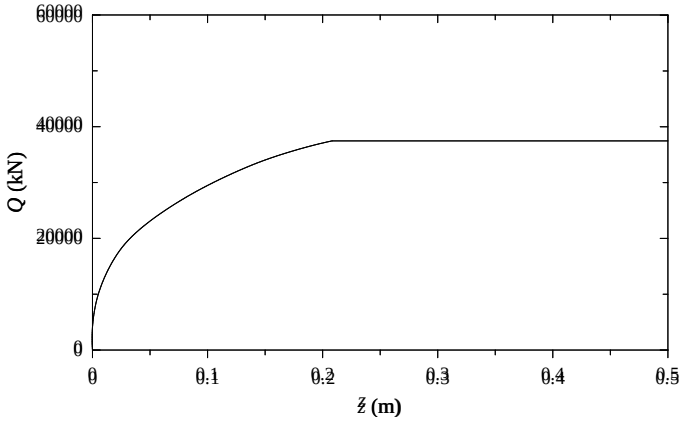

Q-z law given in Section 6.7.3 of API code (ref. [46] in the paper)

APPENDIX B

Axial force demands at the piles head in load cases LC1-LC2-LC3

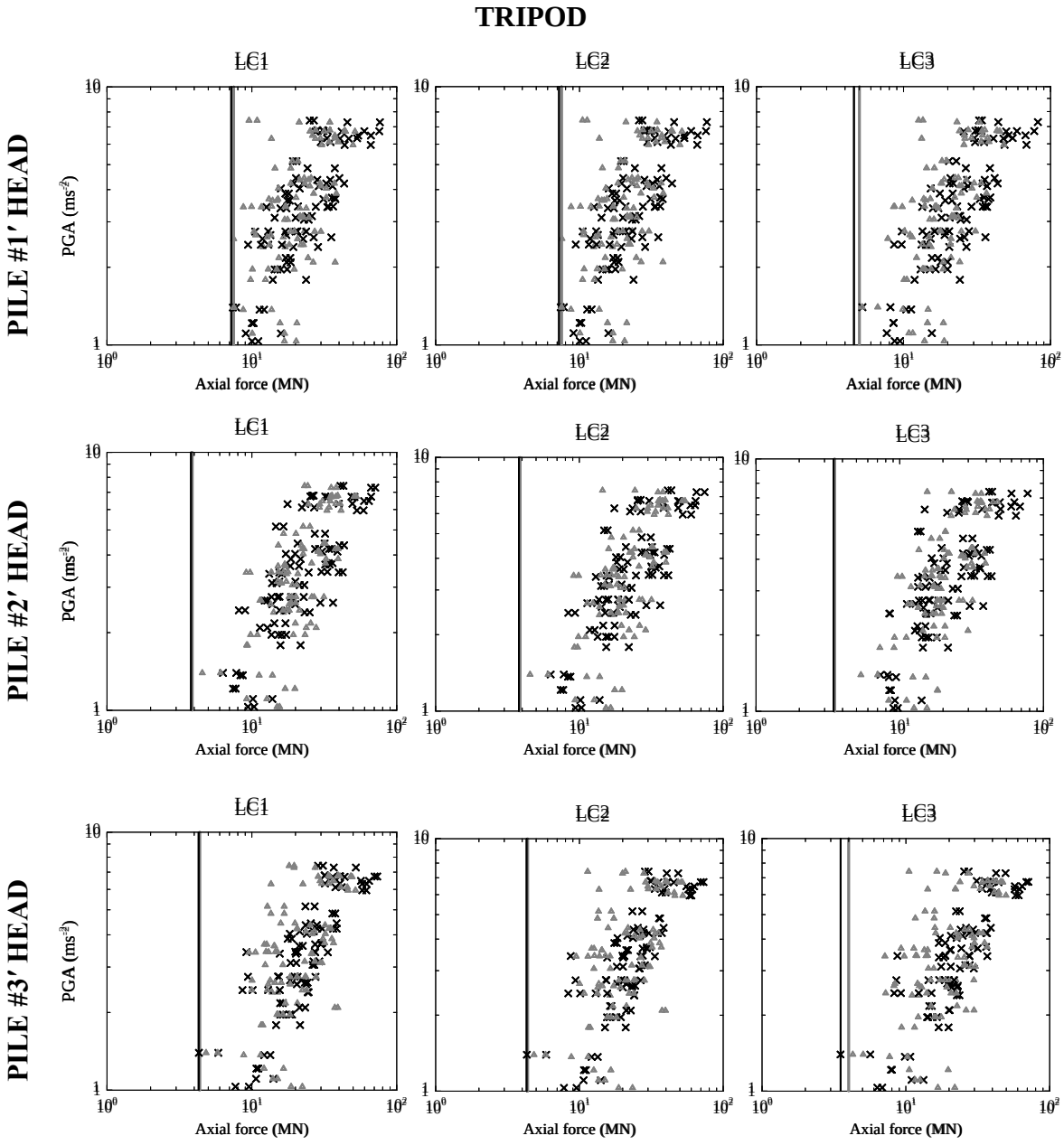

Axial force demands at the piles head in load cases LC1-LC2-LC3

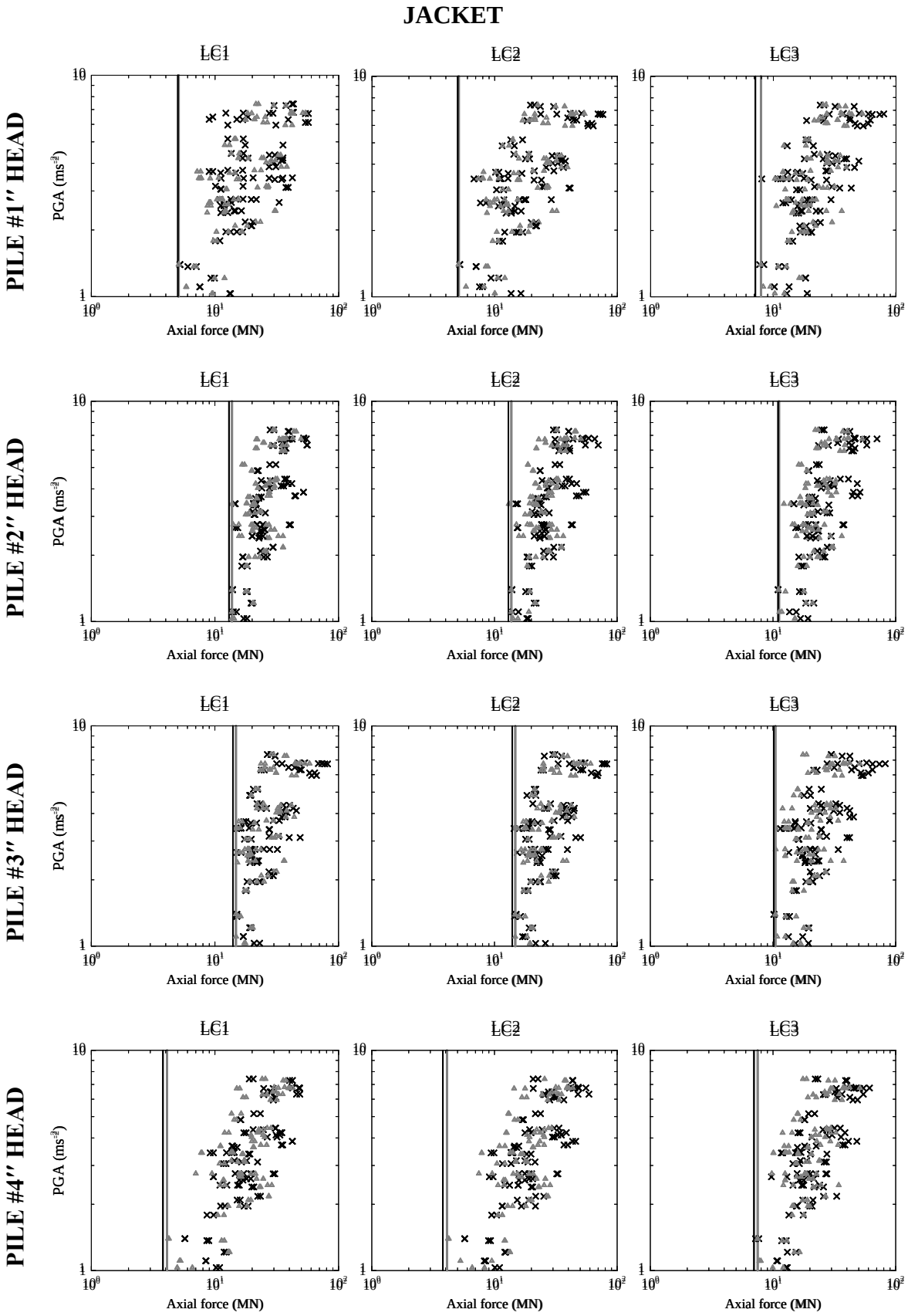

APPENDIX C

Details for IEC load case in Table 3.4

DLC 1.3

Extreme turbulence model (ETM) – Section 6.3.2.3 in IEC61400-1[40]

I_{ref} = 0.14 (Medium turbulence characteristics B)

V_{ave} =0.2V_{ref} = 10 ms-1 for V_{ref} = 50 ms^{-1}.

Normal sea state (NSS) - Section 6.4.1.1 in IEC61400-3 [15]

Normal current model (NCM) – Sections 6.4.2.4 and 6.4.2.2 in IEC61400-3 [15]

V_{hub} (ms^{-1})	$V_{1\text{-}hour}$ (z =10m) (ms^{-1})
10	6.98
15	10.47
20	13.96
25	17.45

$V_{1\text{-}hour}$ (z =10m) = k_1 V_{10min} (z =10m); k_1 = 0.95; V_{10min} (z =10m) = $V_{hub}(z/z_{hub})^{0.14}$

Mean sea level (MSL) – Section 6.4.3 in IEC61400-3 [15]

DLC 1.6a

Normal turbulence model (NTM) - Section 6.3.1.3 in IEC61400-1[40]

I_{ref} = 0.14 (Medium turbulence characteristics B).

Severe sea state (SSS) - Section 6.4.1.3 in IEC61400-3[15]

$H_{s,SSS}$ = $H_{s,50}$ = 8.0 m.

Normal current model (NCM) – Sections 6.4.2.4 and 6.4.2.2 in IEC61400-3 [15]

V_{hub} (ms^{-1})	$V_{1\text{-}hour}$ (z =10m) (ms^{-1})
10	6.98
15	10.47
20	13.96
25	17.45

$V_{1\text{-}hour}$ (z =10m) = k_1 V_{10min} (z =10m); k_1 = 0.95; V_{10min} (z =10m) = $V_{hub}(z/z_{hub})^{0.14}$

Normal water level range (NWLR) - Section 6.4.3.1 in IEC61400-3[15]

NWLR = MSL ± 2 m = 50 ± 2 m.

DLC 6.1a

Extreme wind speed model with turbulence (EWM) – Section 6.3.2.1 in IEC61400-1[40]

k_1 = 0.95 – Section 7.4.6 in IEC61400-3 [15]

V_{ref} = 50 ms^{-1}.

Extreme sea state (ESS) - Section 6.4.1.5 in IEC61400-3[15]

k_2 = 1.09 – Section 7.4.6 in IEC61400-3 [15]

Hs,50 = 8.0 m.

Misaligned (MIS) – Section 6.4.1 in IEC61400-3 [15]

β=0°, ± 30°.

Extreme current model (ECM) – Sections 6.4.2.5, 6.4.2.1 and 6.4.2.2 in IEC61400-3 [15]

V_{hub} = $k_1 V_{ref}$ = 47.5 ms^{-1}; $V_{1\text{-}hour}$ (z =10m) = $V_{hub}(z/z_{hub})^{0.11}$ = 37.3 ms^{-1}; $U_{ss}(0)$ = 3.0 ms^{-1}.

Extreme water level range (EWLR) - Section 6.4.3.2 in IEC61400-3[15]

EWLR = MSL ± 3 m = 50 ± 3 m.

APPENDIX D

Axial force demands at the piles head in some IEC load cases (Table 3.4 in the paper)

TRIPOD

Operational state	Pile #1′ head (MN)		Pile #2′ head (MN)		Pile #3′ head (MN)	
	Fixed FM	Flex. FM	Fixed FM	Flex. FM	Fixed FM	Flex. FM
DLC 1.3_1	6.85	7.63	3.95	4.24	4.53	5.02
DLC 1.3_2	7.04	7.66	3.31	3.74	5.17	5.18
DLC 1.3_3	7.10	7.68	3.71	3.92	5.34	5.22
DLC 1.3_4	7.20	8.32	3.82	4.54	5.71	6.05
DLC 1.6a_1	10.72	12.06	5.31	6.03	6.21	6.82
DLC 1.6a_2	7.38	7.90	3.70	4.10	4.32	4.67
DLC 1.6a_3	9.52	9.73	4.94	4.96	5.34	5.90
DLC 1.6a_4	9.97	9.02	5.31	4.75	5.58	5.63
DLC 1.6a_5	10.30	11.73	5.95	6.54	6.45	7.04
DLC 1.6a_6	7.79	7.58	4.45	4.45	5.17	4.91
DLC 1.6a_7	9.34	9.09	5.33	5.23	5.98	6.19
DLC 1.6a_8	9.66	8.80	5.87	5.39	5.71	6.18

Axial force demands at the piles head in some IEC load cases

TRIPOD

Parked state	Pile #1′ head (MN)		Pile #2′ head (MN)		Pile #3′ head (MN)	
	Fixed FM	Flex. FM	Fixed FM	Flex. FM	Fixed FM	Flex. FM
DLC 6.1a_1	9.06	10.32	5.96	6.15	8.93	10.02
DLC 6.1a_2	10.05	11.51	8.79	9.39	7.01	7.73
DLC 6.1a_3	9.06	10.35	10.86	11.66	6.82	7.00
DLC 6.1a_4	8.01	9.86	6.62	6.66	9.25	10.43
DLC 6.1a_5	8.96	10.65	9.06	9.72	7.39	8.09
DLC 6.1a_6	7.99	9.83	10.92	11.87	7.29	7.38

Axial force demands at the piles head in some IEC load cases

JACKET

Operational state	Pile #1″ head (MN)		Pile #2″ head (MN)		Pile #3″ head (MN)		Pile #4″ head (MN)	
	Fixed FM	Flex. FM	Fixed FM	Flex. FM	Fixed FM	Flex. FM	Fixed FM	Flex. FM
DLC 1.3_1	8.79	8.64	14.52	14.50	16.10	15.96	9.38	9.13
DLC 1.3_2	9.59	9.23	14.01	14.26	16.97	16.52	10.12	10.37
DLC 1.3_3	9.93	9.35	14.47	14.38	17.31	16.86	10.46	10.64
DLC 1.3_4	11.39	9.95	15.64	16.17	18.24	17.49	11.08	11.05
DLC 1.6a_1	9.62	9.35	18.51	18.80	20.01	20.57	10.05	9.71
DLC 1.6a_2	9.83	9.11	14.84	15.03	16.34	16.61	9.89	9.49
DLC 1.6a_3	10.08	9.49	15.16	15.01	17.83	17.73	10.81	10.47
DLC 1.6a_4	10.59	10.49	16.29	15.45	18.56	18.16	11.63	10.80
DLC 1.6a_5	9.61	9.54	18.29	18.73	20.03	20.23	9.93	9.72
DLC 1.6a_6	9.72	9.13	14.47	14.96	15.98	16.46	9.37	9.96
DLC 1.6a_7	9.72	9.37	14.94	14.98	17.70	17.26	10.46	10.22
DLC 1.6a_8	10.27	10.40	15.76	15.11	18.21	17.95	10.90	10.57

Axial force demands at the piles head in some IEC load cases

JACKET

Parked state	Pile #1″ head (MN)		Pile #2″ head (MN)		Pile #3″ head (MN)		Pile #4″ head (MN)	
	Fixed FM	Flex. FM	Fixed FM	Flex. FM	Fixed FM	Flex. FM	Fixed FM	Flex. FM
DLC 6.1a_1	16.48	12.10	20.50	21.10	30.27	25.34	13.99	13.33
DLC 6.1a_2	11.76	10.35	25.28	24.35	25.49	23.18	13.59	12.57
DLC 6.1a_3	10.57	10.63	27.90	27.01	21.06	22.25	13.99	14.03
DLC 6.1a_4	14.45	11.31	20.17	20.87	28.04	24.39	13.96	13.30
DLC 6.1a_5	10.30	10.32	24.36	23.53	23.86	22.68	13.72	12.73
DLC 6.1a_6	10.43	10.47	26.67	25.90	21.21	22.27	13.52	13.06

Publications

[1] Alati N, Nava V, Failla G, Arena F and Santini A. 2013, Fatigue Analysis of Offshore Wind Turbines on Fixed Support Structures, *Key Engineering Materials*, Vols. 569-570 pp 539-546. DOI:10.4028/www.scientific.net/KEM.569-570.539

[2] Alati N, Nava V, Failla G, Arena F and Santini A. 2014, On the fatigue behavior of support structures for offshore wind turbines, *Wind and Structures*, Vol. 18, **2**, 117-134. DOI: http://dx.doi.org/10.12989/was.2014.18.2.117

[3] Alati N, Failla G and Arena F. 2015, Seismic analysis of offshore wind turbines on bottom-fixed support structures, *Philosophical Transactions of the Royal Society A*, Vol. 373, n. 2035 20140086. DOI: 10.1098/rdsta.2014.0086

[4] Alati N, Failla G and Arena F. 2015, Coupled vs. Uncoupled Analyses for Seismic Assessment of Offshore Wind Turbines, *Advances in Mathematics and Statistical Sciences*. ISBN: 978-1-61804-275-0